THE UNIVERSITY
of EDINBURGH

Hippocampal Theta Sequences: From Phenomenology to Circuit Mechanisms

Angus Chadwick

Doctor of Philosophy

Institute for Adaptive and Neural Computation
School of Informatics
University of Edinburgh

2016

Abstract

The hippocampus is a brain structure involved in episodic memory and spatial cognition. Neuronal activity within the hippocampus exhibits intricate temporal patterning, including oscillatory and sequential dynamics, which are believed to underlie these cognitive processes. In individual cells, a temporal activity pattern called phase precession occurs which leads to the organisation of neuronal populations into sequences. These sequences are hypothesised to form a substrate for episodic memory and the representation of spatial trajectories during navigation.

In this thesis, I present a novel theory of the phenomenological properties of these neuronal activity sequences. In particular, I propose that the sequential organisation of population activity is governed by the independent phase precession of each cell. By comparison of models in which cells are independent and models in which cells exhibit coordinated activity against experimental data, I provide empirical evidence to support this hypothesis. Further, I show how independent coding affords a vast capacity for the generation of sequential activity patterns across distinct environments, allowing the representation of episodes and spatial experiences across a large number of contexts.

This theory is then extended to account for grid cells, whose activity patterns form a hexagonal lattice over external space. By analysing simple forms of phase coding in populations of grid cells, I show how previously undocumented constraints on phase coding in two dimensional environments are imposed by the symmetries of grid cell firing fields. To overcome these constraints, I propose a more complex phenomenological model which can account for phase precession in both place cells and grid cells in two dimensional environments.

Using insights from this theory, I then propose a biophysical circuit mechanism for hippocampal sequences. I show that this biophysical circuit model can account for the proposed phenomenological coding properties and provide experimentally testable predictions which can distinguish this model from existing models of phase precession. Finally, I outline a scheme by which this biophysical mechanism can implement supervised learning using spike time dependent plasticity in order to learn associations between events occurring on behavioural timescales.

The models presented in this thesis challenge previous theories of hippocampal circuit function and suggest a much higher degree of flexibility and capacity for the generation of sequences than previously believed. This flexibility may underlie our ability to represent spatial experiences and store episodic memories across a seemingly unlimited number of distinct contexts.

Acknowledgements

Firstly, I would like to thank my supervisors Mark van Rossum and Matthew Nolan for all of their support and advice throughout my PhD. I would also like to thank all of my friends and colleagues at the ANC who have made my time here so enjoyable. Thanks to everyone from the Nolan lab for being friendly and welcoming from the beginning. Thanks to the DTC for all of the journal clubs, conference trips and research visits and for allowing me the freedom to discover and pursue my own interests throughout my PhD. Thanks to Geraint Rees, Vincenzo Romei and Joe Brooks for welcoming me into a new city during my Masters project and devoting so much time towards helping my with my project. Thanks to Gyuri Buzsaki and everyone at the Buzsaki lab for providing a friendly and intellectually stimulating environment during my stay at NYU. Finally, I would like to thank my friends and family for being continually supportive, both before and throughout my PhD.

Declaration

I declare that this thesis was composed by myself, that the work contained herein is my own except where explicitly stated otherwise in the text, and that this work has not been submitted for any other degree or professional qualification except as specified.

(*Angus Chadwick*)

Table of Contents

Chapter 1

Background

1.1 Functions of the hippocampus

Episodic memory

The hippocampus is a brain area central to episodic, spatial and declarative memory. The importance of the hippocampus for episodic and declarative memory was famously demonstrated in patient H.M., whose hippocampi (along with most of his medial temporal lobes) were bilaterally removed in a surgical procedure for the treatment of epilepsy (Penfield and Milner, 1958). Following this procedure, H.M. exhibited severe anterograde amnesia, being unable to form new explicit memories. Despite this deficit, he maintained relatively intact cognitive function in the majority of other domains, including the ability to recall memories of events several years earlier and the ability to form new implicit and procedural memories. These observations motivated the hypothesis, now known as the Standard Model of Systems Consolidation (Squire and Alvarez, 1995), that new memories are formed in the hippocampus but later migrate to cortex, after which the hippocampus is no longer required for their retrieval.

Based on these insights, a highly influential theory of hippocampal function was developed by David Marr (Marr, 1971). Marr proposed that the hippocampus indexes the distributed pattern of cortical activity associated with a particular experience via the activation of a unique subset of hippocampal neurons. According to this theory, memory traces are formed rapidly in the hippocampus by the modification of synaptic efficacies between these cells during the experience. Once this memory trace has been established within the hippocampus, these strengthened synaptic connections allow the pattern of hippocampal activity which indexes the experience to be reactivated

whenever a sufficiently large subset of that pattern is activated, in a process known as *pattern completion*. Thus, a small part of the cortical activation pattern associated with the original experience will be completed within the hippocampus. In turn, this completed pattern of hippocampal activity will reinstate the full cortical activation pattern, resulting in the re-experiencing of the event and thus retrieval of the memory. Over time, this hippocampal memory trace is then transferred to cortex, at which time it becomes hippocampus-independent (but see multiple trace theory for an alternative hypothesis (Nadel et al., 2000)).

Cognitive map

Evidence for the involvement of the hippocampus in spatial cognition emerged later from studies in rodents. The theoretical basis for this work lies in the pioneering behavioural studies of Edward Tolman, a psychologist who had been investigating the ability of rodents to navigate flexibly in complex environments. Arguing against the prominent stimulus-response theory of navigation in which navigational choices in a maze are posited to arise from the sequential chaining of conditioned responses to sensory stimuli (Hull, 1943), Tolman proposed the concept of a cognitive map. According to Tolman, rodents maintain a cognitive map of their environment containing information about the relative locations and attributes of objects, allowing them to flexibly navigate towards a particular goal even if conditioned responses to sensory stimuli have not been established (Tolman, 1948).

To test this hypothesis, Tolman performed experiments in which rats were placed in one arm of a cross shaped maze and learned to take a right turn to a reward at the end of the adjacent arm. After this paradigm had been learned, rats were then placed in a different arm of the maze for the first time. Rather than engaging in the conditioned right turn response as predicted by the stimulus-response theory, rats successfully took the correct path towards the reward using the novel direct route. Despite such evidence, however, the existence of cognitive maps of the form proposed by Tolman in rodents is still debated (Amsel, 1993; Bennett, 1996), and the stimulus-response theory remains a highly influential view of learning and behaviour (Toates, 1997; Holland, 2008).

While Tolman's studies were purely behavioural, neurobiological evidence for the cognitive map hypothesis was subsequently obtained by John O'Keefe and Jonathan Dostrovsky. Recording from the hippocampus of freely moving rodents, they found that individual neurons became active at particular locations in an environment (O'Keefe

and Dostrovsky, 1971). When recording from an ensemble of hippocampal cells, different cells became active at different locations, such that the activity patterns formed a map of the environment from which the animal's location at each instant could be inferred. The theoretical implications of this work were expounded in "The Hippocampus as a Cognitive Map", in which O'Keefe argued that these cells form the biological substrate of Tolman's cognitive map, which had previously only been conceived at a behavioural and psychological level (O'Keefe and Nadel, 1978).

On a philosophical level, it was argued that these findings constitute a scientific basis for Immanuel Kant's theory of space, in which spatial representations are hypothesised to exist prior to all sensory inputs, and this innate cognitive apparatus is hypothesised to provide a fixed architecture within which sensory inputs are integrated in order to construct an experience (O'Keefe and Nadel, 1978). In support of this view, empirical evidence that spatial representations exist in the hippocampus upon first spatial experience has since emerged (Wills et al., 2010). This Kantian view of space runs in contrast to the Lockean view, in which spatial representations are proposed to be learned from sensory inputs, or simply inherited from their structure, such as the spatial patterning of light on the retina (O'Keefe and Nadel, 1978). In the context of hippocampal function, the Kantian view suggests that fixed spatial representations exist and that, upon exposure to a novel environment, sensory inputs simply select from a set of possible preconfigured modes of network dynamics. The Lockean view suggests instead that no such preconfigured representations exist, and that arbitrary spatial representations may be constructed de novo based on sensory experience.

General theories of hippocampal function

Today, the debate over the functional role of the hippocampus continues. A large body of work demonstrates that neurons in the rodent hippocampus convey both spatial and nonspatial information (Hampson et al., 1999; Allen et al., 2012; Cohen et al., 2013). Recently, evidence has emerged which implicates the hippocampus in the representation of elapsed time (MacDonald et al., 2011; Mankin et al., 2012). Several proposals to unify various aspects of the memory-related, spatial and temporal functions of the hippocampus have been made, drawing upon similarities between these apparently disparate functions at a more fundamental level.

In order to unify the spatial view of hippocampal function with the representation of time, it has been proposed that these phenomena are manifestations of a more general

mathematical computation, the Laplace transform, which the hippocampus performs on its inputs in order to generate an integrated representation of spatiotemporal context (Howard et al., 2014). In addition to this unification of the temporal and spatial processing roles of the hippocampus, proposals have been made to unify the spatial and memory-related functions. For example, memory may be viewed as navigation in mental space, or mental time travel (Buzsáki and Moser, 2013). Alternatively, the structure of physical space may share commonalities with the structure of a more abstract space of overlapping memories, such that relational networks of memories organised in terms of similarity or common features may be subserved by the same neural architectures that encode the relational structure of objects in physical space, organised according to relative location (Eichenbaum, 2004). As such, it has been proposed that the hippocampus generates a "memory space" (Eichenbaum et al., 1999).

Several studies support a role for the hippocampus in the processing of relational properties of objects, events and stimuli in various settings, both in rodents and higher primates (Dusek and Eichenbaum, 1997; Kumaran and Maguire, 2005). For example, the hippocampus is known to be essential for transitive inference (Heckers et al., 2004; Zalesak and Heckers, 2009), a cognitive function in which the ordering of two stimuli (for example, in terms of value) is inferred based on knowledge of their individual orderings relative to a third stimulus (i.e., $A > B$, $B > C$, therefore $A > C$). Such a transitivity property is fundamental to space, time, and therefore presumably also the relational memory networks proposed by Eichenbaum and colleagues (which are hypothesised to have an analogous structure to a spatial map). Hence, while the precise function of the hippocampus remains unknown, the organisation of information into abstract, structured spaces of interrelated elements appears to be a fundamental and unifying feature of hippocampal processing.

1.2 Anatomy of the hippocampus

The hippocampus is a three-dimensional subcortical structure located within the medial temporal lobe (Amaral and Witter, 1989). The hippocampus is divided into several histologically and functionally distinct subregions, including four cornu Ammonis subfields (CA1-CA4), the dentate gyrus and subiculum (Figure 1.1). The hippocampus also borders on the entorhinal cortex, which is both a major source of input to and a major recipient of output projections from the hippocampus. These subfields differ in terms of their internal synaptic connectivity as well as their interconnectivity to other

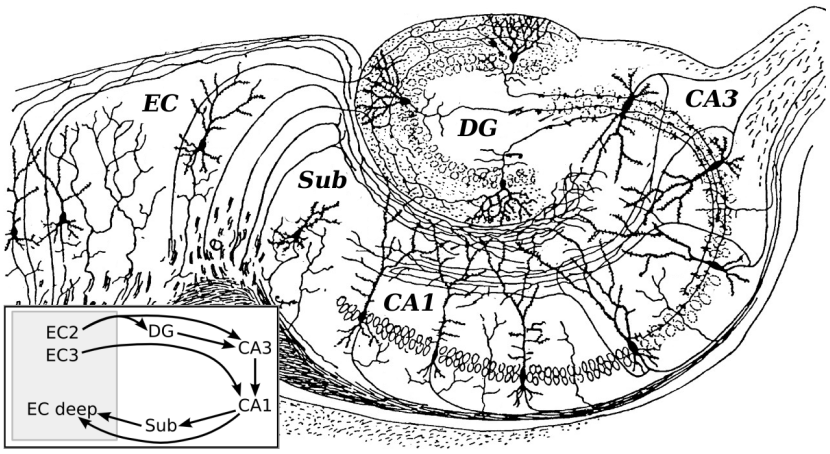

Figure 1.1: Anatomicalrganisation of the hippocampus, showing the entorhinal cortex (EC), subiculum (Sub), dentate gyrus (DG) and subfields CA1 and CA3. Modified figure from Ramon y Cajal (1911).

subfields and external brain areas (Anderson et al., 2007).

In a canonical view of hippocampal function, information enters the hippocampus primarily via the entrorhinal cortex, which projects to regions CA3, CA1 and dentate gyrus (Figure 1.1, inset). Dentate gyrus provides further inputs to CA3 which in turn provides further inputs to CA1, which finally projects back to entrorhinal cortex (Anderson et al., 2007). In addition to the canonical processing loop described above, however, the hippocampus forms reciprocal loops with a multitude of other brain areas such as amygdala (Pitkänen et al., 2000), prefrontal cortex (Thierry et al., 2000), striatum, ventral tegmental area (Floresco et al., 2001; Lisman and Grace, 2005; Luo et al., 2011) and medial septum (Freund and Antal, 1988; Tóth et al., 1993). Further to the division of the hippocampus into histologically distinct subfields, the hippocampus extends spatially across an anatomically defined axis known variously as the dorsoventral, septotemporal or longitudinal axis (Amaral and Witter, 1989).

Distinct subfields of the hippocampus have markedly different cellular and circuit properties. In the CA3 region of the hippocampus, extensive recurrent collaterals between pyramidal cells are hypothesised to underlie associative memory dynamics such as pattern completion (Le Duigou et al., 2014). In the CA1 region, however, there is a dearth of excitatory synapses between pyramidal cells (Anderson et al., 2007). These differences in anatomical structure are often taken to imply distinct functional roles for each subregion in pattern completion and pattern separation for the storage and retrieval of memories (Marr, 1971), and indeed differential coding properties and dynamics are often observed (e.g., Leutgeb et al., 2004).

1.3 Global activity states of the hippocampus

Activity within the hippocampus can be divided into two distinct states, each of which is associated with a different behavioural state (Vanderwolf, 1969). During periods of slow-wave sleep, rest, or immobility, the hippocampus generally enters a state known as large irregular activity (LIA). Within this background state, extracellular recordings of the local field potential (LFP) exhibit occasional large amplitude deflections termed sharp waves, followed by high frequency oscillations termed ripples (around 200 Hz, Buzsáki et al. (1992)). These events are known as sharp wave ripples (SWR). During rapid eye movement (REM) sleep, locomotion, and other active behaviours, the hippocampus enters the theta state (Buzsáki, 2002). This state is characterised by prominent oscillations in the 8-12 Hz range of the LFP, with faster gamma oscillations nested within each theta cycle (Bragin et al., 1995; Lisman and Jensen, 2013). In addition to theta and LIA states, a small irregular activity state has been proposed, which occurs during small movements and is associated with a reduced amplitude and frequency of irregular activity (Vanderwolf, 1969).

Local field potentials are believed to reflect the collective synchronisation of neuronal populations at the mesoscopic scale (Buzsáki et al., 2012). Accordingly, activity at the single neuron and neuronal circuit levels exhibit distinct dynamics in SWR events and theta states (Klausberger et al., 2003). During theta states, hippocampal neurons are rhythmically active at theta frequency, with subtype- and subregion-specific modulation depths and phase preferences (Mizuseki et al., 2009). Similarly, neurons are generally phase-locked to ripple oscillations during SWR events (Csicsvari et al., 2000; Le Van Quyen et al., 2008). During theta states neuronal activity is relatively sparse and asynchronous, whereas during SWR events activity is highly synchronous (Mizuseki and Buzsaki, 2014).

Theta oscillations and SWR events arise through distinct mechanisms. It is generally believed that SWR events emerge due to a combination of neocortical inputs (Sirota et al., 2003) and intrinsic hippocampal dynamics, including synchronous discharge from pyramidal cells in CA3 (Buzsáki et al., 1992) and recurrent inhibitory circuits in CA1 which generate a high frequency ripple oscillation (Schlingloff et al., 2014). The mechanisms of theta oscillations are manifold (Buzsáki, 2002), including intrinsic biophysical rhythmicity at the cellular level (Leung and Yu, 1998), rhythmicity at the level of large-scale neuronal circuits (Stark et al., 2013) and external drive at theta frequency (Bland and Bland, 1986; Stewart and Fox, 1990).

A major generator of hippocampal theta oscillations is the medial septum. In particular, the medial septum is known to send GABAergic projections which target hippocampal interneurons and entrain theta frequency oscillations (Freund and Antal, 1988). In addition to these septohippocampal projections, hippocamposeptal projections form a reciprocal processing loop (Tóth et al., 1993), which has been suggested to be a requirement for theta rhythmogenesis (Wang, 2002). Medial septal theta activity has been shown to lead hippocampal theta oscillations, consistent with its role as a generator rather than inheritor of theta activity (Hangya et al., 2009). Surgical or pharmacological lesions of the medial septum abolish hippocampal theta oscillations in vivo (Petsche et al., 1962; Brandon et al., 2011; Wang et al., 2015). However, theta oscillations can emerge in vitro in an intact hippocampal preparation, despite the absence of septal inputs (Goutagny et al., 2009).

These distinct states of hippocampal activity form the basis of a widely influential view of hippocampal function, termed the two-stage model of memory formation (Buzsaki, 1989). According to this model, experiences are first stored via synaptic plasticity during theta oscillations, while the animal actively explores an environment. During subsequent SWR events as an animal sleeps or rests, experiences are further consolidated into long term memories through interactions between cortex and hippocampus in order to establish stable and permanent cortical representations of experienced events, which may eventually become hippocampus-independent.

1.4 Spatial coding during theta states

Phase precession

During navigation, pyramidal cells in the rodent hippocampus fire action potentials in a limited region of space called their place field (O'Keefe and Dostrovsky, 1971). However, the firing patterns generated by these cells as the animal travels through the place field are also modulated by the theta rhythm. Place cells tend to fire in bursts of spikes within the place field, with a single burst occurring within each cycle of the theta rhythm. In a seminal study, O'Keefe and colleagues asked whether these bursts occur at a fixed phase of the theta cycle, or whether the phase of spiking shifts depending on some spatial or behavioural factors. By plotting the phase at which spikes occur against the location of the animal when the spike occurred, they found that the spikes shift systematically in phase against the LFP theta rhythm as the animal crosses the

place field (Figure 1.2), a phenomenon they termed *phase precession* (O'Keefe and Recce, 1993).

While place cells generally show an increase and then decrease in firing rate and the animal crosses the place field, the firing phase precesses continuously, starting around the peak of the LFP at place field entry and shifting through around 180 - 360 degrees of extracellular theta before place field exit (Schmidt et al., 2009). By breaking the symmetry of the rate code, phase precession provides information about the location of the animal which cannot be extracted from firing rate alone, such as whether the animal has just entered or is about to exit the place field. These observations have therefore been interpreted as evidence for a temporal coding scheme in individual place cells, which both enhances and disambiguates the spatial information contained within the firing rate code. Indeed, it was later shown directly that phase precession increases the spatial information contained within the firing pattern of a place cell (Jensen and Lisman, 2000).

Importantly, spike phase within the place field correlates best with the animal's location, rather than other variables such as the time since the animal entered the place field (Huxter et al., 2003) (Figure 1.2d, e). This occurs despite the fact that the animal may travel through the place field at different speeds on different laps, suggesting that the dynamics of phase precession are configured so as to maintain a stable relationship between spike phase and spatial location across variable behavioural conditions. Later studies confirmed this hypothesis directly, demonstrating that the intrinsic theta frequency of cells in CA1 vary with the running speed of the animal, allowing spike phase to precess more slowly or rapidly in order to maintain a robust phase-position relationship in the face of changing running speeds (Geisler et al., 2007). For these reasons, phase precession is widely viewed as a canonical example of temporal coding within the nervous system, not least because it occurs far from sensory inputs against a temporal reference frame which is internally constructed rather than inherited from external events.

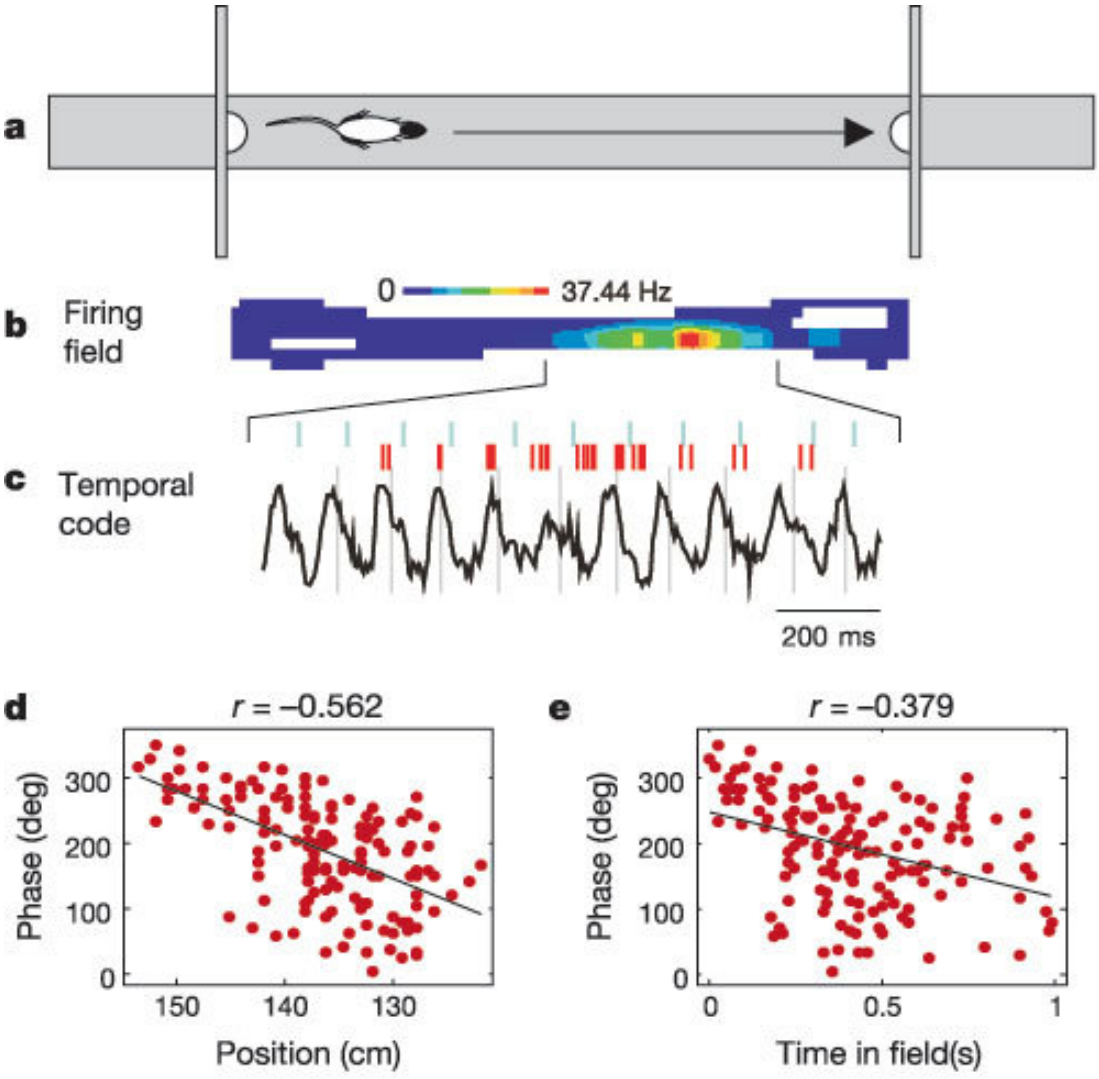

Figure 1.2: Phase precession in place cells. (a) An animal runs from left to right along a linear track. (b) An individual place cell fires in a particular region of the track (the place field). (c) When plotting the spikes on a single lap through the place field against the simultaneously recorded LFP theta oscillation, spikes are seen to shift backwards in phase as the animal crosses the place field. (d) When plotting the pooled set of spike phases over all laps against the position of the animal at the time of the spike, a strong correlation is observed. (e) When plotting the pooled set of spike phases against the time since the animal entered the place field, a weaker correlation is observed. Figure taken from Huxter et al. (2003).

Theta sequences

While the interpretation of phase precession as a single cell temporal coding scheme continues to be viewed by many as attractive, evidence for an alternative interpretation emerged early on from the study of timing relationships between pairs of cells displaying phase precession. Specifically, it was observed that pairs of phase precessing place cells with overlapping place fields tend to be active in a particular temporal order during theta cycles, and that this ordering reflects the ordering of their place fields in physical space (Skaggs et al., 1996). Moreover, it was found that the temporal lag between place cells within theta cycles reflects the distance between their place field centres in physical space.

Thus, phase precession was shown to compress the pairwise ordering of place cells along a behavioural route into a faster ordering within theta cycles, generating a nested representation at behavioural and theta timescales of the ordering at which places were visited. It was therefore proposed that the function of phase precession may be to bridge the gap in timescales between behavioural events and the faster timescales at which neuronal processes such as synaptic plasticity and synaptic integration occur, facilitating the storage and neuronal decoding of extended behavioural events (Skaggs et al., 1996). Such an interpretation suggests that the functional role of phase precession pertains to the dynamics of neuronal populations rather than individual cells.

As technologies for monitoring the activity of large scale neuronal ensembles during behaviour have progressed, further evidence has emerged regarding the coordination of neuronal activity during theta cycles. By recording from groups of place cells coactive within theta cycles, the results of Skaggs and colleagues regarding the theta-ordering of place cell pairs were extended to multi-neuron spike patterns within theta cycles (Dragoi and Buzsáki, 2006; Foster and Wilson, 2007). As expected from the results of Skaggs and colleagues, it was found that groups of place cells fire in sequence within theta cycles, and that the ordering of place cells within a theta sequence reflects the ordering of their place fields on a linear track. However, an unexpected finding of these studies was that the timing relationships present in multi-neuron spike sequences appeared to be more precise and well-organised than would be expected based on the phase precession of each individual cell alone, suggesting some form of additional coordination within the circuit.

Following the discovery of these theta sequences, a shift in the interpretation of phase precession as a spatial coding scheme began to emerge. Whereas studies of

single unit phase precession had assumed that the spike phase provides a temporal code through which the animal's precise location within the place field can be deduced, studies of theta sequences began to view place cell population activity as representing spatial trajectories within theta cycles. Specifically, these studies viewed each place cell as representing only a single location regardless of spike phase, which is generally not the current location of the animal, allowing different cells within a theta cycle to represent locations ahead or behind the animal. Such a view constitutes a fundamental shift in perspective of the information conveyed by the spiking of place cells within theta cycles - in the first view, a population of phase precessing place cells active within a theta cycle would simply represent the animal's instantaneous location at high resolution (Jensen and Lisman, 2000), while in the second view the population of place cells represents an extended trajectory spanning around one metre of physical space (e.g., Gupta et al., 2012).

By decoding the spatial trajectories represented by place cell populations within theta cycles according to the second view, subsequent studies attempted to probe the spatial representations active at theta timescales. By pooling data from many laps across a linear track, Maurer and colleagues were amongst the first to demonstrate that such spatial representations are not fixed, but may vary depending on behavioural conditions (Maurer et al., 2011). They found that the running speed of the animal modulates the length of trajectory generated within a population of place cells, with greater running speeds generating longer spatial trajectories. Shortly thereafter, Gupta and colleagues performed the first single cycle analysis of theta sequences. Using Bayesian decoding algorithms, they found that theta sequences appear to represent salient segments of the environment, such as the region of space between two landmarks, and that decoded trajectories can shift to represent locations further ahead or behind the animal as the animal approached or departed from a landmark (Gupta et al., 2012).

These discoveries gave rise a fundamental shift in thinking regarding the circuit operations underlying phase precession and theta sequences. Rather than viewing phase precession as a cellular coding scheme which generates population sequences, the sequential organisation of neuronal activity began to be viewed as fundamental to hippocampal function (Lisman and Redish, 2009; Wikenheiser and Redish, 2015). In this view, phase precession is an epiphenomenon reflecting a limited sampling of a network-wide pattern of sequentially organised ensemble activity, which arises due to an intrinsic functional organisation of the circuit. More recently, it has been suggested that not only phase precession, but also place fields themselves may emerge from this

sequential organisation of hippocampal activity dynamics (Aghajan et al., 2015; Wang et al., 2015).

1.5 Spatial coding during sharp wave-ripples

Following the discovery of sequential activity patterns representing spatial trajectories during theta cycles, the nature of the activity patterns occurring within high frequency oscillations during sharp wave-ripples was investigated. By analysing the population spiking activity patterns during sharp wave-ripple events, it was demonstrated that neurons fire in sequence during ripples (Lee and Wilson, 2002). These sequences replay experienced events in either forwards or reversed order (Foster and Wilson, 2006; Diba and Buzsáki, 2007). This phenomenon is observed both during slow wave sleep (Diba and Buzsáki, 2007) and during awake immobility (Foster and Wilson, 2006). Decoding of these sequences during awake immobility demonstrated that, unlike theta sequences, SWR sequences represent trajectories through locations distant from the animal (Davidson et al., 2009) and even in entirely different environments (Karlsson and Frank, 2009).

The content of SWR sequences often reflects recent experiences. Such SWR sequences are therefore thought to consolidate experienced events by repetitively replaying experienced episodes in order to establish stable cortical representations for long term memory. However, SWR sequences have also been implicated in the planning of routes through space, leading to a hypothesised role in decision making (Johnson and Redish, 2007; Singer et al., 2013). The functional role of SWR activity for learning in a decision making task has been causally established by selectively disrupting SWRs as an animal learns the structure of a novel task (Jadhav et al., 2012) or during post-training consolidation (Girardeau et al., 2009).

In addition to replaying experienced events and constructing trajectories in decision making tasks, SWR sequences have been observed to show a third spatial correlate called preplay. By analysing the sequential structure of SWR activity during slow wave sleep in naive animals who had never before been exposed to a linear track, and subsequently comparing these sequences to the activity maps generated for de novo runs on linear tracks, Dragoi and colleagues demonstrated that SWR sequences can predict the structure of spatial maps in subsequent experience (Dragoi and Tonegawa, 2011, 2013b). These findings were interpreted as evidence for an innate, preconfigured organisation of hippocampal place maps out of which novel spatial experiences are

constructed, in contrast to the alternative possibility of a truly de novo experience created on a "blank slate" or tabula rasa. In line with O'Keefe's earlier proposal, the observation that novel spatial representations utilise existing network dynamics was seen to support the Kantian view of space (Dragoi and Tonegawa, 2014).

1.6 Coding across the dorsoventral axis

The observations and theories discussed above are largely a product of experimental investigations into the dorsal region of the CA1 subfield of the hippocampus, where the majority of large-scale recordings of neuronal ensembles are carried out. However, the hippocampus is a spatially extended structure, and its properties vary according to anatomical location. Across the dorsoventral axis of the CA1 region of the hippocampus, a systematic shift in coding properties occurs. On the one hand, the size of place fields increases from dorsal to ventral locations from < 1 metre at the dorsal pole to ~ 10 metres at the ventral pole (Kjelstrup et al., 2008). In line with this change in place field size, there is a commensurate change in phase precession slope. At the same time, the information carried by place cells varies across this axis, with highly spatial representations occurring at the dorsal pole and more complex, conjunctive representations combining spatial and emotional variables such as fear and anxiety occurring at the ventral pole (Kjelstrup et al., 2002; Bannerman et al., 2003).

In addition to changes in spatial representations across the dorsoventral axis, there is a gradient in theta dynamics. Measurements of LFP and single unit activity at different dorsoventral locations show a gradient in LFP theta phase (Lubenov and Siapas, 2009; Patel et al., 2012). From the dorsal pole to the ventral pole, theta phase shifts monotonically through around 180 degrees (Patel et al., 2012). Rather than acting as a coherent, global unit, the hippocampus therefore generates theta waves which travel along the dorsoventral axis. As local neuronal populations lock to their local theta rhythm rather than a global rhythm (Patel et al., 2012), neuronal spiking activity also travels along this axis during theta cycles. The functions and mechanisms of this travelling wave, and how these relate to gradients in place field size, precession frequency and spatial information, are largely unclear.

1.7 Mechanisms of phase precession and theta sequences

Understanding the cellular and circuit mechanisms of theta dynamics in the hippocampus has been a major challenge and the focus of considerable research effort. Several theories of the mechanisms underlying phase precession and sequences have been proposed. O'Keefe and colleagues originally proposed a simple mechanism which they termed the oscillatory interference model in order to simultaneously explain the place field of the cell and the precession of spiking activity across this place field (O'Keefe and Recce, 1993). The oscillatory interference model proposes that place cells receive two oscillatory inputs at nearby frequencies. When two such oscillations are summed, the resulting signal generates "beat frequencies", which consist of an oscillation at a frequency midway between that of the two individual oscillators, with a periodic amplitude modulation at a much slower frequency than the individual oscillators. O'Keefe proposed that place cells receive one input at LFP theta frequency and one input at a slightly higher frequency, causing the cell to oscillate at a frequency higher than the LFP theta (and hence precess in phase). The slower modulatory beat frequency then generates the place field. To avoid periodically repeating place fields, O'Keefe proposed that an additional mechanism is in place to silence the place cell outside of the place field. By varying the frequency of the faster oscillator with the running speed of the animal, it is then possible to vary the precession frequency of the cell in order to maintain a fixed relationship between spike phase and the animal's location. Hence, a fundamental prerequisite for the oscillatory interference model is the existence of velocity-controlled oscillators which provide inputs to hippocampal place cells.

Following the discovery that phase precession compresses behavioural sequences into faster sequences within theta cycles, a circuit mechanism was proposed based directly the sequential ordering of place cell activity (Tsodyks et al., 1996). In this model, asymmetric synaptic connectivity between place cells generates a sequence of spiking activity which propagates synaptically through a population of place cells. Due to the presence of feedback inhibition and an oscillatory theta drive to the network, these sequences of excitation are eventually overcome by inhibition towards the end of the theta cycle, causing them to collapse before a new sequence begins at the start of the next cycle. Due to the presence of a place field drive to specific subpopulations of cells depending on the location of the animal, sequences begin with place cells representing locations behind the animal and sweep forward to locations ahead of the animal before collapsing and reinitiating again behind the animal. Phase precession

in each place cell emerges as a consequence of these network-level activity dynamics. As such a model relies on excitatory synaptic connectivity between place cells, it is not consistent with the architecture of CA1, but can account for phase precession in upstream CA3 which could then be inherited in CA1 through phase precessing synaptic inputs. The possibility of inheritance of phase precession has since been analysed in detail (Jaramillo et al., 2014).

Based on observations of an experience dependent, asymmetric expansion of place fields during learning of a novel environment, an alternative explanation of single cell phase precession has been proposed (Mehta et al., 2002). Specifically, it was hypothesised that place cells receive an oscillatory theta input as well as an asymmetric ramp-like input over the place field. As the animal crosses the place field, the increasing amplitude of the ramp input causes spikes to occur at an earlier phase of the oscillatory input, generating precession through up to 180 degrees. While this model cannot account for 360 degrees of phase precession, it was argued that phase precession is generally bimodal in experimental data, displaying relatively robust phase precession through the first 180 degrees before becoming noisier and less selective towards the end of the place field.

While Mehta and colleagues proposed an asymmetric firing rate field in order to explain phase precession, a mechanism using symmetric firing rate fields combined with spike train adaptation has also been proposed in order to generate a monotonic shift in firing phase across the place field. Harris and colleagues suggested that the phase precession dynamics of place cells might not be dependent on the location of the animal in the place field per se, but may instead depend on the firing rate dynamics of the cell regardless of the spatial context (Harris et al., 2002). They proposed that spike train adaptation occurs in place cells, so that changes in dynamics over the place field can break the firing rate symmetry in order to continue to precess over the second half of the firing rate field. However, the close relationship between firing rate and phase observed by Harris and colleagues was called into question by another study which found that firing rate varies independently of firing phase in order to encode the running speed of the animal (Huxter et al., 2003).

Based on experimental observations showing that the inputs to CA1 arriving from CA3 and the medial entorhinal cortex occur at different phases of the theta cycle (Mizuseki et al., 2009), a model was proposed based on the interference of oscillators at the same frequency but with different phases and amplitudes (Chance, 2012). In this model, it is assumed that the temporal profile of inputs to CA1 arriving from CA3

and entorhinal cortex take the form of a Gaussian envelope modulated by the theta oscillation. However, the two inputs have a phase offset in their theta component and a temporal (or equivalently spatial) offset in their Gaussian envelopes. By correctly configuring these offsets, the summation of these two inputs generates phase precession across the place field of the CA1 cell.

Most recently, the model of Tsodyks et al. (1996) has been modified to include synaptic facilitation and depression (Wang et al., 2015). In this model, sequences are again generated by asymmetric excitatory synaptic connections, but the slow rate coded firing fields can emerge due to the intrinsic synaptic dynamics of the circuit, without spatially structured external drive to the network. In particular, short term synaptic modification leaves a synaptic footprint within the network, such that after the collapse of a theta sequence, the new theta sequence will naturally reinitiate at the correct location and the slow firing rate fields can stably propagate forward through the network. In this model, external input can calibrate and stabilise rate coded firing fields in order to anchor them to sensory cues and spatial locations, but these firing field activity patterns will nevertheless persist in the network when these external drives are removed.

Despite this abundance of models for phase precession and theta sequences, however, the cellular and circuit mechanisms remain obscure. While many features of phase precession can be explained in isolation within a given model, several features of phase precession have proven difficult to explain in combination and by any one particular model - for example, the change in precession frequency with running speed and ability to generate phase precession along arbitrary two-dimensional trajectories (Geisler et al., 2007; Huxter et al., 2008). Moreover, the relationship between phase precession, theta sequences and firing rate fields remains unknown. Whether sequences arise through the compression of place field activity generated by phase precession across a place field (Skaggs et al., 1996), or whether phase precession and place fields emerge through the anchoring of intrinsically organised sequential activity to landmarks and other sensory cues (Wang et al., 2015; Aghajan et al., 2015) remains to be determined.

1.8 Functions and mechanisms of grid cells

While it was the discovery of place cells which prompted O'Keefe's original cognitive map hypothesis, namely that the dynamics of place cell ensembles generates a spatial

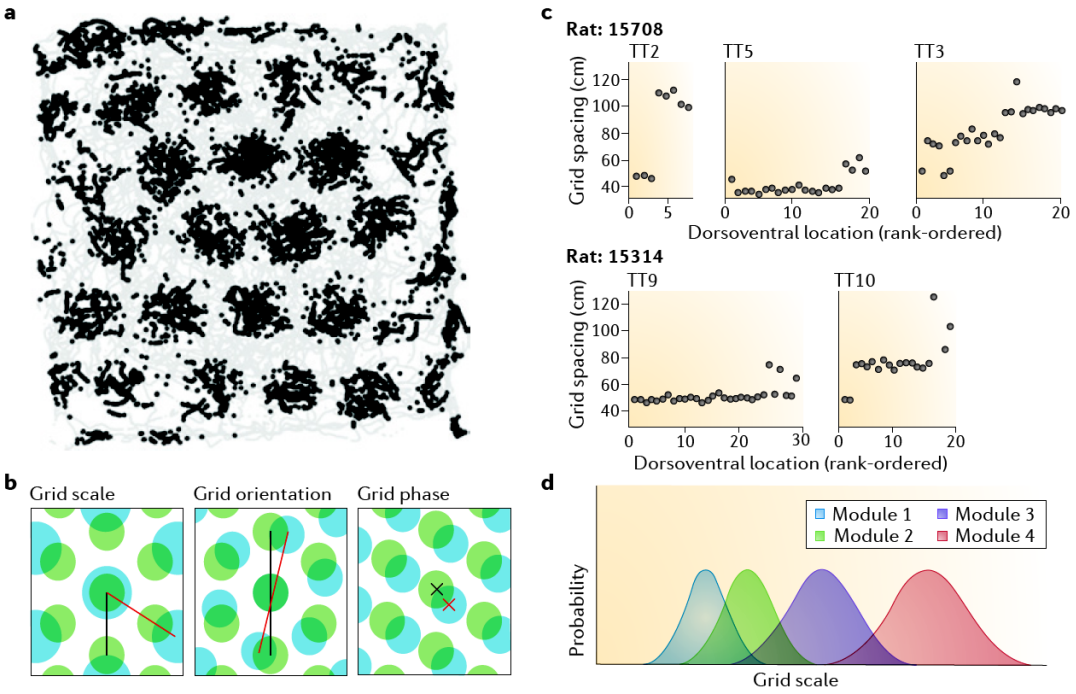

Figure 1.3: Spatial coding in grid cells. (a) Spiking activity of a single grid cell as an animal explores a square arena. The animal's trajectory over a long period of time is shown as a grey line, and the locations where spikes occurred are illustrated with black dots. (b) Illustration of spatial scale, orientation and phase of grid cells. (c) Discrete changes in grid scale along the dorsoventral axis of the medial entorhinal cortex. (d) A schematic of the modular organisation of grid cell representation over the dorsoventral axis. Figure taken from Moser et al. (2014).

map based on which an animal can localise itself in space and calculate routes towards desired objects and locations, later discoveries revealed the existence of various other cell types whose activity provides spatial information, suggesting a broader neural system which comprises the cognitive map. Perhaps most strikingly, the discovery of grid cells in the medial entorhinal cortex revealed the existence of a cell type with highly precise, metric-like firing rate properties which appear well suited perform to spatial calculations such as path-integration (Hafting et al., 2005). The defining property of grid cells is an activity map which tessellates physical space with triangular firing rate fields, the so-called grid (Figure 1.3a). When measuring from a population of grid cells, individual cells exhibit a variety of grid orientations, spatial scales and spatial phases (Figure 1.3b). However, these properties do not vary randomly amongst grid cells, but are instead organised into discrete modules (Figure 1.3c, d), which share a common spatial scale and orientation but a full spectrum of spatial phases (Stensola

et al., 2012).

Due the highly organised and geometrical properties of grid cells, they have been suggested to be an ideal candidate for path integration (McNaughton et al., 2006). An apparent drawback to the use of grid cells for spatial coding, however, is their periodicity. The firing rate of an individual grid cell is highly non-unique, due to the translational symmetry of its activity map over space. However, detailed mathematical analysis has shown that the modular organisation of grid cells into subsets at different spatial scales allows a highly informative population code in which location can be extracted with exponential resolution in the number of grid cells, outperforming place cells considerably (Sreenivasan and Fiete, 2011; Mathis et al., 2012).

Similarly to place cells, grid cells also show phase precession (Hafting et al., 2008). Moreover, phase precession in grid cells persists even in the absence of hippocampal inputs. Firing phase precesses over each individual grid firing field, much like phase precession across a place field. As an animal travels through multiple successive grid fields, precession over each field appears to be independent of the previous and subsequent fields, suggesting that a grid cell's intrinsic theta activity may be reset between fields (Reifenstein et al., 2012).

In order to explain the firing fields and phase precession of grid cells, the oscillatory interference model has been extended to account for grid cells (Burgess et al., 2007). On a linear track, the oscillatory interference model already accounts for these properties, due the natural oscillatory nature of the interference pattern which generates slow amplitude oscillations (which had previously been removed to account for the unimodal firing fields of place cells). In open environments, however, the tessellated firing rate fields of grid cells require a more complex interference of oscillators. To account for two dimensional grid cell activity, the oscillatory interference model was therefore extended to include six (or more) velocity controlled oscillators which integrate self-motion over different symmetry axes of the triangular grid map (Burgess, 2008). Support for the oscillatory interference model comes from experimental data showing a disruption of grid cell firing fields following manipulations which reduce the power of theta oscillations in the network (Koenig et al., 2011). However, evidence from bats challenges these findings by demonstrating a robust grid cell maps in the absence of theta oscillations (Yartsev et al., 2011).

A second hypothesised mechanism postulates that grid cell activity patterns form through attractor dynamics in networks of grid cells. In networks with geometrically organised synaptic weights, self-sustaining bump-like network activity profiles can be

achieved. These networks can be organised such that multiple equally spaced bumps occur, which tessellate the network with a grid-like activity pattern (Fuhs and Touretzky, 2006). Alternatively, if the network has a closed topology with periodic boundary conditions, a single activity bump can emerge which generates a grid cell firing rate map in physical space (Guanella et al., 2007; Pastoll et al., 2013). External current inputs to the network can move the activity bump(s) through the network at a speed which depends on the current amplitude. Hence, by including input currents which vary with the running speed of the animal, an attractor network can perform path integration to keep track of the animal's location in space (Burak and Fiete, 2009). Such attractor models can also be extended to incorporate phase precession (Navratilova et al., 2012), and can also coexist with oscillatory interference mechanisms (Bush and Burgess, 2014).

In addition to the discovery of grid cells, several other spatially selective cell types have been discovered. Head direction cells, which fire selectively for certain head directions of the animal, appear to act as an integrator of angular velocity in order to maintain an internal compass (Taube, 2007). In rodent medial entorhinal cortex, conjunctive cells maintain a joint grid and head direction representation (Sargolini et al., 2006). These conjunctive representations are contingent on theta oscillations within the circuit, such that disruption of theta oscillations abolishes the grid component while leaving the head direction component intact (Brandon et al., 2011). In addition to place, grid, head direction and conjunctive cells, a further cell type termed border cells generates an activity pattern which correlates with the animal's distance from an environmental boundary (Solstad et al., 2008). In combination, the variety of spatially selective cell types in the hippocampus, entorhinal cortex and adjacent structures appears well suited to perform the spatial computations needed to navigate flexibly within complex environments.

1.9 Place field remapping

So far, we have focussed on how the hippocampus represents an animal's location within a single environment. However, when an animal is exposed to multiple distinct environments, or when manipulations of a familiar environment are made, or even under changes in cognitive or behavioural conditions within a fixed environment, the nature of these representations can change dramatically. The process by which hippocampal place field representations change across these conditions is known as

remapping (Colgin et al., 2008).

When an animal is moved from a familiar environment in which a stable place field representation has emerged into a novel environment, a phenomenon known as global remapping occurs. Global remapping is a change in relative spatial locations at which place fields are expressed in a population of cells (Wilson and McNaughton, 1993). Additionally, global remapping selects a different (but partially overlapping) subset of pyramidal cells which are active in the novel environment, with CA3 generally displaying a low degree of overlap between spatial representations and CA1 displaying a higher degree of overlap which varies depending on the similarity between spatial contexts (Leutgeb et al., 2004). Through this remapping procedure, multiple stable spatial representations can be established in order to encode events occurring in different environments (Alme et al., 2014). Remapping between environments appears to be statistically random, with no discernible relationship between the place field map in each environment (e.g., O'Keefe and Conway, 1978; Wilson and McNaughton, 1993).

One explanation for ability to store multiple statistically independent spatial representations within a network of place cells is the multiple charts model (Samsonovich and McNaughton, 1997). This model proposes that maps are stored within the synaptic connections between place cells, which generate activity bumps via attractor mechanisms. The synaptic connectivity patterns associated with each map are superimposed onto the same network. However, as maps are statistically independent, the connections associated with one map would appear as unstructured noise in the spatial frame of the second, and hence interference between multiple stored maps is minimal, allowing the network to switch between stable maps depending on the structure of external inputs.

In addition to this global form of remapping, subtler forms of activity changes can occur when smaller changes are made within an environment, or as other cognitive variables vary within the same environment. This form of remapping is known as rate remapping (Wood et al., 2000; Dupret et al., 2010; Allen et al., 2012). Rate remapping occurs when the firing rate of a place cell changes within the place field, without changes in the place field map. Hence, rate remapping allows additional information to be multiplexed onto spatial representations. Examples of rate and global remapping are shown in Figure 1.4.

In grid cells, remapping is more stereotyped than in place cells. Individual grid cells generally remap by a combination of rotation, scaling, shear and translation of their grid maps (Fyhn et al., 2007). These remappings are coherent between all grid

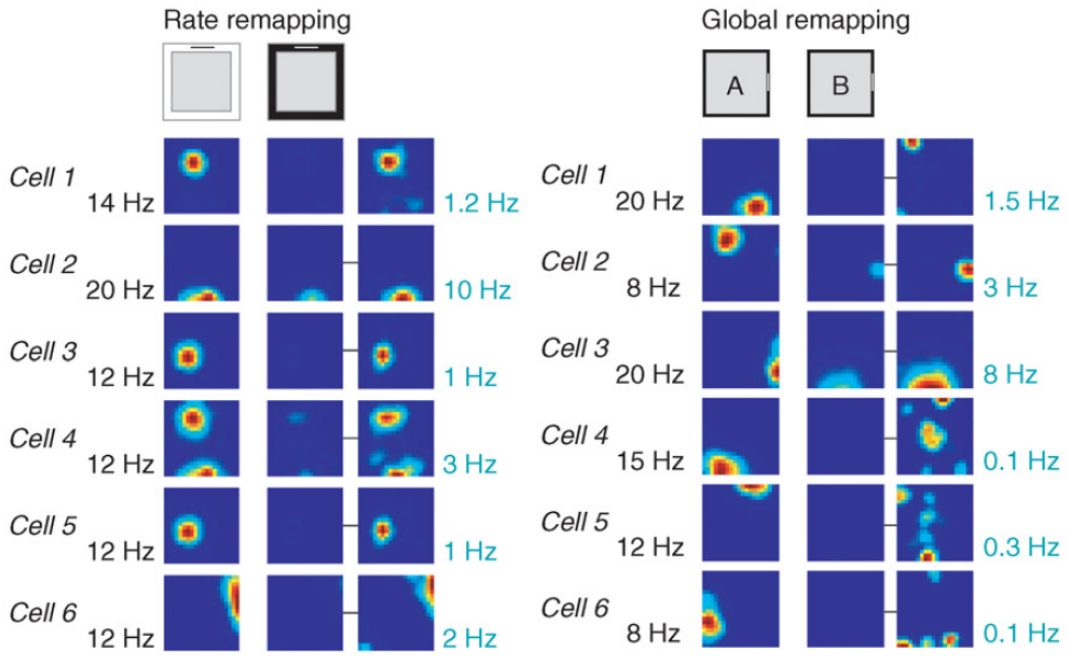

Figure 1.4: Examples of rate remapping and global remapping. Left: Rate remapping when rats were exposed to arenas with different colours but identical spatial configurations. Right: Global remapping when rats were tested in identical arenas in different locations. Figure taken from Colgin et al. (2008)

cells within a module, but may vary randomly between distinct modules (Stensola et al., 2012). Remapping in grid cells predicts whether downstream place cells will exhibit global or rate remapping. Place cell rate remapping is associated with stable grid representations, whereas global remapping is associated with remapping of upstream grid cell maps (Fyhn et al., 2007).

Place field remapping is thought to allow multiple memories to be storied without interference by establishing maximally decorrelated place field representations of different environments and contexts (Colgin et al., 2008). However, the relationship between phase precession, theta sequences and place field remapping has received little attention. How sequential activity patterns can be maintained in multiple spatial maps, and whether interference between sequential dynamics associated with different spatial representations might occur, is not yet clear.

1.10 Thesis overview

This thesis provides an investigation into the phenomenological, mechanistic and functional properties of population activity in the rodent hippocampus during theta oscillations. In Chapter 2, we develop phenomenological models of the activity of place cell populations in the CA1 region of the hippocampus during navigation. We go on to test these models against experimental data, before investigating the relationship between theta sequences and place field remapping in each model. In Chapter 3, we extend these models to account for the properties of grid cells during theta oscillations. We demonstrate that the translational symmetry of grid cell activity maps imposes constraints on theta dynamics which require more complex phenomenological models. In Chapter 4, we propose a biophysical mechanism for phase precession consistent with the architecture of the CA1 circuit. We show that this model can account for many features of phase precession which have proven challenging for previous models. Finally, we propose a functional role for this mechanism in the performance of supervised learning during behaviour.

Chapter 2

Phenomenological Models of CA1 Theta Sequences

2.1 Introduction

Cognitive processes are thought to involve the organisation of neuronal activity into phase sequences, reflecting sequential activation of different cell assemblies (Hebb, 1949; Harris, 2005; Buzsáki, 2010; Wallace and Kerr, 2010; Palm et al., 2014). During navigation, populations of place cells in the CA1 region of the hippocampus generate phase sequences structured around the theta rhythm (e.g., Skaggs et al., 1996; Dragoi and Buzsáki, 2006; Foster and Wilson, 2007). As an animal moves through the firing field of a single CA1 neuron, there is an advance in the phase of its action potentials relative to the extracellular theta cycle (O'Keefe and Recce, 1993). Thus, populations of CA1 neurons active at a particular phase of theta encode the animal's recent, current, or future positions (Figure 2.1A, B). One explanation for these observations is that synaptic output from an active cell assembly ensures its other members are synchronously activated and in addition drives subsequent activation of different assemblies to generate a phase sequence (Figure 2.1C) (Harris, 2005). We refer to this as the *coordinated assembly hypothesis*. An alternative possibility is that independent single cell coding is sufficient to account for population activity. According to this hypothesis, currently active assemblies do not determine the identity of future assemblies (Figure 2.1D). We refer to this as the *independent coding hypothesis*.

Since these coding schemes lead to different views on the nature of the information transferred from hippocampus to neocortex and on the role of CA1 during theta states, it is important to distinguish between them. While considerable experimental evidence

has been suggested to support the coordinated assembly hypothesis (e.g., Harris et al., 2003; Dragoi and Buzsáki, 2006; Foster and Wilson, 2007; Maurer et al., 2011; Gupta et al., 2012), the extent to which complex sequences of activity in large neuronal populations can be accounted for by independent coding is not clear. To address this we developed phenomenological models of independent and coordinated place cell activity during navigation. In the independent coding model, the spiking activity of each cell is generated by rate coding across its place field and phase precession against a fixed theta rhythm. We show that in this model phase coding generates a travelling wave which propagates through the population to form spike sequences. This wave is constrained by a slower moving modulatory envelope which generates spatially localised place fields. In the coordinated assembly model, the spikes generated by each cell are also influenced by the activity of other cells in the population. As a result, population spike patterns are further entrained by population interactions which counter the effects of single cell spike time variability and increase the robustness of theta sequences.

The independent coding hypothesis predicts that a population of independent cells will be sufficient to explain the spatiotemporal dynamics of cell assemblies in CA1. In contrast, the coordinated assembly hypothesis predicts that groups of cells show additional coordination beyond that imposed by a fixed firing rate and phase code (Harris et al., 2003; Harris, 2005). We show that the independent coding model is sufficient to replicate experimental data previously interpreted as evidence for the coordinated assembly hypothesis (Harris et al., 2003; Dragoi and Buzsáki, 2006; Foster and Wilson, 2007; Maurer et al., 2011; Gupta et al., 2012), despite the absence of coordination within or between assemblies. Moreover, novel analyses of experimental data support the hypothesis that place cells in CA1 code independently. Independent coding leads to new and experimentally testable predictions for membrane potential oscillations and place field remapping that distinguish circuit mechanisms underlying theta sequences. In addition we show that, despite the apparent advantage of coordinated coding in generating robust sequential activity patterns, it suffers from an inability to maintain these patterns in a novel environment. Thus, a key advantage of sequence generation through independent coding is to allow flexible global remapping of population activity while maintaining the ability to generate coherent theta sequences in multiple environments.

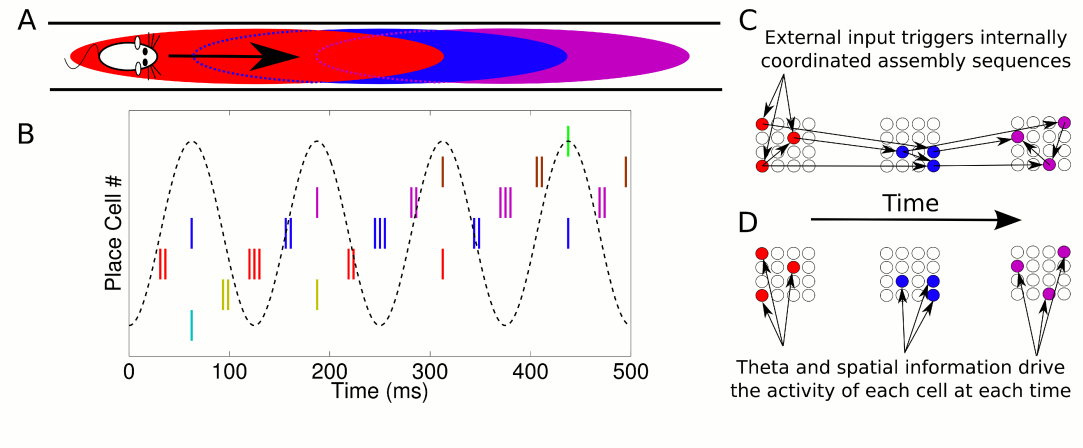

Figure 2.1: **Phase sequences in a place cell population.**
(A) During navigation, place cells are sequentially activated along a route. (B) Within each theta cycle, this slow behavioural sequence of place cell activations is played out on a compressed timescale as a theta sequence. Theta sequences involve both rate and phase modulation of individual cells, but it remains unclear whether additional coordination between cells is present. (C) Internal coordination may bind CA1 cells into assemblies, and sequential assemblies may be chained together synaptically. This would require specific inter- and intra-assembly patterns of synaptic connectivity within the network. (D) Alternatively, according to the independent coding hypothesis, each cell is governed by theta phase precession without additional coordination.

2.2 Single cell coding model

To test the independent coding hypothesis, we developed a phenomenological model which generates activity patterns for place cell populations during navigation. While a phenomenological model of CA1 phase precession has previously been developed (Geisler et al., 2010), several features of this model limit its utility for investigation of coordination across neuronal populations. First, the previous model addresses only the temporal dynamics of single unit activity and population average activity, without addressing the spatiotemporal patterns of spiking activity within the population, the nature of which is a central question in the present study. Second, the previous model assumes coordination between cells in the form of fixed temporal delays and is formulated for a fixed running speed. In contrast, we wish to understand in detail the temporal relationships between cells arising in populations with no direct coordination and how these temporal relationships might depend on factors such as running speed. To this end, we now develop a model of a single cell with a given place field and phase

code and proceed to derive the patterns of population activity under the independent coding hypothesis.

List of parameters and variables used within this thesis.

Parameter /Variable	Description
x_c	Location of firing field centre.
x	Physical location of the animal in space.
$\phi(x)$	Encoded phase - the phase of the local field potential theta oscillation at which a cell will preferentially fire given the animal's location x.
ϕ_0	The encoded fire at place field entry.
$\Delta\phi$	The total phase precessed over the place field.
R	The radius of the place field, quantified via phase precession.
σ	The spatial width of the place field, quantified via firing rate tuning curves.
v	The animal's running speed.
x_s	The animal's location at time $t = 0$.
f_θ	The frequency of the local field potential theta oscillation.
$\theta(t)$	The instantaneous phase of the local field potential theta oscillation.
θ_s	The phase of location field potential theta at time $t = 0$.
t_0	The time of place field entry.
x_0	Location of place field entry (start of place field).
f_ϕ	Rate of phase precession (in cycles of LFP theta per second).
$r_x(x)$	Average firing rate when animal is at location x.
A	Maximum (averaged) firing rate, at centre of place field.
$r_\phi(\phi(x),\theta(t))$	The phasic tuning curve, which modulates instantaneous firing rate as a function of theta phase and location.
k	Phase locking, a measure of the depth of modulation of a cell by the theta rhythm.
$r(t)$	Instantaneous firing rate of a cell.
N_{spikes}	The average number of spikes fired by a cell on a single pass through its place field.
c	The compression factor of the population.
D	The sequence path length of the population.

$\psi(x_c,t)$	The total phase of a cell with place field centre x_c, i.e., the phase of its ongoing intrinsic cellular theta oscillations.
ω	The angular frequency of the cell, i.e., the frequency of ongoing intrinsic cellular theta oscillations.
κ	The wavenumber of the population travelling wave, measured in radians per metre.
ψ_s	The initial phase offset of the population travelling wave.
v_p	The propagation speed of the population travelling wave.
w_{ij}	The total interaction weight from cell j to cell i in the coordinated coding model.
w_E	The magnitude of the excitatory component of the interaction weight.
ℓ	The interaction length of the excitatory component of interactions.
w_I	The magnitude of the inhibitory component of the interaction weight.

Analysis of linear phase coding

Here, we provide a simple mathematical description of the phase and frequency of a place cell firing relative to the LFP theta rhythm as a function of the animal's location, running speed and the place field size. The properties of the cell's firing rate are discussed in the following section. A table containing a list of mathematical variables and parameters used throughout this thesis is provided below.

Consider a place field with centre x_c on a linear track. We define the encoded phase $\phi(x)$ which assigns a firing phase to each location x inside the place field. The encoded phase $\phi(x)$ is defined so that the cell fires spikes which precess linearly in phase against the LFP theta rhythm over the place field (Figure 2.2A, bottom panel). The parameters describing the encoded phase are the firing phase at place field entry ϕ_0, the total phase precessed $\Delta\phi$, and the distance over which this phase is precessed $2R$. The encoded phase is given by:

$$\phi(x) = \phi_0 - \Delta\phi\frac{x - x_c + R}{2R} \tag{2.1}$$

so that the phase of spiking relative to the LFP theta rhythm at place field entry $x_c - R$ is ϕ_0 and at place field exit $x_c + R$ is $\phi_0 - \Delta\phi$ as required. The parameter R therefore determines the spatial range of phase precession, whereas the width of the firing rate field σ is considered separately in the following section.

By considering locomotion along a linear track, we can then analyse how ϕ varies over time. If the rat moves at a constant running speed v, starting from a position x_s at time $t = 0$, and the LFP theta phase advances with a constant frequency f_θ with an initial phase offset θ_s, then:

$$x(t) = x_s + vt \tag{2.2}$$

$$\theta(t) = \theta_s + 2\pi f_\theta t \tag{2.3}$$

$$\phi(t) = \phi_0 - 2\pi f_\phi (t - t_0) \tag{2.4}$$

where $t_0 = (x_0 - x_s)/v$ is the time that the rat reaches location $x_0 = x_c - R$, the start of the place field. Combined with Equation (2.1), this gives the rate of phase precession

$$f_\phi = \frac{\Delta\phi}{2\pi}\frac{v}{2R} \tag{2.5}$$

and provides a complete description of the firing phase of a cell for arbitrary place field locations, running speeds, LFP phase offsets and initial locations on a linear track.

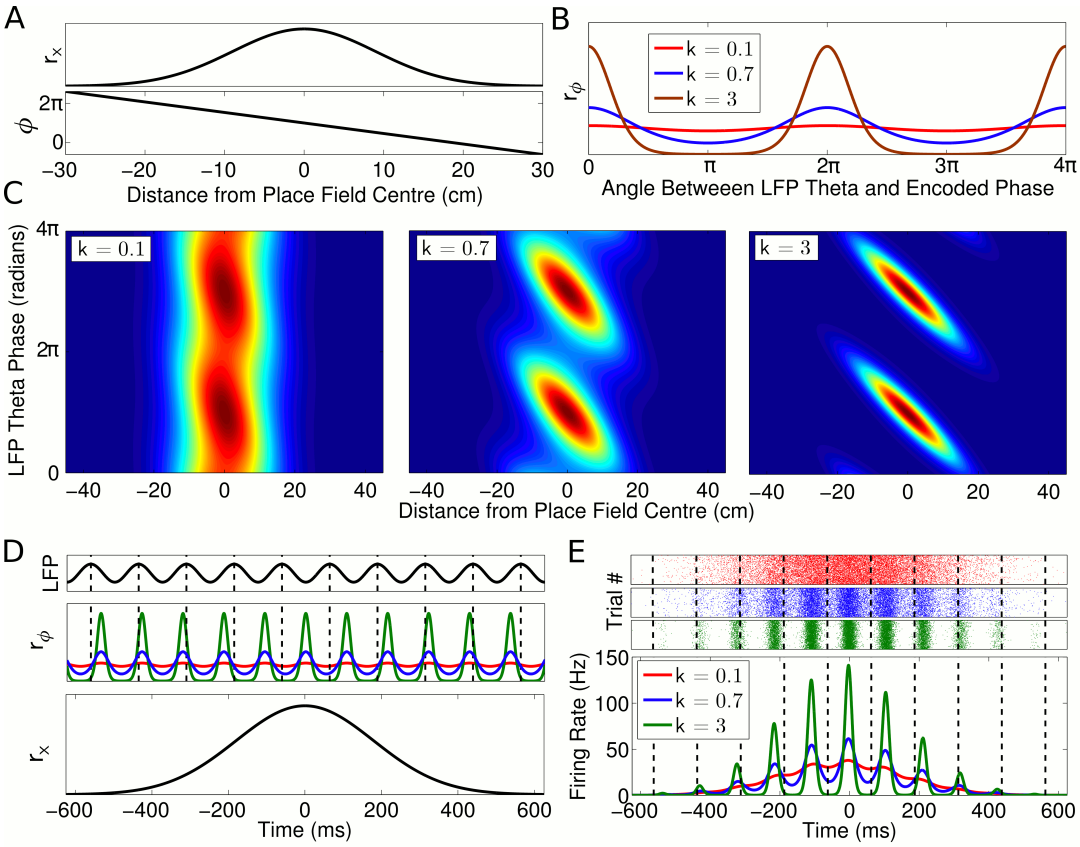

Figure 2.2: **Single cell coding model.**

(A) Firing rate and phase at different locations within a cell's place field are determined by a Gaussian tuning curve r_x and linearly precessing encoded phase ϕ respectively. (B) The dependence of single cell activity on the LFP theta phase θ is modelled by a second tuning curve r_ϕ which depends on the angle between the LFP theta phase θ and encoded phase ϕ at the animal's location. The phase locking parameter k controls the precision of the phase code. (C) The combined dependence of single cell activity on location and LFP theta phase. (D) Temporal evolution of the rate and phase tuning curves for a single cell as a rat passes through the place field at constant speed. (E) The total firing rate corresponding to (D), and spiking activity on 1000 identical runs.

Analysis of dual rate and phase coding

Given the above description of the animal's movement through space together with evolution of the LFP theta oscillation and the resultant change in firing phase in a given cell, we proceeded to model the firing rate in order to arrive at a unified description of the coding properties of an individual place cell during locomotion on a linear track. We modelled the firing rate field for each neuron using a Gaussian tuning curve:

$$r_x(x) = A \exp\left(-\frac{(x-x_c)^2}{2\sigma^2}\right) \tag{2.6}$$

where r_x describes firing rate when the animal is at location x within a place field with centre x_c, width σ and maximum rate A (Figure 2.2A, top panel). Simultaneously, we modelled the firing phase using a circular Gaussian:

$$r_\phi(\phi(x), \theta(t)) = \exp\left(k\cos(\phi(x) - \theta(t))\right) \tag{2.7}$$

where r_ϕ describes the firing probability of the neuron at each theta phase at a given location (Figure 2.2B). The *phase locking* parameter k determines the precision at which the encoded phase is represented in the spike output (Figure 2.2B). The instantaneous firing rate of the cell is given by the product of these two components $r = r_x r_\phi$. The phase locking can be set so that the cell exhibits only rate coding (at $k = 0$, where $r = r_x$), only phase coding (as $k \to \infty$, where all spikes occur at exactly the encoded phase $\phi(x)$) or anywhere in between (Figure 2.2C).

For a constant running speed (Equations (2.2, 2.3, 2.4)), the firing rate for a cell during place field crossing is:

$$r(t) = r_x(x(t)) r_\phi(\phi(x(t)) - \theta(t)) \tag{2.8}$$

$$= A \exp\left(-\frac{(x_s + vt - x_c)^2}{2\sigma^2}\right) \exp\left(k\cos(2\pi(f_\theta + f_\phi)t - \phi_0 + \theta_s - 2\pi f_\phi t_0)\right) \tag{2.9}$$

Figure 2.2E shows the firing rate distribution for different values of k. Note that the phase precessed across the firing rate field depends on the relative values of R and σ. Hence, to model ranges of phase precession other than 2π, we are free to fix $\Delta\phi = 2\pi$ and vary R.

To generate spikes we can use an inhomogeneous Poisson process with an instantaneous rate given by Equation (2.9). In experiments, the number of spikes fired by a place cell is uncorrelated with the running speed of the animal, and is around $10-20$ spikes per pass (Huxter et al., 2003). Hence, using Equation 2.9, the amplitude A can be set such that $\int_{-\infty}^{\infty} r(t)dt = N_{\text{spikes}}$, which normalises the average number of spikes

fired per pass through the place field to N_{spikes} (Figure 2.3). A good approximation to this integral can be obtained by setting r_ϕ to be a constant in order to average out its oscillatory component:

$$\langle r_\phi \rangle = \frac{1}{T}\int_0^T r_\phi(t)dt = I_0(k) \tag{2.10}$$

where $I_0(k)$ is the modified Bessel function of order zero and T is the period of $r_\phi(t)$. Hence, the firing rate of the cell is modulated by running speed as:

$$A(v) \approx \frac{N_{\text{spikes}}}{I_0(k)} \frac{v}{\sqrt{2\pi\sigma^2}} \tag{2.11}$$

This approximation is accurate when the number of oscillatory cycles within the place field is high. For very high running speeds (or small place fields), this approximation will be less accurate.

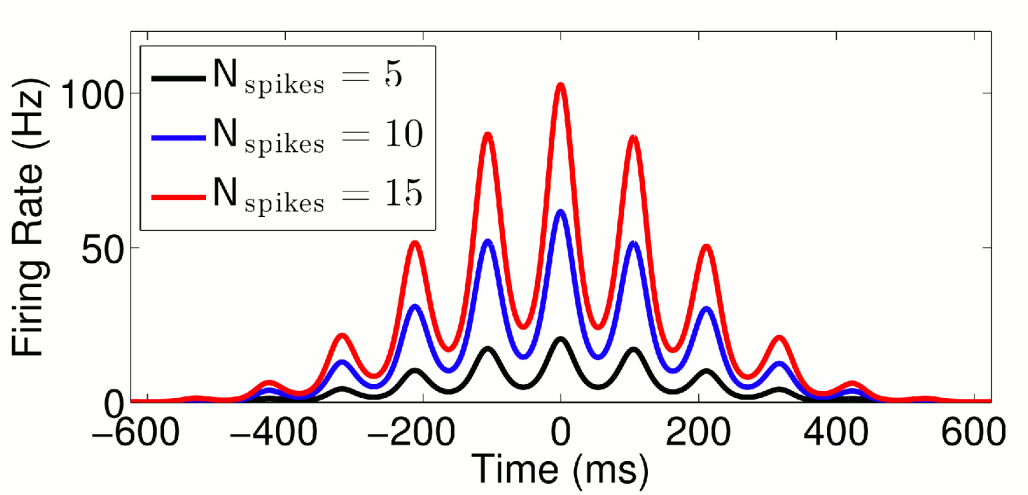

Figure 2.3: **Effect of normalisation factor (N_{spikes}).**
Firing rate vs time for runs with $v = 50$cm/s, $k = 0.7$ and 3 different values of N_{spikes}.

If the phase $\phi(x)$ at each location in the place field is fixed, the full rate and phase coding properties of a cell are encompassed by three independent parameters - the width of the spatial tuning curve σ, the degree of phase locking k and the average number of spikes per pass N_{spikes}. Phase precession (Figure 2.2C) and firing rate modulation as a function of time in this model (Figure 2.2E) closely resemble experimental observations, including the single lap firing rate and theta modulation (e.g., Mizuseki and Buzsaki, 2014) as well as the pooled place field and phase precession structure (e.g., Skaggs et al., 1996). However, as discussed below, experimental data can show properties not accounted for by this simple model, such as asymmetries in place fields and phase precession slopes.

Place cells often show variations in firing rate in response to nonspatial factors relevant to a particular task (e.g., Wood et al., 2000; Griffin et al., 2007; Fyhn et al., 2007; Allen et al., 2012). In our model, such multiplexing of additional rate coded information can be achieved by varying the number of spikes per pass N_{spikes} without interfering with the other parameters $\phi(x)$, σ and k (Figure 2.3).

While we have modelled firing fields using simple, symmetric Gaussian functions and precession using simple linear functions of phase versus position, it is worth noting that experimental recordings often show more complex relationships of firing rate and phase as a function of position. For example, firing fields are often asymmetric (Mehta et al., 2002) and firing phase often varies nonlinearly as a function of location (Skaggs et al., 1996; Mehta et al., 2002). Due to the simplicity of our model, we are able to investigate analytically the properties of spike sequences generated within theta cycles and their spatial coding properties. However, the implications of place field asymmetries and phase precession nonlinearities for theta sequences and the spatial information contained within them is also of interest, and could be investigated through relatively straightforward extensions of the model presented within this chapter.

Single cell coding with trial to trial variability

For completeness, we note here that some studies suggest a more complex single cell coding scheme than that outlined above. In particular, phase precession in single trials may reflect a greater degree of coordination against the theta rhythm than that suggested from the pooled data (Schmidt et al., 2009). The key differences observed in single trials compared to surrogate trials sampled from the pooled data were a higher phase-position correlation and slope and a lower phase range and spatial range. The single cell model we developed above can be extended to incorporate such properties by replacing the fixed phase precession parameters with random variables which vary from trial to trial. For example, a single trial phase offset ϕ_0 sampled from a normal distribution with a variability of $\sigma_{\phi_0} = \pi/2$, together with a fixed phase range of $\Delta\phi = \pi$ on each trial gives a pooled phase range of 2π as well as a lower pooled phase position-correlation, in line with experimental observations.

If, on each trial, each cell samples its parameters from these distributions independently of other cells, the population code will be independent. If instead this trial to trial variability is shared across the population a coordinated population code will result. For simplicity, we will not consider these trial to trial properties of phase pre-

cession in the following analyses.

Sequence properties for independent coding in the high phase locking limit

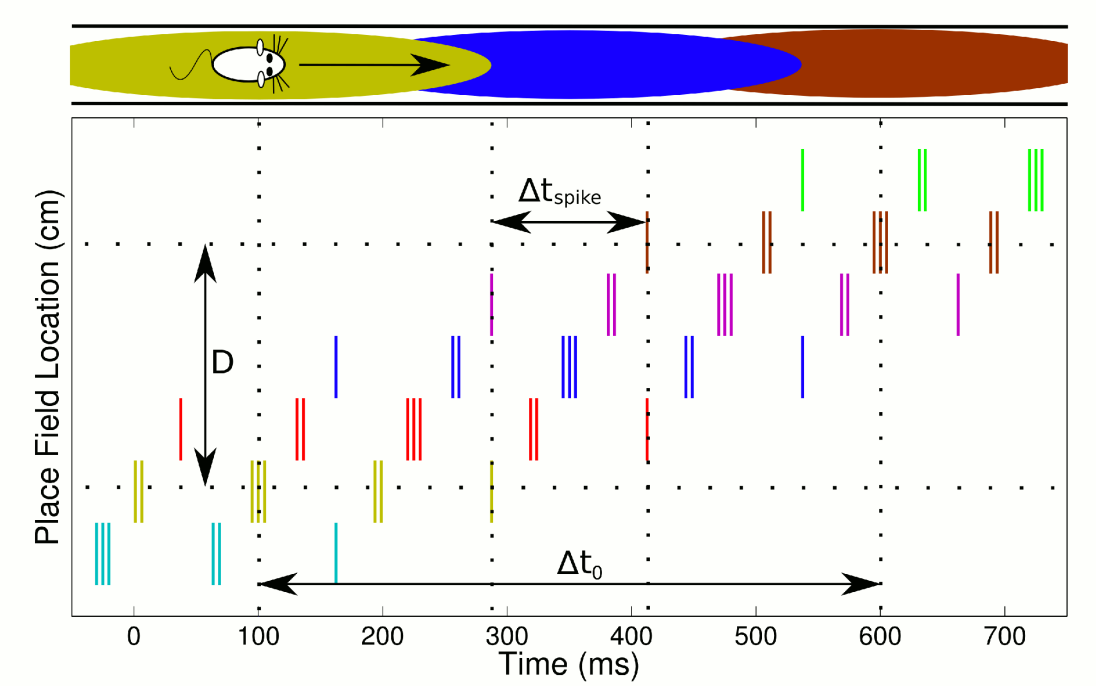

Figure 2.4: **Definitions of compression factor and sequence path length.** Shown are the sequence path length D, which is defined as the largest distance between place field centres for any two cells active in a single theta cycle, the time Δt_0 to travel between place field centres of a pair of cells and the time interval Δt_{spike} between spikes fired in a theta cycle by this cell pair. The compression factor is the ratio of these two timescales. (The cell pair illustrated is the first and last cell on the track above: only three place fields are shown for clarity, the rest are omitted.)

Based on the above description of coding in a single place cell, we can already derive some interesting properties of population theta sequences in special cases. In particular, when the phase locking k is very high, the above stochastic model achieves its deterministic limit in which exact analytical expressions for certain properties of theoretical and experimental interest can be found.

Here, we derive analytical expressions for two key quantities which are often measured in experiments: the compression factor and the sequence path length. These expressions are strictly only valid in the limit that phase locking is strong, but are use-

ful for understanding how behavioural variables such as running speed can influence sequence properties. Moreover, as solutions for the $k = 0$ case are trivial, it is possible to compare the cases of pure rate coding vs strong phase coding in order gain intuition into how intermediate dual rate and phase coding schemes might behave depending on the value of k. In this section, we assume that the activity of each cell is governed by Equation (2.9), i.e. that the activity of each cell depends only on the animal's location in the place field and the LFP theta phase, and not explicitly on the activity of other cells in the population.

The compression factor measures the ratio between the sequence compressed timescale and the behavioural timescale along a trajectory. Given any two cells active within the same theta cycle, the compression factor is defined as:

$$c = \frac{\Delta t_0}{\Delta t_{\text{spike}}} \tag{2.12}$$

where Δt_0 is the time it takes the animal to travel between the place field centres of the two cells and Δt_{spike} is the time lag between the spikes of the two cells within the theta cycle (Figure 2.4). Note that some studies invert this definition of c (e.g., Geisler et al., 2010). These two timescales are generally measured in experiments as peaks in the cross-correlogram of the cell pair following filtering at behavioural and theta timescales.

In the limit of high phase locking ($k \to \infty$), the spikes occur exactly at the peaks of the phasic tuning curve, i.e.:

$$\theta(t_{\text{spike}}) - \phi(t_{\text{spike}}) \equiv 0 \mod 2\pi \tag{2.13}$$

Figure 2.5 provides a graphical illustration of the spike sequence in this limit. Using Equations (2.3) and (2.4) in this limit:

$$t_{\text{spike}} = \frac{(\phi_0 - \theta_s)/(2\pi) + f_\phi t_0 + n}{f_\theta + f_\phi} \tag{2.14}$$

where n is an integer introduced to account for the resetting of phases $\phi(t)$ and $\theta(t)$ each cycle under the modulo arithmetic. If we further assume that each cell precesses over a range of phases of one cycle or less $0 \leq \phi < 2\pi$, then the integer n is simply an index labelling the LFP theta cycle, since ϕ is never reset. Hence, when calculating Δt_{spike} for a cell pair, we can assume n is the same for each spike, since we are considering only spike sequences contained within a single theta cycle. Assuming the cells also share the same phase precession parameters ϕ_0 and f_ϕ, we find $\Delta t_{\text{spike}} = \Delta t_0 f_\phi/(f_\theta + f_\phi)$, so

that the compression factor is:

$$c = 1 + \frac{f_\theta}{f_\phi} = 1 + f_\theta \frac{2\pi}{\Delta\phi}\frac{2R}{v} \tag{2.15}$$

The sequence path length D measures the distance swept out by a sequence during a theta cycle (Figure 2.4). We define this as the difference between the maximum and minimum place field locations of cells active in a single theta cycle $D = \max(\Delta x_c) = \max(x_c) - \min(x_c)$. Again, we take the limit $k \to \infty$ where spike times are given by Equation (2.13). The distance between place field centres is $\Delta x_c = v\Delta t_0 = cv\Delta t_{\text{spike}}$, and the sequence path length D is the largest distance Δx_c for cells with spikes within the time window of one theta cycle, $\Delta t_{\text{spike}} \leq 1/f_\theta$:

$$D = \frac{v}{f_\theta}c = \frac{2\pi}{\Delta\phi}2R + \frac{v}{f_\theta} \tag{2.16}$$

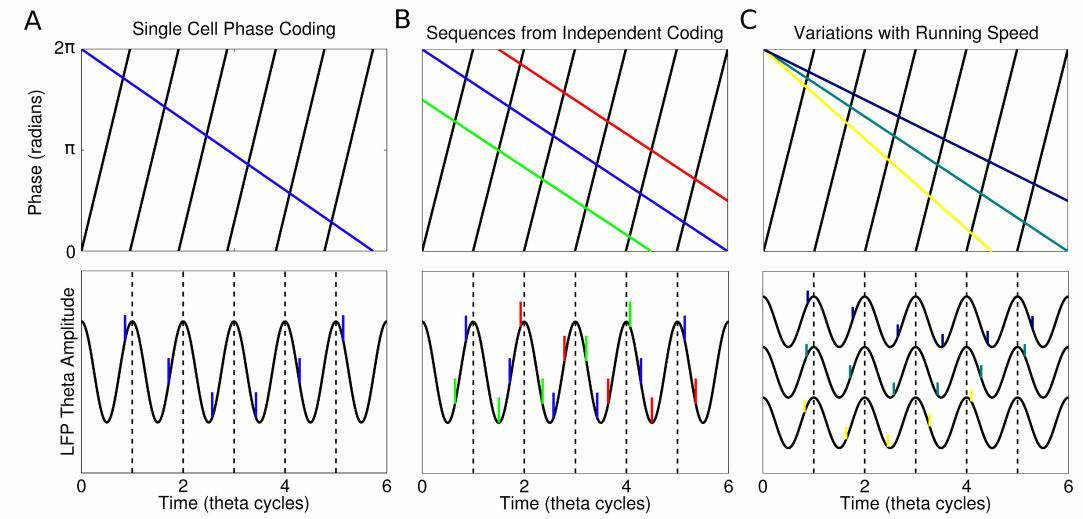

Figure 2.5: **Sequences in the high phase locking limit ($k \to \infty$).**
Black lines show LFP theta phase $\theta(t)$, coloured lines show single cell encoded phase $\phi(t)$. Spikes occur when the encoded phase equals the LFP phase. (A) Single cell coding. (B) A sequence generated through independent phase coding in three cells. (C) Running speed v determines the slope of phase precession f_ϕ in single place cells, which in turn affects sequence properties. Here, three separate runs through the same place field at different speeds are shown for comparison.

2.3 Independent phase coding generates travelling waves

Given the single cell model and assuming an independent population code, we next investigated the spatially distributed patterns of spiking activity generated in a CA1 population more generally. To map the spatiotemporal dynamics of the population activity onto the physical space navigated by the animal, we analysed the distributions of the rate components r_x and phase components r_ϕ of activity in cell populations sorted according to the location x_c of each place field. In order to make the step from the single cell coding model described above to the population coding model we present in this section, it is necessary to invoke the independent coding hypothesis. If cells do not code independently of each other then further information is needed to develop an account of population activity, which we discuss subsequently.

Derivation of travelling wave dynamics for independent coding

We now investigate the behaviour of a place cell population under the assumption that each cell is governed independently by the above single cell coding model. Note that, in Equation (2.9), we have eliminated the rat's location x in favour of time t, since we have assumed a constant running speed. In this way, we would like to understand the firing rate in the population both as a function of time t, and place field centre x_c during locomotion on a linear track. In Equation (2.9), the remaining t_0 can be expressed in terms of x_c as $t_0 = (x_c - R - x_s)/v$. We then define the total phase of each cell as $\psi = \phi - \theta$, which gives :

$$\psi(x_c,t) = 2\pi(f_\theta + f_\phi)t - 2\pi\frac{f_\phi}{v}(x_c - x_s) + \frac{\Delta\phi}{2} - \phi_0 + \theta_s \tag{2.17}$$

We can set the initial position of the rat as $x_s = 0$ for simplification. Inspecting the structure of this population phase, we see it has the form $\psi(x_c,t) = \omega t - \kappa x_c + \psi_s$. This is the form of a travelling wave of angular frequency $\omega = 2\pi f$, wavenumber $\kappa = 2\pi/\lambda$ and phase offset ψ_s. The frequency and wavelength of the travelling wave are:

$$f(v) = f_\theta + f_\phi(v) \tag{2.18}$$

$$\lambda = \frac{v}{f_\phi} = \frac{2\pi}{\Delta\phi}2R \tag{2.19}$$

so that the frequency increases with running speed, but the wavelength stays constant. Hence, the propagation speed of the wave is:

$$v_p = f\lambda = (f_\theta + f_\phi)\frac{v}{f_\phi} = cv \tag{2.20}$$

where c is the compression factor. The compression factor is equivalent to the ratio of the rat's actual velocity and the velocity of the representation within a theta cycle. While the compression factor has been quantified in previous experimental work (Skaggs et al., 1996; Dragoi and Buzsáki, 2006; Geisler et al., 2007; Maurer et al., 2011), the relationship to the travelling wave model developed here was not previously identified.

The propagation speed shows a constant relationship to the running speed of the rat:

$$v_p = v + \frac{2\pi}{\Delta\phi} 2Rf_\theta \tag{2.21}$$

At this point, we also see that (assuming $\Delta\phi = 2\pi$, which are free to choose by varying R) the sequence path length in Equation (2.16) is just the distance travelled by this wave in a theta cycle, since $D = v_p/f_\theta$. Putting everything together, the population firing rate is given by:

$$r(x_c,t) = A\exp\left(-\frac{(x_c - vt)^2}{2\sigma^2}\right)\exp\left(k\cos\left(\frac{2\pi f}{cv}(cvt - x_c) + \psi_s\right)\right) \tag{2.22}$$

which is an equivalent form of Equation (2.9) and was used to produce Figure 2.6. Hence, our model naturally generates population activity at two different timescales: the slow behavioural timescale at which the rat navigates through space and a fast theta timescale at which trajectories are compressed into theta sequences. While the rat moves through the environment, the spatial tuning curves $r_x(x)$ generate a slow moving 'bump' of activity which, by definition, is comoving with the animal (Figure 2.6A top, black). Simultaneously, the phasic component $r_\phi(\phi(x),\theta(t))$ instantiates a travelling wave (Figure 2.6A top, red). Due to the precession of $\phi(t)$, the wave propagates forward through the network at a speed faster than the bump, resulting in sequential activation of cells along a trajectory on a compressed timescale. The slower bump of activity acts as an envelope for the travelling wave, limiting its spatial extent to one place field (Figure 2.6A bottom). The continuous forward movement of the travelling wave is translated into discrete, repeating theta sequences via a shifting phase relationship to the slow moving component (Figure 2.6B-D). From the above analysis we find an alternative expression for the compression factor derived earlier $c = v_p/v$, i.e. the compression factor is the ratio of the propagation speed of the travelling wave to the speed of the envelope.

Finally, it is useful to inspect the phase offset ψ_s of the travelling wave. In particular, if we assume a full cycle of phase precession $\Delta\phi = 2\pi$ starting at $\phi_0 = 2\pi$, with initial position $x_s = 0$, we see from Equation (2.17) that the population phase offset

is $\psi_s = \theta_s - \pi$. The maximum population activity occurs at the trough of LFP theta, where zero LFP phase is defined as the peak. Hence, there is a half cycle phase shift between the population waveform and the LFP waveform (although experimentally this effect depends on the recording depth, since the LFP phase varies with depth (Buzsáki, 2002)).

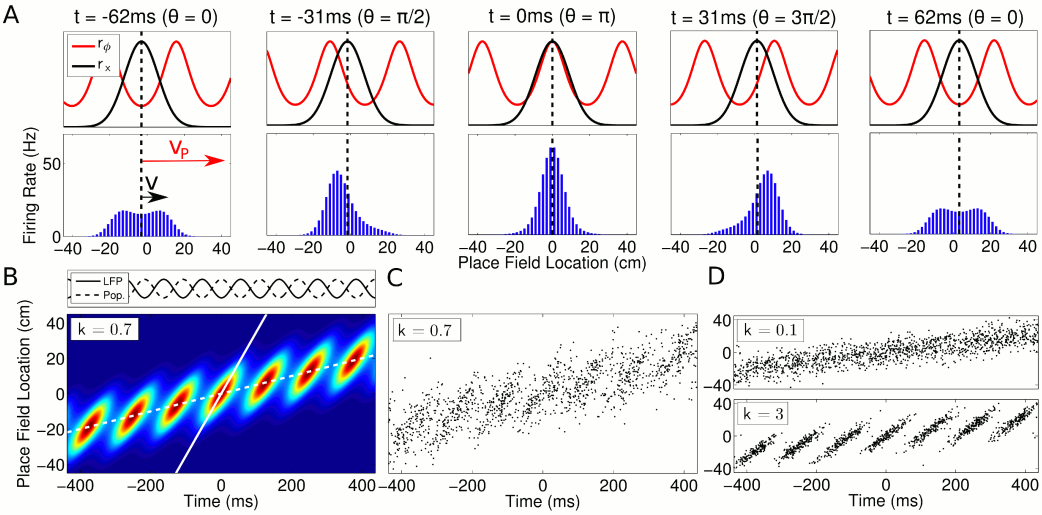

Figure 2.6: **Spatiotemporal dynamics of CA1 populations governed by independent coding.**

(A) *Top:* Population dynamics during a single theta cycle on a linear track after ordering cells according to their place field centre x_c in physical space. The two components of the population activity are shown - the slow moving envelope (black) and the fast moving travelling wave (red), which give rise to rate coding and phase coding respectively (cf. Figure 2.2). *Bottom:* Resulting firing rates across the population. When the travelling wave and envelope are aligned, the population activity is highest (middle panel). The dashed line shows the location of the rat at each instant. (B) Firing rate in the population over seven consecutive theta cycles. The fast and slow slopes are shown (solid and dashed lines respectively), corresponding to the speeds of the travelling wave and envelope as shown in part (A). The top panel shows the LFP theta oscillations and emergent population theta oscillations, which are generated by the changing population activity as the travelling wave shifts in phase relative to the slower envelope. (C, D) The spiking activity for a population of 180 cells. All panels used $v = 50$ cm/s, so that $v_p = 350$ cm/s and $c = 7$.

Analysis of population theta rhythm

Here, we show how a slower LFP theta rhythm arises within the population, despite the higher frequency of individual cells. In particular, we see from the above analysis that the frequency of a single cell is higher than the LFP theta since $f = f_\theta + f_\phi$. However, if we change variables to view the travelling wave in coordinates comoving with the envelope, the fast population activity is decoupled from the slow movement of the animal, allowing the population theta frequency to be analysed.

To see this, we make the change of coordinates $X = x_c - vt$, after which $\psi(X = 0, t)$ measures the phase of the travelling wave relative to the slow moving envelope, since $X = 0$ is the centre of the envelope. In these coordinates, the population phase is:

$$\psi(X,t) = \theta(t) - 2\pi\frac{X}{\lambda} \tag{2.23}$$

Equation (2.23) shows that $\theta(t) = \psi(X = 0, t)$, and therefore that the LFP theta phase is equal to the phase difference between the travelling wave and envelope. To further illustrate this point, we note that the LFP theta frequency is equal to the time taken for the fast wave to overtake the slow envelope, i.e. from Equation (2.21):

$$f_\theta = \frac{v_p - v}{\lambda} \tag{2.24}$$

so that the LFP theta frequency is simply the frequency of the interference pattern of the two components. Thus, the shifting phase relationship between the slow and fast components of population activity generates global theta oscillations at exactly the LFP frequency that cells were defined to precess against (Figure 2.6B top panel). Our single cell model can therefore be recast in terms of the dynamics of a propagating wavepacket comprising two components, with network theta resulting from their interaction. While we define single cells to precess against a reference theta rhythm (i.e., the LFP), we now see that this same reference oscillation emerges from the population, despite the higher frequencies of individual cells.

This prediction of global theta oscillations emerging in networks of faster oscillating place cells is consistent with a previous phenomenological model which assumed a fixed running speed and fixed, experimentally determined temporal delays between cells (Geisler et al., 2010). However, in contrast to previous models, our model based on experimentally observed single-cell coding properties allows an analysis in which only place field configurations and navigational trajectories are required to fully predict at any running speed both the global theta oscillation and the detailed population

dynamics. Experimental data show that the frequency of LFP theta oscillations is relatively insensitive to the running speed of the animal, showing a mild increase with running speed compared to a larger single unit increase (Geisler et al., 2007). Similarly, in our model the change in compression factor with running speed ensures that the network maintains a fixed population theta frequency while running speed and single unit frequency vary. In predicting a compression factor which changes with running speed, independent coding equivalently predicts temporal delays which are dependent on running speed. Conversely, our analysis shows that models incorporating fixed temporal delays between cells (e.g., Diba and Buzsáki, 2008; Geisler et al., 2010) cannot maintain an invariant relationship between spike phase and location without producing a population theta oscillation whose frequency decreases rapidly with running speed, in conflict with experimental observations (Geisler et al., 2007).

Linear phase coding in open environments

To complete our phenomenological model of phase coding in independent coding populations, we now consider the population activity for arbitrary trajectories $\mathbf{x}(t)$ in two dimensions.

The most natural extension is to modulate the direction of the travelling wave with heading direction, via a wavevector $\boldsymbol{\kappa}(t) = \kappa \mathbf{v}(t)/v(t)$. It is necessary to align the wavevector with heading direction to account for data showing phase precession in two dimensions regardless of the direction of travel through a place field (Huxter et al., 2008). The previous results can then be extended using the phase:

$$\begin{aligned}\psi(\mathbf{x_c}, t) &= \int_0^t \omega(t')dt' - \boldsymbol{\kappa}(t) \cdot \mathbf{x_c} + \psi(\mathbf{x_c}, 0) \\ &= 2\pi f_\theta t + \frac{\Delta\phi}{2\pi}\frac{\pi}{R}\left(\int_0^t v(t')dt' - \frac{\mathbf{v}(t)\cdot\mathbf{x_c}}{v(t)}\right) + \psi_s \end{aligned} \tag{2.25}$$

where we introduced an integral to account for variations in frequency due to changes in running speed along the trajectory and expanded out expressions for frequency and wavenumber. In this case, the phase offset $\psi(\mathbf{x_c}, 0)$ is the same for all neurons, since the phase gradient is enforced by the dot product term. In line with a recent report (Jeewajee et al., 2014), the relative firing phases of each cell depend on the current direction of motion rather than past trajectory in this model.

2.4 Assembly coordination stabilises sequential activation patterns

In order to compare activity patterns predicted by independent coding schemes with those predicted when interactions between cell assemblies are present, we developed a second model in which the spiking activity of each place cell influences the spiking activity of peer cells within the population. While single-cell rate and phase tuning curves in this coordinated assembly model are identical to those in the independent coding model, a peer weight function also modulates the probability of a spike occurring in each cell depending on the spikes of its peers (Figure 2.7A). In this model, asymmetric excitation stabilises the temporal relationship between sequentially activated assemblies, while feedback inhibition between place cells normalises firing rates (cf. Tsodyks et al., 1996; Wang et al., 2015). The resulting sequences are considerably more robust than those generated by independent coding with the same single cell properties (Figure 2.71B-C). Assembly interactions also amplify theta oscillations in the network (Figure 2.7D) (Stark et al., 2013). Hence, assembly coordination provides a potential mechanism for stabilising the sequential activity patterns generated by noisy neurons, as interactions entrain cells in the population into coherent activation patterns within each theta cycle. The precise formulation of the coordinated coding model is described below.

Model of coordinated assembly dynamics

While the previous sections assumed that cells are are independent of each other once their mutual dependence on the animal's location and the LFP theta rhythm are accounted for, we now model the case in which cells have additional interdependencies arising from interactions within the local CA1 population. Therefore, we introduce a weight function through which the spiking activity of any given cell will influence the probability of another cell to spike:

$$w_{ij} = \frac{w_E}{\ell} e^{-(x_c^i - x_c^j)/\ell} \Theta\left(x_c^i - x_c^j\right) - w_I \tag{2.26}$$

where w_E is the magnitude of the excitatory weights, ℓ is the peer interaction length, Θ is the Heaviside step function, w_I is the magnitude of the inhibitory weights and x_c^i, x_c^j are the place field centres of cells i and j. This weight function is comprised of two components - an excitatory feedforward interaction with an interaction length ℓ, and a global inhibitory interaction.

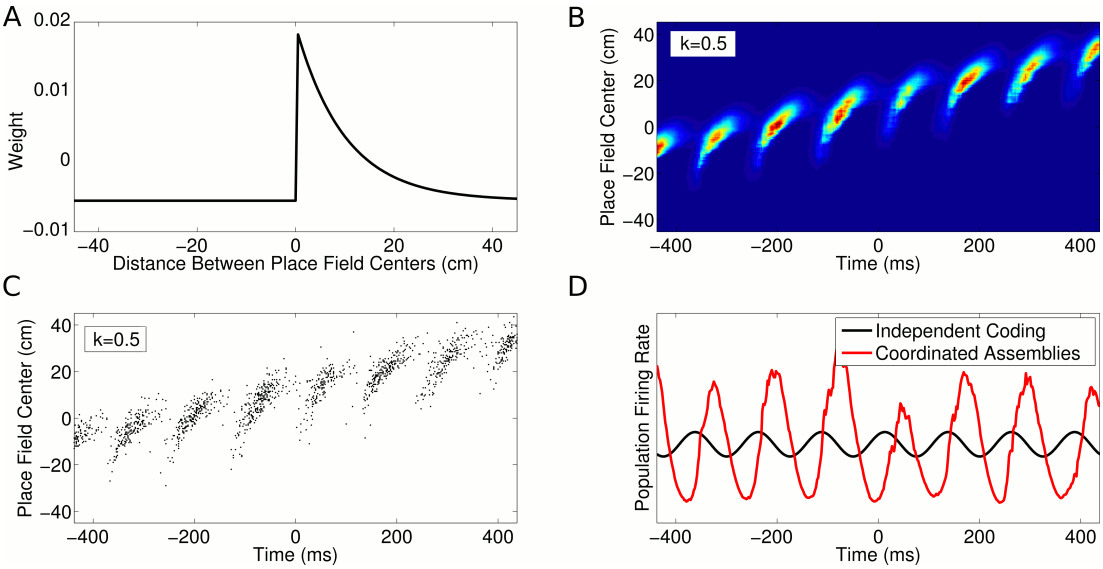

Figure 2.7: **CA1 population activity governed by coordinated assemblies.** (A) The simulated place cells interact via a combination of asymmetric excitation and feedback inhibition. The weights plotted here govern how the spikes emitted by a given cell will influence the spiking activity of its peers depending on their relative place field locations. (B) Population firing rate on a single run along a linear track (180 cells with $v = 50$ cm/s and $k = 0.5$). The firing rate in each cell is a product of the animal's location, the LFP theta phase and the influence of recent peer spiking activity. (C) The spiking activity, generated using an inhomogeneous Poisson process. (D) Comparison of the global population firing rate for an independent coding population (black) and a coordinated population (red), with identical single cell properties. Interactions between cells amplify theta oscillations and introduce a shift in firing phase.

To incorporate the dynamics of peer interactions into our existing single cell model, we follow a similar approach to that used by Harris et al. (2003) when estimating peer interactions from data. Specifically, peer spike trains are smoothed in time:

$$s_i(t) = \frac{1}{\sqrt{2\pi\tau^2}} \sum_{t_{ij}<t} e^{-\left(t_{ij}-t\right)^2/2\tau^2} \tag{2.27}$$

where the smoothing kernel width τ determines the peer interaction timescale - i.e., the timescale at which spiking activity from one cell will influence the activity of another cell (cf., the peer prediction timescale defined by Harris et al. (2003)). Here, s_i is the smoothed spike train of cell i and t_{ij} is the jth spike of cell i, where the sum is over j only. Note that the above sum is causal, i.e. only previous spikes will influence present and future activity. The influence of a set of peer spike trains on a particular cell i is

then determined by the peer factor $P_i(t)$:

$$P_i(t) = g\left(\sum_j s_j(t) w_{ij}\right) \tag{2.28}$$

which is the weighted sum of the smoothed peer spike trains, followed by a nonlinear transformation g:

$$g(x) = \begin{cases} x+1 & \text{if } x \geq 0 \\ \exp(x) & \text{if } x < 0 \end{cases} \tag{2.29}$$

We note that, apart from some minor adjustments, Equations (2.27-2.29) are essentially an inversion of the peer prediction method of Harris et al. (2003) such that, with our particular choice of weights, we can generate data for an interacting population rather than estimate these interactions from that data.

The firing rate of each cell is simply modelled as the product of the activity generated by phase and rate coding alone with the additional peer factor $P_i(t)$. To simplify notation, we let $P_i(t) = P(x_c, t)$ where x_c is the place field centre of cell i. The total firing rate of the cell is then:

$$r(x_c,t) = A \exp\left(-\frac{(x_c - vt)^2}{2\sigma^2}\right) \exp\left(k \cos\left(\kappa x_c - \omega t + \psi_s\right)\right) P\left(x_c, t\right) \tag{2.30}$$

While alternative forms of assembly coordination might also be considered, we choose the present model for two key reasons. First, this model is simple, containing relatively few adjustable parameters while capturing the essential features of sequence generation via assembly coordination. Second, as we will show below, the coordination between cells under this model is sufficient to evaluate statistical tests of independence, allowing a systematic framework with which to interpret the results of such tests on experimental data. Nevertheless, it should be noted that the results obtained for coordinated coding simulations are specific to the model outlined here, and that other forms of coordination may behave differently.

2.5 Independent coding accounts for apparent peer dependence of CA1 activity

We next investigated the extent to which models for population activity based on independent coding and coordinated assemblies can account for observations previously suggested to imply coordination within and between assemblies (Harris et al., 2003;

Dragoi and Buzsáki, 2006; Foster and Wilson, 2007; Maurer et al., 2011; Gupta et al., 2012). We show below that, although these observations at first appear to imply assembly coordination, they can be accounted for by the independent coding model. We go on to establish the power of several tests to distinguish spike patterns generated by independent and coordinated coding models. By applying these tests to experimental data, we provide further evidence that CA1 population activity is generated through independent coding.

Prediction analysis of Harris et al., 2003

We first assessed whether independent coding accounts for membership of cell assemblies. A useful measure of the coding properties of place cell populations is to test how accurately single-unit activity can be predicted from different variables. If, after accounting for all known single-cell coding properties, predictions of the activity of individual place cells can be further improved by information about firing by their peer cells, it is likely that such cells are interacting through cell assemblies (Harris, 2005). Initial analysis of CA1 place cell firing suggested this is the case, with coordination between cells at the gamma timescale being implicated (Harris et al., 2003). Because this improved predictability directly implies interactions between CA1 neurons, it would constitute strong evidence against the independent coding hypothesis. However, in accounting for single-cell phase coding properties, the prediction analysis of Harris et al. (2003) assumed that firing phase is independent of movement direction in an open environment. In contrast, more recent experimental data show that in open environments firing phase always precesses from late to early phases of theta, so that firing phase at a specific location depends on the direction of travel (Huxter et al., 2008; Climer et al., 2013; Jeewajee et al., 2014). Therefore, to test if the apparent peer dependence of place cell activity is in fact consistent with independent coding, the directionality of phase fields must be accounted for.

To address this we first considered whether the assumption of a non-directional phase field would lead to an erroneous conclusion of coordinated coding when analysing spike patterns generated by the independent coding model. To do this, we used the above extension of the travelling wave model to two dimensional environments. We constructed phase fields from simulated spiking data following the approach of Harris et al. (2003), in which firing phase is averaged over all running directions, and separately constructed directional phase fields consistent with recent experimental ob-

servations (Huxter et al., 2008; Climer et al., 2013; Jeewajee et al., 2014). We then calculated the predictability of neuronal firing patterns generated by the independent coding model using each of these phase fields. For simplicity, we considered the problem in one dimension, treating separately passes from right to left, left to right and the combined data in order to generate the directional and nondirectional phase fields (Figure 2.8A&B respectively). We did not model shifts in place field centres for different running directions (e.g., Battaglia et al., 2004; Huxter et al., 2008) and assumed that the place cells did not engage in multiple reference frames (Jackson and Redish, 2007; Fenton et al., 2010).

For the independent coding model, we find that peer prediction provides a higher level of information about a neuron's firing than predictions based on place and nondirectional phase fields, despite the absence of intra-assembly coordination in our simulated data (Figure 2.8C, green and purple). However, prediction based on place fields and directional phase fields outperforms both of these metrics (Figure 2.8C, red). Therefore, previous evidence for intra-assembly coordination can be explained by a failure to account for the phase dependence of CA1 firing. Instead, our analysis indicates that independent phase precession of CA1 neurons is sufficient to account for observations concerning membership of CA1 assemblies. We also find that nondirectional phase fields (Figure 2.8B), as assumed by (Harris et al., 2003), yield little improvement in predictability of a neuron's firing compared with predictions based on the place field alone, and for high phase locking are detrimental (Figure 2.8C, blue vs black). While Harris et al. (2003) found that nondirectional phase fields generally do improve prediction, this discrepancy may arise from more complex details of experimental data in open exploration, for example a nonuniform distribution of running directions through the place field, which would cause the information in nondirectional phase fields to increase.

Because peers share a relationship to a common theta activity and implement similar rules for generation of firing, a cell's activity in the independent coding model can nevertheless be predicted from that of its peers in the absence of information about location or theta phase (Figure 2.8C, green). The quality of this prediction is dependent on the timescale at which peer activity is included in the analysis, so that the optimal timescale for peer prediction provides a measure of the temporal resolution of assembly formation. In experimental data the optimal timescale for peer prediction is approximately 20 ms, which corresponds to the gamma rhythm and the membrane time constant of CA1 neurons (Harris et al., 2003). We find that in the independent

coding model the optimal peer prediction timescale depends strongly on phase locking (Figure 2.8D). Even though the model does not incorporate gamma oscillations or neuronal membrane properties, high values of phase locking also show a striking peak in peer predictability around the 20 ms range (Figure 2.8D). We show below that for running speeds in the range $35 - 75$ cm/s phase locking is likely to lie within the range at which the observed 20 ms prediction timescale dominates. Thus, the 20 ms timescales found both here and experimentally are explainable as a signature of the common, independent phase locking of place cells to the theta rhythm, rather than transient gamma coordination or intrinsic properties of CA1 neurons.

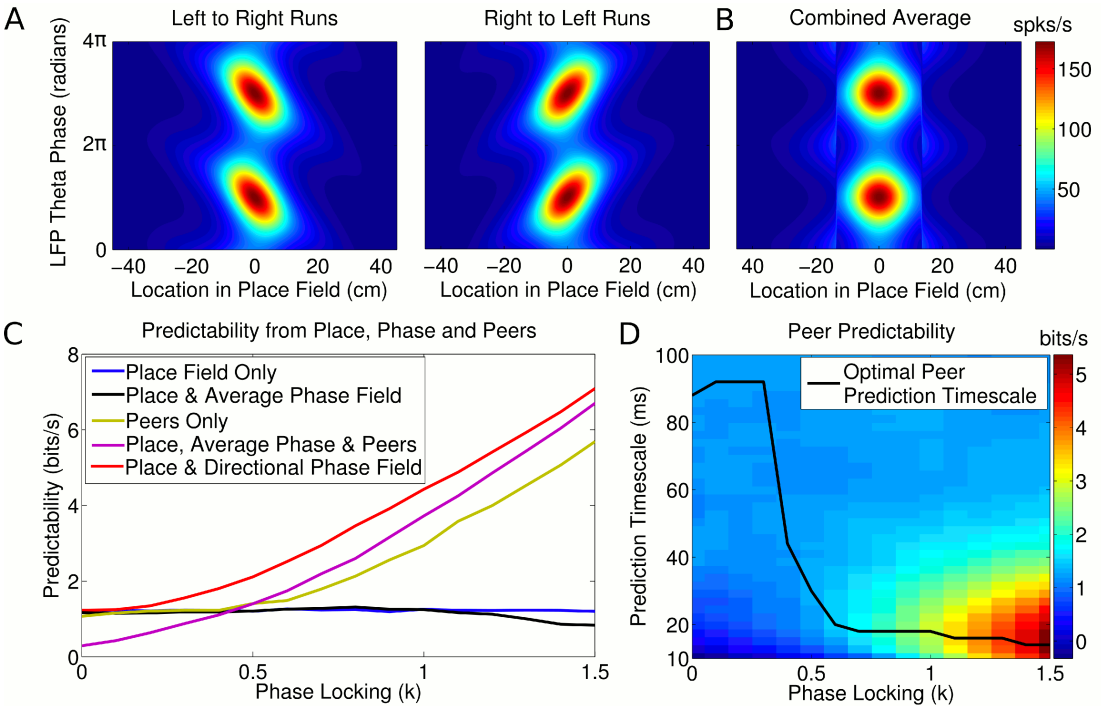

Figure 2.8: **Peer prediction analysis for an independent population code.** (A) Combined place and phase fields constructed from simulated data using only runs with a single direction. (B) Place/phase field constructed from a combination of both running directions, as used by Harris et al. (2003). (C) Predictability analysis, using various combinations of place, phase and peer activity. When using the nondirectional phase field of Harris et al. (2003), an additional peer predictability emerges (black vs green and purple). However, this additional predictability is seen to be erroneous if the directional phase field is used to predict activity (red). (D) Dependence of peer predictability on the peer prediction timescale and phase locking of individual cells, for an independent population code. The heat map shows the predictability of a cell's activity from peer activity (cf. part C, green line). The optimal peer prediction timescale depends on the amount of phase locking. The 20 ms characteristic timescale of peer correlations reflects independent phase precession of single cells rather than transient gamma synchronisation of cell assemblies.

Modified prediction analysis

While the above analysis demonstrates that independent coding is consistent with previous experimental results, it does not exclude the presence of coordinated assemblies. In particular, it is not clear whether, when applied to experimental data, including information about peer activity would continue to improve prediction compared to place and directional phase fields alone. We therefore applied the prediction analysis based on directional phase fields to experimental datasets recorded from CA1 place cells (Mizuseki et al., 2014). To provide benchmarks for the interpretation of experimental results, we also analysed simulated datasets generated with either independent coding or coordinated assemblies. We simulated datasets with the same number of sessions and recorded cells per session as the experimental dataset in order to obtain measures of peer prediction performance expected under each hypothesis (see Methods). In simulations of independent cells, we found that information about peer activity continues to improve predictability compared to prediction from place and directional phase fields alone. The source of this predictability was found to be the common modulation of firing rate in each cell with the running speed of the animal, which is a further single-cell coding feature not previously accounted for in prediction analyses (McNaughton et al., 1984; Czurko, 1999; Huxter et al., 2003; Ahmed and Mehta, 2012). We therefore included in our analysis an additional prediction factor, termed the velocity modulation factor (see Methods).

After accounting for rate fields, directional phase fields and velocity modulation factors, inclusion of peer information increased the predictability of 84% of place cells simulated through coordinated coding, but only 38% of cells simulated through independent coding (see Table 1 for a summary of all prediction metrics). On average, information decreased by 0.047 bits/s for each cell simulated by independent coding and increased by 0.24 bits/s for coordinated coding when peer information was added (Wilcoxon signed rank test, $p = 3.9 \times 10^{-17}$ and $p = 9 \times 10^{-83}$ respectively, Figure 2.9). Thus, this new prediction analysis which accounts for directional phase fields and velocity modulation can effectively distinguish between independent and coordinated coding.

When we applied this prediction analysis to experimental data, prediction performance improved for 75.7% ($\pm$ 5.7%, SEM, $n = 10$ sessions) of experimentally observed place cells when phase fields were included and 77.8% ($\pm$ 3.7%) of place cells when velocity modulation factors were included. In contrast, prediction performance

Prediction Metric	Independent Coding	Coordinated Coding	Experimental Data
Location	100%	100%	44.6% (SEM 5.8%)
Running Speed	99.3%	99.7%	77.8% (SEM 3.7%)
Phase Field	99.3%	100%	75.7% (SEM 5.7%)
Peer Activity	38%	84.3%	32.5% (SEM 11%)

Table 1: **Performance of prediction metrics on experimental and simulated data.** The percentage of cells for which prediction performance increased with the addition of each metric. Percentages refer to the number of cells for which information increased when the specified metric was included in addition to those listed in rows above. Note that for velocity, phase and peer prediction, only those cells for which prediction performance improved with information about location were considered. Simulations demonstrate that, after taking into account place fields, velocity modulation factors and phase fields, information about peer activity improves prediction for the majority of cells when coordination is present, but not when cells are independent. Experimental data are consistent with independent coding.

improved for only 32% ($\pm$ 11%) of the experimentally observed place cells when peer information was included after accounting for single-cell coding properties (Figure 2.10 shows the results for individual experimental sessions). On average, addition of peer information decreased the predictability of each cell by 0.049 bits/s ($\pm$ 0.013, SEM, $n = 270$ cells, Wilcoxon signed rank test, $p = 1.4 \times 10^{-6}$), in agreement with independent coding simulations and in contrast to coordinated coding simulations. Hence, after fully accounting for the directional properties of phase fields and the dependence of firing rate on running speed, peer prediction analysis supports independent coding as the basis of experimentally observed place cells in CA1. Therefore, based on comparison of simulated with experimental datasets, coordinated assemblies appear unlikely to account for the observed activity in CA1.

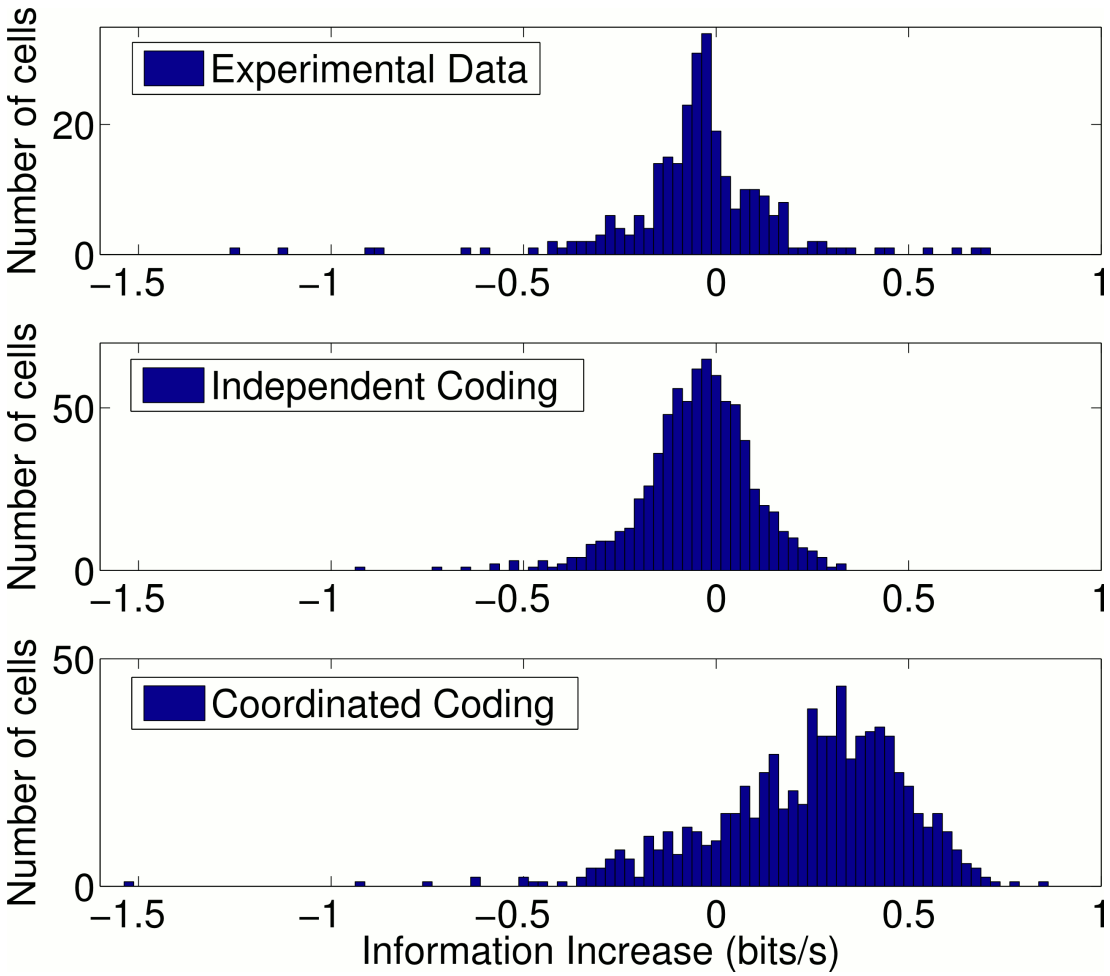

Figure 2.9: **Change in information after addition of peer activity to prediction metrics.**

Distributions of information gain/loss in individual cells after including peer activity in addition to all other prediction metrics. For independent coding and experimental data, peer prediction causes a decrease in information on average ($p = 3.9 \times 10^{-17}$ and $p = 1.4 \times 10^{-6}$ respectively). For coordinated coding, peer prediction causes an increase in information on average ($p = 9 \times 10^{-83}$). The decrease in information observed for independent coding simulations when peer activity is included occurs due to overfitting on a dataset of finite size. Due to statistical fluctuations in the data, peer weights are generally estimated as non-zero. Both the peer weights and the change in information when peers are included would be expected to approach zero as the amount of data increases for independent coding simulations, but not for coordinated coding simulations.

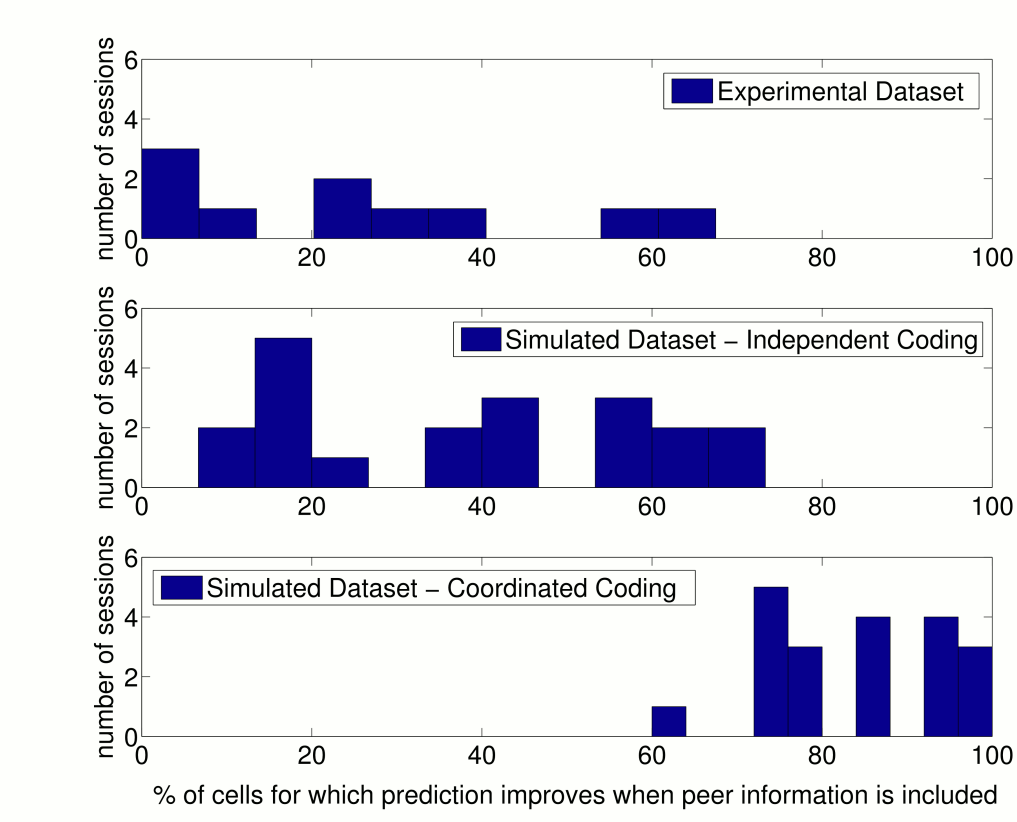

Figure 2.10: **Results of prediction analysis on individual sessions.**
Top: Number of cells for which prediction improved with peers after place fields, velocity modulation factors and directional phase fields had been fitted, shown for each session/running direction in the experimental dataset. *Middle:* The results when the same analysis were applied to data simulated with independent coding (twice as many sessions were simulated for comparison). *Bottom:* The results when data were simulated with coordinated assemblies.

2.6 Independent coding accounts for phase sequences

While the above analysis demonstrates that intra-assembly interactions are not required to account for membership of CA1 assemblies, several studies support a role for inter-assembly coordination in the generation of theta sequences (Dragoi and Buzsáki, 2006; Foster and Wilson, 2007; Maurer et al., 2011; Gupta et al., 2012). We therefore investigated whether the independent coding or coordinated assembly model would better account for the results of these studies.

Changes with running speed

We focus initially on the path length encoded by spike sequences, which we define as the length of trajectory represented by the sequence of spikes within a single theta cycle. Experimental data show that this path length varies with running speed (Maurer et al., 2011; Gupta et al., 2012), but it is not clear whether this phenomenon is a feature of independent coding or instead results from coordination between assemblies. Our analytical solutions to the sequence path length for strong phase coding, where $k \to \infty$ predict a linear increase in sequence path length with running speed, but with a lower gradient than that found experimentally (Maurer et al., 2011). Hence, independent coding with strong phase locking does not quantitatively explain the changes in sequence properties with running speed.

We reasoned that independent coding might still explain observed sequence path lengths if a more realistic tradeoff between rate and phase coding is taken into account. To test this, we varied phase locking k and decoded the path length following the method of Maurer et al. (2011), which decodes the location represented by the population at each time bin in a theta cycle to estimate the encoded trajectory. We found that a good match to the data of Maurer et al. (2011) can be obtained by assuming that the degree of phase locking increases with running speed (Figure 2.11A). This is due to the dependence of the decoded path length on the strength of phase locking (Figure 2.12A).

Maurer et al. (2011) found that the compression factor c, which measures the compression of an encoded trajectory into a single theta cycle, also depends on running speed. To test whether independent coding might account for this observation, we investigated the behaviour of the fast and slow slopes of population activity (as shown in Figure 2.6B), representing assembly propagation at theta timescales and behavioural timescales respectively (i.e., v_p and v). In the analysis of Maurer et al. (2011), the

compression factor was estimated as the ratio of these two quantities. Following again the methods used by Maurer et al. (2011) to decode the fast and slow slopes from spiking data, we found that the dependence of the decoded fast slope on running speed in our simulated data matches experimental data provided that phase locking is again made dependent on running speed (Figure 2.11B, Figure 2.12B). However, the slower behavioural timescale dynamics did not match those reported by Maurer et al. (2011). Our decoded values for the slow slope closely matched the true value based on the rat's running speed. In contrast, the values reported by Maurer et al. (2011) are considerably lower (Figure 2.11C) which, if correct, would suggest that the population consistently moved more slowly than the rat, even moving backwards while the animal remained still. Because of this discrepancy we could not reproduce the compression factor reported by Maurer et al. (2011). Nevertheless, the independent coding model accurately reproduces the theta timescale activity reported by Maurer et al. (2011).

The above analysis has two important implications. First, both the decoded sequence path length and theta-compressed propagation speed in the independent coding model match experimental data provided the degree of theta modulation of spike output increases linearly with running speed. This dependence of phase locking on running speed is consistent with the observed increase in LFP theta amplitude (McFarland et al., 1975; Maurer et al., 2005; Patel et al., 2012), and is a novel prediction made by our model. Second, since the temporal delays between cells are determined by the propagation speed v_p, the close match of this quantity to experimental data confirms the dependence of temporal delays on running speed predicted by our model, and argues against models based on fixed delays (Diba and Buzsáki, 2008; Geisler et al., 2010).

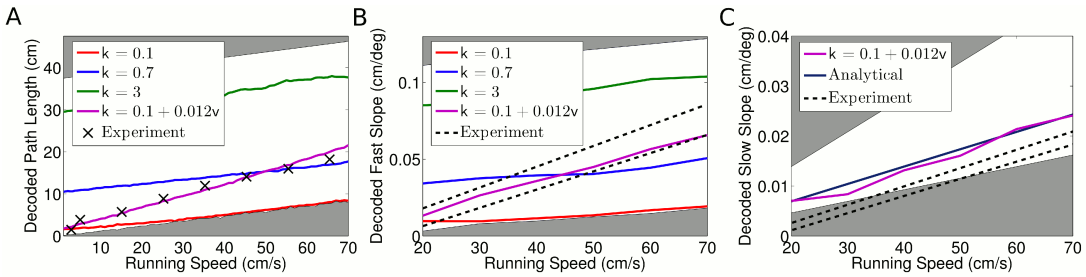

Figure 2.11: **Decoded sequence path lengths and population activity propagation speeds.**

This figure shows the results of analytical and numerical analyses of the changes in theta sequence properties with running speed in the independent coding model, and a comparison to the reported data of Maurer et al., 2011. (A) With constant phase locking, the decoded path length increases linearly with running speed, but to account for experimental data a dependence of phase locking on running speed is required. The shaded regions show lower and upper bounds ($k = 0$ and $k = \infty$). (B) Dependence of decoded fast slope on running speed (cf. our Figure 2.6B; Maurer et al. (2011) Figure 3). Again, a match to the data requires a velocity dependent phase locking. (C) The decoded slow slope matches the analytical value, where the population travels at the running speed v. Bounds show LFP theta frequencies below 4 Hz (upper bound) and above 12 Hz (lower bound) at each given running speed.

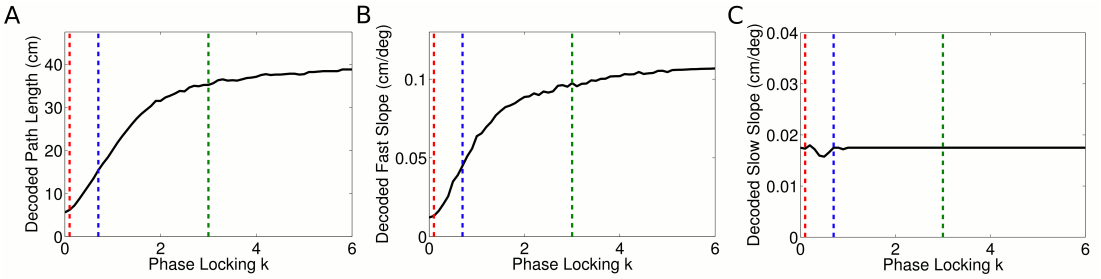

Figure 2.12: **Dependence of decoded sequence path lengths, fast slopes and slow slopes on phase locking.**

(A) The decoded path length depends on the phase locking of individual cells. For zero phase locking, the decoded path length is the distance travelled by the rat in a theta cycle. This is because the decoded location in each time bin is simply the location of the rat. As phase locking is increased the path length increases asymptotically towards our analytical result, which is the distance travelled by the rat plus one full place field. This effect arises due to the gradual separation of cells representing different locations into separate theta phases, as seen explicitly in Figure 2.6C&D. Phases within a single theta cycle represent past, present and future locations along the track. Dashed lines show the phase locking values plotted in Figures 2 and 3. (B) Dependence of decoded fast slope on phase locking. While the analytical result for v_p is independent of phase locking, the decoded value shown here is consistent with the intuitive notion that the sequence path length D is equal to the distance travelled by the fast moving wave in a theta cycle. (C) The decoded slow slope does not depend on phase locking, which is expected given the separation of timescales involved.

Sequence disruption by spike shuffling

Further experimental support for the notion of inter-assembly coordination has come from an analysis suggesting that single cell phase precession is less precise than observed theta sequences (Foster and Wilson, 2007). This conclusion relies on a shuffling procedure which preserves the statistics of single cell phase precession yet reduces intra-sequence correlations. However, performing the same shuffling analysis on data generated by our independent coding model also reduced sequence correlations (t-test, $p < 10^{-46}$) (Figure 2.13). The effect arises because the shuffling procedure does not preserve the temporal structure of single cell phase precession, despite preserving the phasic structure (Figure 2.13A, B). Hence, the phase-position correlations are unaffected, while the time-position correlations and hence sequence correlations are disrupted (Figure 2.13C, D). Thus, inter-assembly coordination is not required to account for these findings.

Nevertheless, although these results are reproducible by the independent coding model, it remains possible that coordinated assemblies underlie the observed theta sequences. In particular, it is unclear whether this shuffling procedure could be modified to obtain a test for assembly coordination with greater statistical specificity and if so, whether it would reveal assembly coordination within experimental datasets. To address these questions, we analysed experimental data along with data generated by independent coding and coordinated assembly models, using a modified version of this shuffling procedure (see Methods). Briefly, this modified shuffling procedure improves upon the previous version by using a circular-linear correlation between spike phase and location, avoiding the conversion between phases and times which introduced errors in the original approach. We found that the new shuffling procedure successfully detected assembly coordination with a statistical power of 81% (calculated for datasets containing the same number of sessions, cells and sequences as our experimental dataset). When applied to experimental data from CA1, the shuffling test failed to detect any significant effect of shuffling (t-test, p=0.28, 2436 events), as in most (74%) of the simulated independent coding datasets (Figure 2.13E, F). This failure to detect evidence of assembly coordination gives further support to the independent coding hypothesis.

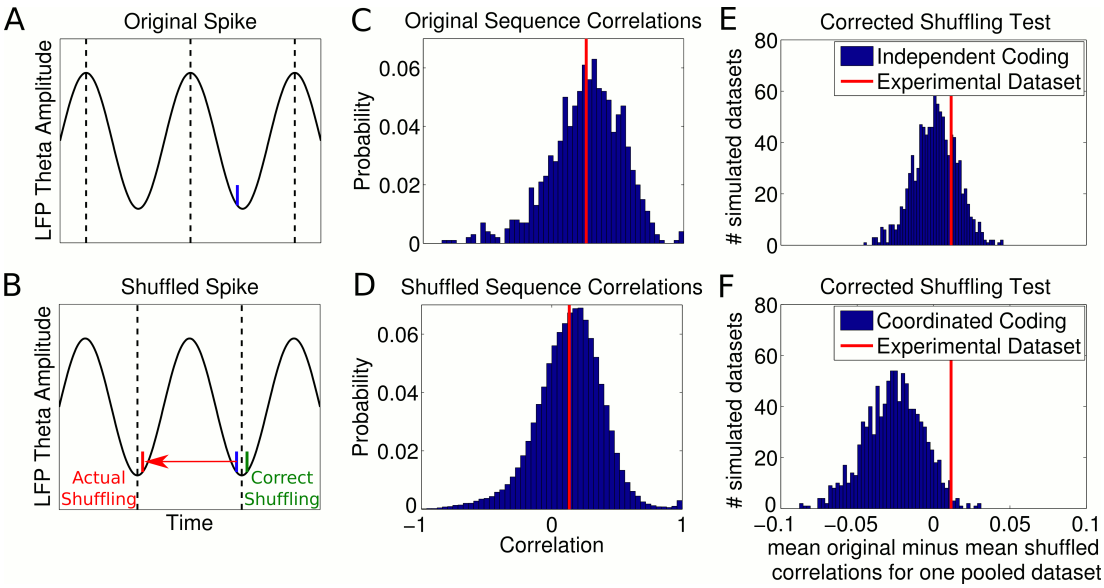

Figure 2.13: **Results of shuffling analysis.**

(A)-(D) show the analysis of Foster and Wilson (2007), (E)-(F) show a corrected analysis. (A) Spike phases were initially calculated by interpolation between theta peaks, shown as dotted lines. (B) After shuffling the phases of spikes, a new spike time is calculated by interpolation between the nearest two theta troughs (dotted lines) to the original spike, which often generates erroneous spike times. The shuffled spike in this case acquires a small phase jitter, but a large temporal jitter. (C)-(D) show the results of this shuffling analysis applied to simulated independent coding data. (C) The unshuffled sequence correlations between cell rank order and spike times. The red line shows the mean correlation. (D) Shuffled sequence correlations remained greater than zero, but were significantly reduced relative to the unshuffled case as in experimental data (Foster and Wilson, 2007). (E) Results of a corrected shuffling procedure applied to simulated independent coding datasets and an experimental dataset (height magnified for comparison). Displayed are the average changes in sequence correlations caused by shuffling for each simulated dataset. In 74% of simulated datasets, there was no significant difference between the original and shuffled distributions. (F) Results of the corrected shuffling procedure when applied to datasets simulated with coordinated assemblies. In 81% of simulated coordinated coding datasets, shuffling significantly changed the distribution of sequence correlations. The experimental dataset was not significantly affected by shuffling (p=0.28, t-test, 2436 putative sequences).

Dependent and independent cell pairs

In additional support for the coordinated assembly hypothesis, Dragoi and Buzsáki (2006) performed an analysis suggesting that, during continuous locomotion around a rectangular track, some cell pairs show a lap by lap covariation of firing rates (termed the dependent pairs). These cell pairs were found to spike with a more reliable temporal lag within theta cycles than cell pairs whose firing rates are independent, which was interpreted as evidence for direct interactions between dependent neurons. To test whether these results are instead consistent with independent coding, we applied the analysis of lap by lap firing rate covariations to data from simulations of the independent coding model. We found a similar fraction of apparently dependent cell pairs to that reported by Dragoi and Buzsáki (2006), despite the absence of any true dependencies between cells in the model (see Methods). Hence, this analysis artificially separates homogeneous populations of place cells into apparently dependent and independent cell pairs. Moreover, these dependent and independent cell groups displayed different spatial distributions of place fields, with dependent cell pairs generally occurring closer together on the track (Wilcoxon rank sum test, $p = 1.8 \times 10^{-16}$). By separating a homogeneous population of cells into dependent and independent groups, the analysis therefore introduces a sampling bias, leading to dependent cell pairs having different properties. While we were unable to reproduce the analysis of the temporal lags in each group due to a lack of information provided within the original study (see Methods), the emergence of dependent cell pairs with measurably different properties in independent coding simulations nevertheless demonstrates that these results are not indicative of interactions between neurons.

Lookahead and lookbehind sequences

Finally, precise coordination of theta sequences has been suggested on the basis that theta sequence properties vary according to environmental features such as landmarks and behavioural factors such as acceleration, with sequences sometimes representing locations further ahead or behind the animal (Gupta et al., 2012). To establish whether independent coding could also account for these results, we generated data from our model and applied the sequence identification and decoding analysis reported by Gupta et al. (2012). We found that, even for simulated data based on pure rate coding with no theta modulation ($k = 0$), large numbers of significant sequences were detected at high running speeds (Figure 2.14A). Therefore, to test the performance of the full

sequence detection and Bayesian decoding protocol used by Gupta et al. (2012), we analysed two simulated datasets - one with a realistic value of phase locking ($k = 0.5$, Figure 2.14B-D, solid lines) and another with zero phase locking (i.e., no theta related activity, Figure 2.14B-D, dashed lines). In both cases, applying the reported Bayesian decoding analysis yielded similar decoded path lengths to those found experimentally (Figure 2.14C, D). Importantly, there was an inverse relationship between the ahead and behind lengths decoded from the simulated data, which reproduces the apparent shift in sequences ahead or behind the animal observed in experimental data (cf. Gupta et al. (2012), Figure 4c). This effect was dependent on the density of recorded place fields on the track and the threshold for the minimum number of cells in a theta cycle required for sequence selection (Figure 2.15). As these results were obtained both in the case with realistic phase coding and in the case with only rate coding (and therefore no theta sequences), the properties of the decoded trajectories are not related to theta activity within the population. Hence, these data do not constrain models of theta activity in CA1.

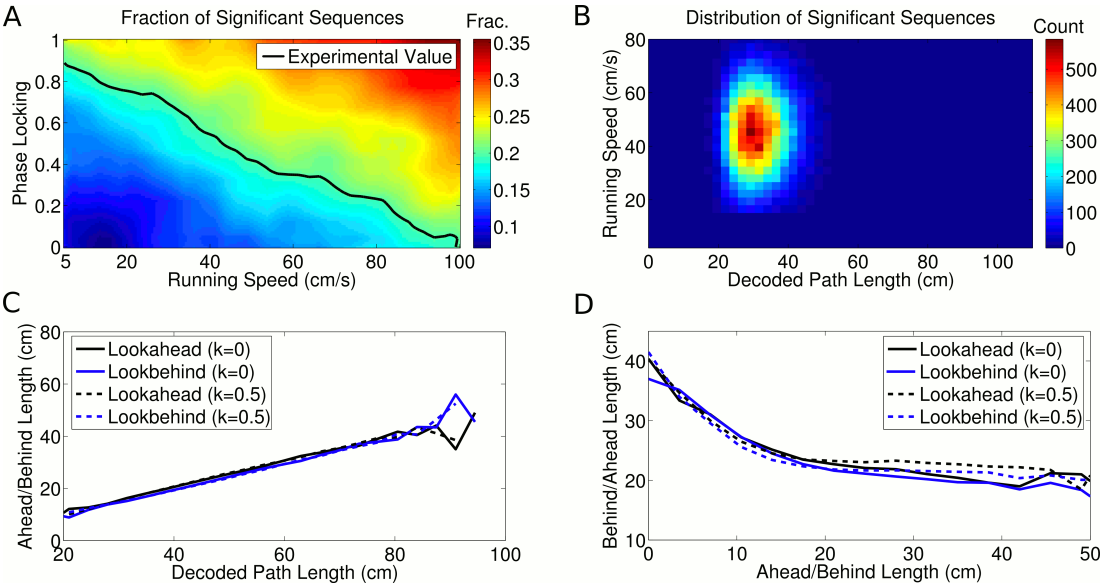

Figure 2.14: **Analysis of individual sequence statistics.**

(A) The fraction of theta cycles which are classified as "significant sequences" according to the Gupta et al. (2012) analysis, as a function of running speed and phase locking (for simulated data generated under the independent coding model). Large fractions of significant sequences are generated even without phase coding or theta sequences within the population (i.e. at $k = 0$). The black line shows the fraction reported experimentally. (B) The distribution of significant sequences over running speed and decoded path length for simulated data with phase locking $k = 0.5$, as calculated by Gupta et al. (2012) (cf. their Fig 1c). (C) The relationship between decoded path length and decoded ahead and behind lengths for significant sequences, calculated for a dataset with no theta activity ($k = 0$) and a dataset with realistic theta activity ($k = 0.5$). (D) The relationship between the ahead length of the sequence and the behind length of the sequence for these two datasets. Note that the properties of the decoded trajectories do not depend on the theta activity in the data. This replicates the experimental data (cf. Fig 4a-c in Gupta et al. (2012)), showing that similar trajectories are decoded by this algorithm regardless of the presence of theta sequences.

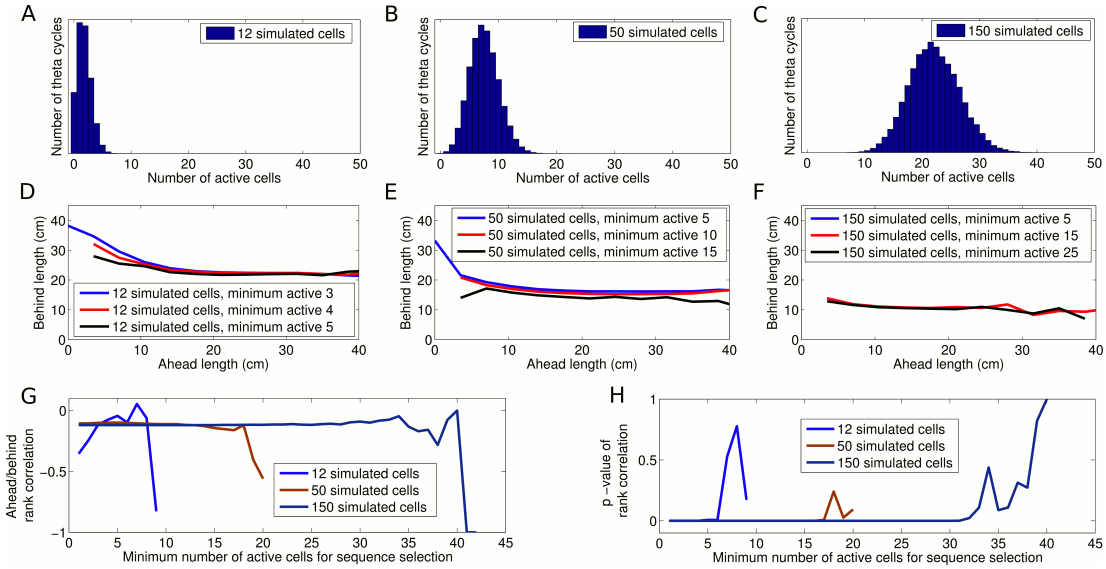

Figure 2.15: **Dependence of decoded trajectories on the number of cells in a sequence.**

(A)-(C) Distributions of the number of cells which spike in a theta cycle, for simulations of the independent coding model with different densities of place fields on the track (i.e., different numbers of place fields on a track of fixed length). (A) shows the cell density used to reproduce the results of Gupta et al. (2012). (B) and (C) show simulations with higher place field densities in which more active cells are recorded in each theta cycle on average. (D)-(F) Relationship between decoded ahead and behind length, calculated as in Gupta et al. (2012), shown for simulations with different place field densities and for different thresholds of the minimum number of cells required for a sequence to be included for analysis. (D) Simulations with 12 cells on the track and a threshold of 3 cells generate results similar to Gupta et al. (2012). (E)-(F) The density of place fields on the track and the threshold for sequence selection affect the decoded trajectories, with higher values for either resulting in a smaller change in behind length as a function of ahead length. (G)-(H) Spearman's rank correlation between ahead length and behind length for different place field densities plotted as a function of the threshold for the minimum number active of cells. Although the magnitude of the effect shown in (D)-(F) is diminished as these quantities increase, the correlation between ahead and behind length stays constant. Moreover, this correlation remains significant despite the decreasing effect size. Only when the number of selected sequences becomes too low to maintain a reliable measure does the effect become insignificant.

Interim summary

In total, our analysis demonstrates that a travelling wave model based on independent phase coding for CA1 theta states is consistent with existing experimental data. Thus, neither intra- nor inter-assembly interactions are required to explain spike sequences observed in CA1 during theta states. Our analyses of experimental data along with simulations from each hypothesis render it unlikely that assembly coordination significantly shapes the structure of theta sequences or CA1 cell assemblies. Below, we investigate some functional consequences of the independent coding and coordinated assembly hypotheses and show that, despite the advantage of assembly coordination in generating robust sequential activity patterns, it suffers from severe limitations in remapping and storage of multiple spatial maps. Independent coding offers a solution to this problem, allowing flexible generation of sequential activity over multiple spatial representations.

2.7 Linear phase coding constrains global remapping

What are the advantages of independent coding compared to sequence generation through interactions between cell assemblies? When an animal is moved between environments, the relative locations at which place cells in CA1 fire seem to remap independently of one another (e.g., O'Keefe and Conway, 1978; Wilson and McNaughton, 1993). This global remapping of spatial representations poses a challenge for generation of theta sequences through coordinated assemblies as synaptic interactions that promote formation of sequences in one environment would be expected to interfere with sequences in a second environment. Indeed, in the coordinated assembly model, simulations of remapping reduced single cell phase precession to below the level of independent cells (i.e., of an identical simulation with interactions between cells removed). Remapping in the coordinated coding model also substantially reduced firing rate and population oscillations (Figure 2.16). This decrease in firing rate following remapping contradicts experimental data showing an increase in firing rate in novel environments (Karlsson and Frank, 2008). It is not immediately clear whether the independent coding model faces similar constraints on sequence generation across different spatial representations. We therefore addressed the feasibility of maintaining theta sequences following remapping given the assumptions that underpin our independent coding model.

We first consider the possibility that following remapping the phase lags between cell pairs remain fixed - that is, while two cells may be assigned new firing rate fields, their relative spike timing within a theta cycle does not change. This scenario would occur if the phase lags associated with phase precession were generated by intrinsic network architectures (e.g., Diba and Buzsáki, 2008; Geisler et al., 2010; Dragoi and Tonegawa, 2011, 2013b) or upstream pacemaker inputs. For fixed phase lags, place cells display linear phase coding, whereby a cell continues to precess in phase outside of its rate coded firing field at a constant rate (Figure 2.17A). In this scenario, the phase lag between two neurons depends linearly on the distance between their place field centres, while cells separated by multiples of a place field width share the same phase (Figure 2.17A). Each cell pair therefore has a fixed phase lag in all environments and all cells can in principle be mapped onto a single chart describing their phase ordering (Figure 2.17A). If this mechanism for determining phase ordering is hardwired, then following arbitrary global remapping, cells with nearby place field locations will in most cases no longer share similar phases (Figure 2.17B). As a result, theta sequences and the global population theta will in general be abolished (Figure 2.17B). However, there exist a limited set of remappings which in this scenario do not disrupt the sequential structure of the population (e.g., Figure 2.17C). On a linear track, these remappings are: translation of all place fields by a fixed amount, scaling of all place fields by a fixed amount and permuting the place field locations of any cell pair with zero phase lag.

When considering global remapping in an open environment similar constraints apply. Because the phase lag between any two cells depends on running direction (e.g., Huxter et al., 2008), the population phase ordering must always be aligned with the direction of movement (Figure 2.17D). Hence, in open environments, the notion of a phase chart must be extended to include a fixed phase ordering for each running direction. Given such a fixed phase chart, a set of remappings known as *affine transformations* preserve the correct theta dynamics (see Appendix A). Such remappings consist of combinations of linear transformations (scaling, shear, rotation and reflection) and translations (Figure 2.17E). Remappings based on permutation of place field locations of synchronous cells, which are permissible in one dimensional environments, are no longer tenable in the two dimensional case due to constraints over each running direction.

Since place cell ensembles support statistically complete (i.e. non-affine) remappings (e.g., O'Keefe and Conway, 1978) while maintaining phase precession, CA1

network dynamics are not consistent with the model outlined above. Moreover, this analysis demonstrates that previous models based on fixed temporal delays between cells (e.g., Diba and Buzsáki, 2008; Geisler et al., 2010) cannot maintain theta sequences following global remapping. Nevertheless, it remains possible that CA1 theta dynamics are based on fixed phase charts, provided that multiple such phase charts are available to the network, similar to the multiple attractor charts which have been suggested to support remapping of firing rate (Samsonovich and McNaughton, 1997). In this case, each complete remapping recruits a different phase chart, fixing a new set of phase lags in the population. The number of possible global remappings that maintain theta sequences is then determined by the number of available phase charts. Such a possibility is consistent with recent suggestions of fixed sequential architectures (Dragoi and Tonegawa, 2011, 2013b) and has not been ruled out in CA1. It is also of interest that affine transformations are consistent with the observed remapping properties in grid modules (Fyhn et al., 2007), suggesting that a single phase chart might be associated with each grid module.

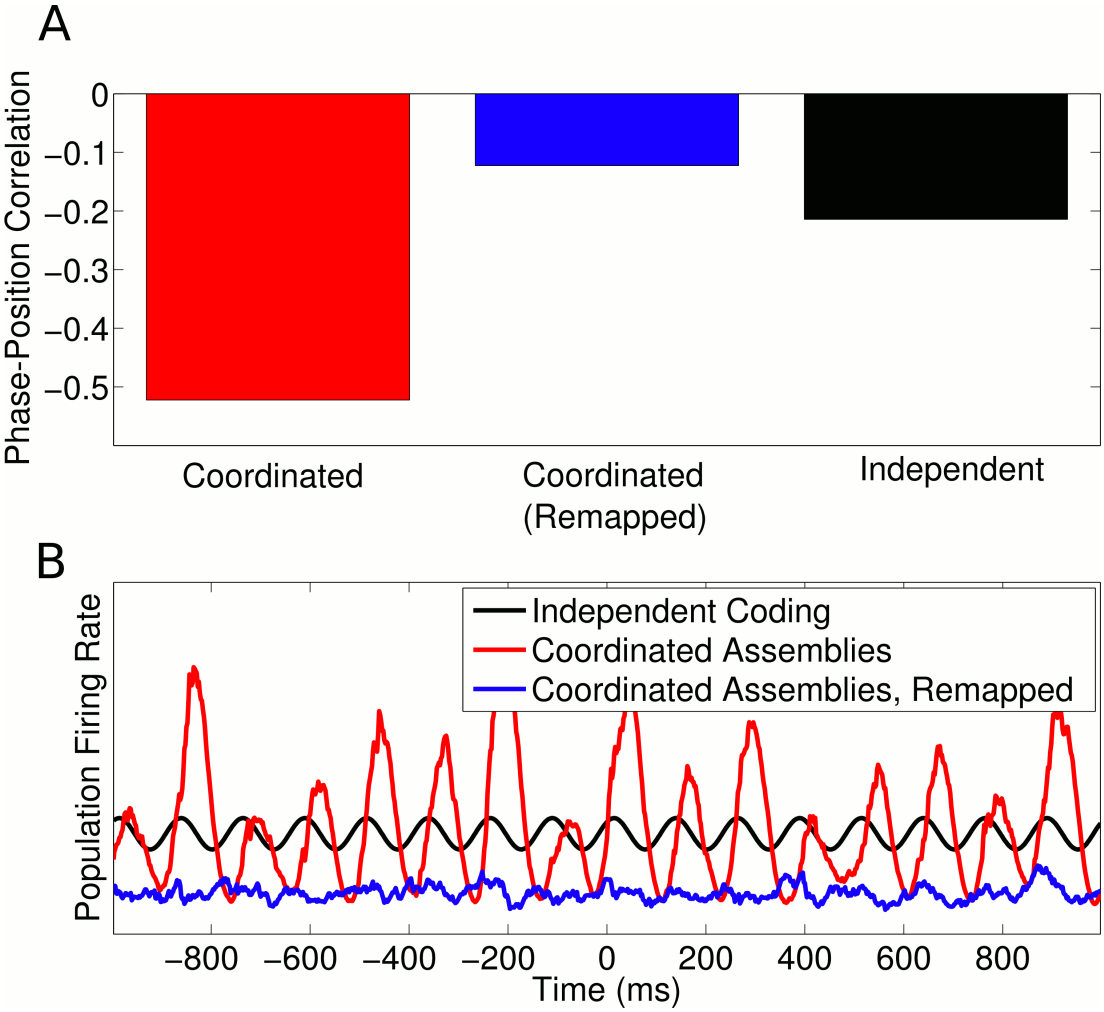

Figure 2.16: **Remapping with coordinated assemblies.**

(A) Comparison of single cell phase precession generated by coordinated assemblies (before and after remapping) and independent coding. For this simulation, single cell phase and rate fields were assumed to be perfectly remapped, so that any changes are purely due to assembly interactions. Note that, while assembly interactions improve phase coding in single cells in the initial environment, after remapping these same interactions disrupt phase precession and cause a lower (circular-linear) correlation between spike phase and animal location than that generated by independent cells. (B) Population firing rate on a single trial along a linear track. While assembly interactions initially entrain and amplify theta oscillations in the population compared to independent cells, after remapping these interactions disrupt theta activity and cause a lower overall activity level.

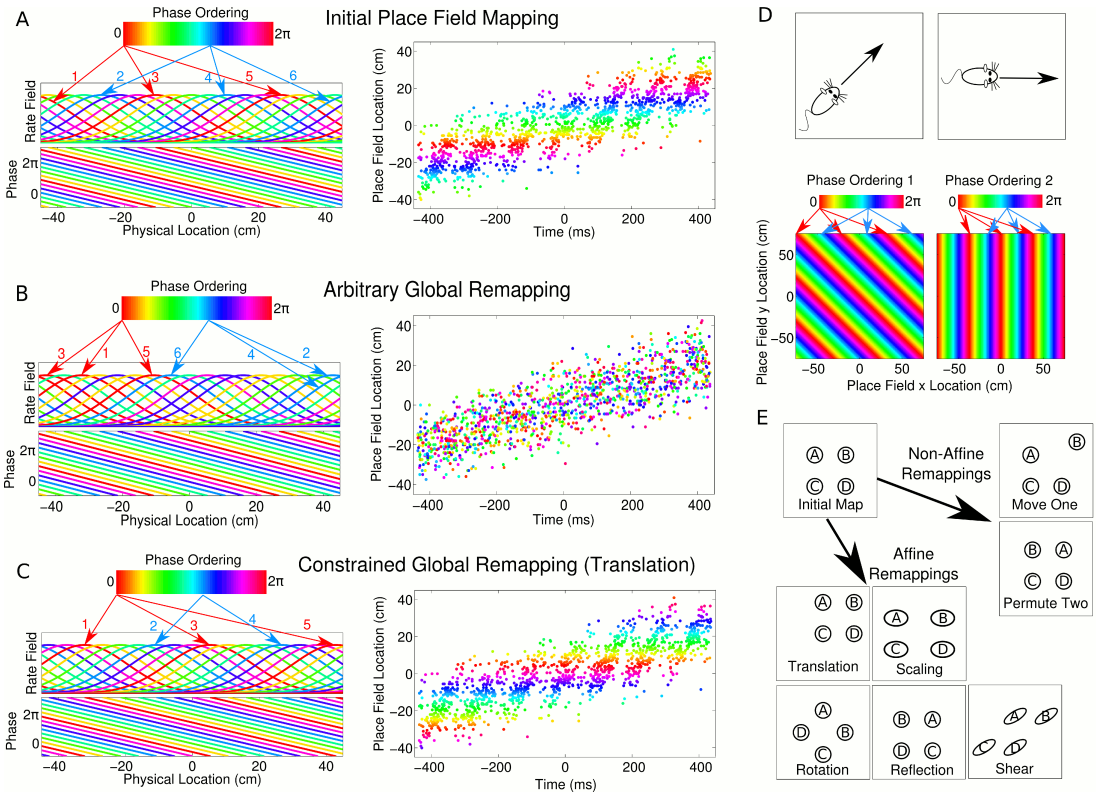

Figure 2.17: **Properties of CA1 populations governed by linear phase coding.** (A) On a linear track, cells which precess linearly in phase maintain fixed theta phase lags. This is illustrated as a phase ordering (coloured bar), which describes the relative phase of each cell (arrows and numbers show locations of place fields at each phase). Each cell has a constant, running speed dependent frequency and a fixed phase offset to each other cell. (B) A complete global remapping with phase lags between cells held fixed. Theta sequences and population oscillations are abolished. (C) In a constrained place field remapping, theta sequences are preserved. (D) In open environments, phase lags depend on running direction. The set of population phase lag configurations needed to generate sequences in each direction is called a phase chart. (E) If a population has a fixed phase chart, the possible remappings are restricted to affine transformations.

2.8 Sigmoidal phase coding enables flexible global remapping

The above analysis demonstrates that both coordination of assemblies and independent, linear phase coding pose severe restrictions on global remapping which appear at odds with experimental observations. We asked if it is possible to overcome these constraints so that phase sequences can be flexibly generated across multiple environments. We reasoned that experimental data on phase precession only imply that phase precesses within a cell's firing field and need not constrain a cell's phase outside of its firing field. In particular, place cells show intrinsic theta frequency membrane potential oscillations (MPOs) even when the animal is outside of their firing rate field, so that the cell is not spiking (e.g., Harvey et al., 2009). This implies that a place cell has a well defined intrinsic theta phase which extends across the environment, even when the cell is not spiking. We therefore implemented a version of the independent coding model in which firing phase has a sigmoidal relationship with location (Figure 2.18A-B, solid line), such that phase precesses within the firing field but not outside of the field. In this case, each cell's intrinsic frequency increases as the animal enters the spatial firing field and drops back to LFP frequency when the animal exits the firing field (Figure 2.18C, solid line). This is in contrast to the linear phase model and previous work with fixed delays (Geisler et al., 2010) in which each cell's intrinsic frequency is always faster than the population oscillation, both inside and outside of the place field (Figure 2.18C, dashed line). In a given environment, spike phase precession and sequence generation in a population of cells with sigmoidal phase coding (Figure 2.18D-F) are similar to models in which cells have linear phase coding. However, in addition, sigmoidal phase coding enables theta sequences to be generated after any arbitrary global remapping (Figure 2.18G). This flexible global remapping is in contrast to the scrambling of theta sequences following global remapping when cells have linear phase coding (Figure 2.18G). Thus, independent sigmoidal coding is able to account for CA1 population activity before and after global remapping. Mathematical details of the sigmoidal phase coding model are given below.

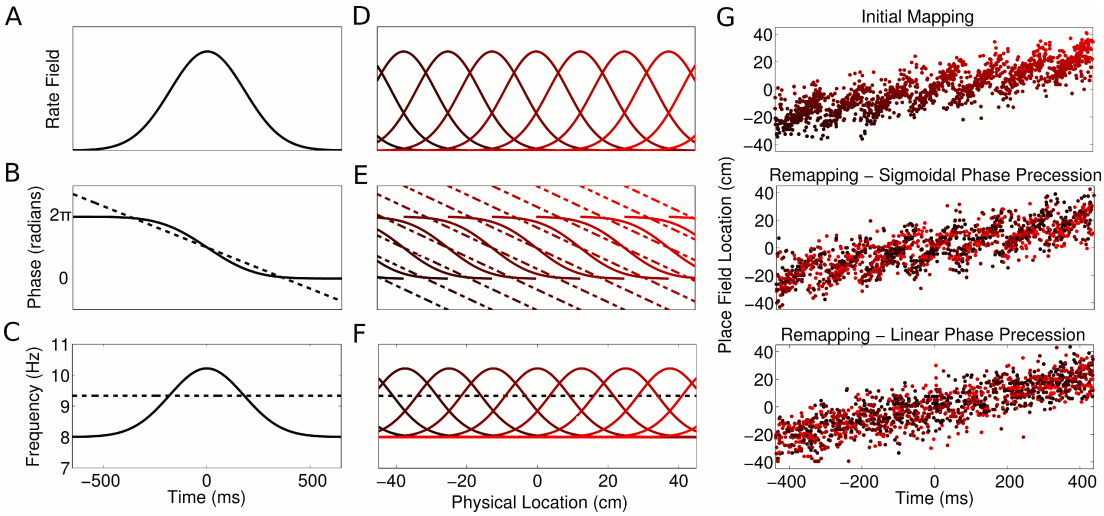

Figure 2.18: **Properties of CA1 populations governed by sigmoidal phase coding.** (A-C) Firing rate and intracellular phase and frequency in the linear (dashed lines) and sigmoidal models (solid lines) during the crossing of a place field. In the sigmoidal model, phase precession is initiated inside the place field by an elevation of intracellular frequency from baseline. (D-F) Firing rate and intracellular phase and frequency for a place cell population on a linear track. In the sigmoidal model, an intracellular theta phase lag between cell pairs develops as the animal moves through their place fields. Outside their place fields, cell pairs are synchronised. (G) Global remapping in the linear and sigmoidal models. The sigmoidal model allows arbitrary remapping without disrupting population sequences.

Analysis of sigmoidal phase coding

Here we propose a model for a cell's intrinsic theta phase which matches the above travelling wave model for cells in the population that are spiking, but which differs outside the place field where the cell is silent. Since the above models were based on considerations of data from spiking neurons, the extension of a linear phase gradient outside of the place field is not guaranteed, and several studies support a sigmoidal phase gradient (Chance, 2012; Diba and Buzsáki, 2008).

To model a sigmoidal phase gradient, we assume that the frequency of a place cell depends only on the distance of the animal from the centre of the place field x_c (Figure 2.18C):

$$f(x_c,t) = f_\theta + \Delta f \exp\left(\frac{-(x_c - vt)^2}{2\sigma^2}\right) \tag{2.31}$$

where Δf is the increase in frequency at the centre of the place field. We can then calculate the phase as a function of time, as the rat moves through the field at constant

velocity v:

$$\begin{aligned}\psi(x_c,t) &= 2\pi\int_0^t f(x_c,\tau)d\tau + \psi(x_c,0)\\ &= 2\pi f_\theta t - \frac{\pi^{3/2}\sqrt{2}\Delta f\sigma}{v}\left(\mathrm{erf}\left(\frac{x_c-vt}{\sqrt{2}\sigma}\right)-\mathrm{erf}\left(\frac{x_c}{\sqrt{2}\sigma}\right)\right)+\psi(x_c,0)\end{aligned} \quad (2.32)$$

If each cell precesses from 2π to 0, we can set $\lim_{t\to-\infty}[2\pi f_\theta t+\theta_s-\psi(x_c,t)]=2\pi$ and $\lim_{t\to+\infty}[2\pi f_\theta t+\theta_s-\psi(x_c,t)]=0$ to find $\psi(x_c,0)$, so that:

$$\psi(x_c,t) = 2\pi f_\theta t - \pi\,\mathrm{erf}\left(\frac{x_c-vt}{\sqrt{2}\sigma}\right)+\theta_s-\pi \quad (2.33)$$

which also gives $\Delta f = v/(\sqrt{2\pi}\sigma)$. This model reduces the number of parameters by explaining the rate of phase precession f_ϕ (Equation (2.5)) purely in terms of the place field width σ, eliminating the second scale parameter R from the model and allowing experimental predictions based on fewer alterable parameters.

For the sigmoidal model, the extension to navigation in two dimensions is straightforward. The frequency of the cell is simply a function of the distance to the centre of the place field, and hence the phase is given by:

$$\psi(\mathbf{x_c},t) = 2\pi f_\theta t + \frac{\sqrt{2\pi}}{\sigma}\int_0^t |\mathbf{v}(t')|\exp\left(-\frac{(\mathbf{x}(t')-\mathbf{x_c})^2}{2\sigma^2}\right)dt' + \psi(\mathbf{x_c},0) \quad (2.34)$$

where we used Equation (2.31) and the expression for Δf.

Experimental predictions for linear vs sigmoidal phase coding

Linear and sigmoidal models of phase coding lead to distinct experimentally testable predictions. Recordings of the membrane potential of CA1 neurons in behaving animals show that although spikes precess against the LFP, they always occur around the peak of a cell's intrinsic membrane potential oscillation (MPO) (Harvey et al., 2009). Therefore the intrinsic phase ϕ of each cell in our model (Figure 2.2D, E) can be interpreted as MPO phase. While data concerning the MPO phase outside of the firing field are limited, such data would likely distinguish generation of theta sequences based on a linear and sigmoidal phase coding. If CA1 implements linear phase coding, then the MPO of each cell should precess linearly in time against LFP theta at a fixed (velocity dependent) frequency, both when the animal is inside the place field and when the animal is at locations where the cell is silent (Figure 2.18A-C, dashed line). Alternatively, sigmoidal phase coding predicts that precession of the MPO against the LFP

occurs only inside the firing rate field (Figure 2.18A, B solid line) and that the MPO drops back to the LFP frequency outside of the place field (Figure 2.18C solid line) as reported by Harvey et al. (2009). A further prediction of sigmoidal coding is that, in contrast to models based on fixed delays (Diba and Buzsáki, 2008; Geisler et al., 2010), the phase lag between any two cells changes when the animal moves through their place fields. Outside their place fields the cells are synchronised with each other and with the LFP, whereas a dynamically shifting phase lag develops as the animal crosses the place fields. Finally, phase precession under the sigmoidal model behaves differently to the linear model in open environments. In the linear model, the phase chart fixes a different population phase ordering for each running direction, so that spike phase depends on the location of the animal and the instantaneous direction of movement. In the sigmoidal model, however, each cell has a location dependent frequency, so that the spike phase depends on the complete trajectory through the place field and no explicit directional information is required. Rather, the directional property of the sequence arises purely through a location dependent oscillation frequency in each cell combined with the trajectory of the animal through each place field. In summary, our analysis demonstrates how evaluation of theta sequences following global remapping and of theta phase within and outside of a cell's firing field will be critical for distinguishing models of CA1 assemblies and theta generation.

2.9 Discussion

Our analysis demonstrates how complex and highly structured population sequences can be generated without coordination between neurons. In contrast to previous suggestions (Harris et al., 2003; Dragoi and Buzsáki, 2006; Foster and Wilson, 2007; Maurer et al., 2011; Gupta et al., 2012), we find that the theta-scale population activity observed in CA1 is consistent with phase precession in independent cells, without interactions within or between cell assemblies. We demonstrate that independent coding enables flexible remapping of CA1 population activity while maintaining the ability to generate theta sequences. These properties are consistent with maximisation of the capacity of CA1 for representation of distinct spatial experiences.

The independent coding hypothesis leads to a novel view of the CA1 population as a fast moving travelling wave with a slower modulatory envelope. This model implements an invariant phase code via a change in the frequency and temporal delay between cells with running speed. Amplitude modulation of the envelope provides a

mechanism for multiplexing spatial with nonspatial information, such as task specific memory items (Wood et al., 2000) and sensory inputs (Rennó-Costa et al., 2010). The independence of each neuron naturally explains the robustness of phase precession against intrahippocampal perturbations (Zugaro et al., 2005), an observation which is difficult to reconcile with models based on assembly interactions. Depending on the exact nature of the single cell phase code, independent phase coding can enable theta sequences to be maintained with arbitrary global remapping. This flexibility may maximise the number and diversity of spatial representations that CA1 can provide to downstream structures, offering a strong functional advantage over mechanisms based on interactions between cell assemblies.

Independent phase coding leads to new and experimentally testable predictions that distinguish mechanisms of CA1 function during theta states. First, an absence of coordination within or between assemblies has the advantage that neural interactions do not interfere with sequence generation after global remapping. Rather, for independent coding models the constraints on sequence generation following remapping arise from the nature of the phase code. With linear phase coding the set of sequences available to the network is fixed, resulting in a limited set of place field configurations with a particular mathematical structure (Figure 2.17). Interestingly, the remappings observed in grid modules (Fyhn et al., 2007), but not CA1, are consistent with those predicted for networks with a single fixed set of theta phase lags called a phase chart. Specifically, grid modules appear to remap via combinations of rotation, scaling, translation and shear as predicted by the linear model (Fyhn et al., 2007). These findings, together with the fact that the temporal delays between cells depend on running speed, argue against previous models based on fixed delays within CA1 populations (Diba and Buzsáki, 2008; Geisler et al., 2010). Nevertheless, more complex scenarios with multiple phase charts could explain CA1 population activity during theta oscillations and "preplay", which suggests a limited remapping capacity for CA1 (Dragoi and Tonegawa, 2011, 2013b). Alternatively, sigmoidal phase coding massively increases the flexibility for global remapping as cells can remap arbitrarily while maintaining coherent theta sequences within each spatial representation (Figure 2.18). Second, linear and sigmoidal phase coding predict distinct MPO dynamics. With linear phase coding the temporal frequency of each MPO is independent of the animal's location. With sigmoidal phase coding, the MPO frequency increases inside the place field, so that phase precession occurs inside but not outside the place field. In this case, only the spiking assembly behaves as a travelling wave, whereas the MPOs of cells with place fields

distant from the animal are phase locked to the LFP. Sigmoidal phase precession could emerge due to inputs from upstream structures (Chance, 2012) or be generated intrinsically in CA1 place cells (Leung, 2011). Finally, in contrast to linear phase coding populations, sigmoidal phase coding populations do not require additional information from head direction or velocity cells to generate directed theta sequences in open environments. Instead, sigmoidal theta sequences are determined solely by the recent trajectory of the rat through the set of place fields together with a location dependent oscillation frequency, consistent with recent observations of reversed theta sequences during backwards travel (Cei et al., 2014; Maurer et al., 2014). In summary therefore, these two models may be distinguished experimentally on the basis of observations of the number of non-affine remappings in CA1, the intracellular frequency and delay between place cells as a function of location and of the dependence of firing phase on the trajectory through a place field in open environments.

While theta sequences of CA1 activity are most commonly observed during spatial navigation, similar activity patterns associated with short term memory have been observed during wheel running (Pastalkova et al., 2008). In this situation each cell's activity depends on the phase of the LFP theta rhythm and on the temporal location within an "episode field" rather than a place field. Our model can be applied equally well to these internally generated sequences if the rate coded episode field is assumed to have a similar temporal structure to a place field. An entirely different class of sequences, however, is observed during non-theta states such as sharp wave ripples (SWR) (Buzsáki et al., 1992; Diba and Buzsáki, 2007). In contrast to theta sequences, SWR sequences are generally observed during states of immobility and are believed to arise from synchronous discharge in CA3 (Buzsaki et al., 1983). Because SWR sequences only occur at a single timscale and are therefore generated without co-occurrence of longer time-scale firing fields or theta oscillations, they cannot be accounted for by the independent coding schemes that we investigate here, in which rate and phase information determine the activity of each cell. Instead, the nature of cell assemblies in CA1 may be highly state dependent, operating in at least two modes. During theta states, sequences are generated by independently precessing neurons, whereas during SWRs sequences may result from interactions between consecutively activated cell assemblies. In particular, theta oscillations have been shown to decorrelate network activity, while more synchronous states in which cell assemblies may exist are observed during sharp wave ripple events (Mizuseki and Buzsaki, 2014)

Can independent coding account for manipulations that modify place cell dynam-

ics? Administration of cannabinoids disrupts phase precession by CA1 neurons and impairs spatial memory, but does not appear to affect the rate coded place firing fields of CA1 neurons (Robbe and Buzsáki, 2009). This dissociation between rate and phase coding can be accounted for in our model by assuming that rate fields are maintained while phase fields are disrupted (Figure 2.2A) or the degree of phase locking (k) is substantially reduced (Figure 2.2B). In contrast, increased in-field firing of place cells following optogenetic inactivation of hippocampal interneurons (Royer et al., 2012) can be accounted for in our model by increased N_{spikes}, while altered phase of place cell firing following inactivation of parvalbumin interneurons can be accounted for in our model by modifying the phase fields (Figure 2.2A) of the place cells. Important future tests of the independent coding model will include comparison of its predictions of sequence activity, remapping and intracellular dynamics to experimental measures made during these kinds of manipulations.

Our independent coding model offers a comprehensive account of population activity in CA1 during theta states and makes new predictions for coordination of network dynamics and remapping at the population level, but it does not aim to distinguish cellular mechanisms for phase precession. Nevertheless, by demonstrating that existing observations of population sequences can be explained by independent coding our model argues against mechanisms for phase precession that rely on synaptic coordination at theta time scales (e.g., Tsodyks et al., 1996; Maurer and McNaughton, 2007; Lisman and Redish, 2009). In contrast, our model does not distinguish between specific single cell mechanisms for phase precession such as dual oscillators (Lengyel et al., 2003; Burgess et al., 2007), depolarising ramps (Mehta et al., 2002), intrinsic membrane currents (Leung, 2011) or dual inputs from CA3 and entorhinal cortex (Chance, 2012). Our model is also consistent with inheritance of phase precession in CA1 from upstream circuits in CA3 and entorhinal cortex (Jaramillo et al., 2014). However, it argues against the possibility that CA1 inherits coordinated sequences from CA3 (Jaramillo et al., 2014). It is possible that CA3 nevertheless generates sequences by synaptic coordination. Because CA3 neurons are connected by dense recurrent collaterals (Miles and Wong, 1986; Le Duigou et al., 2014), there are likely to be substantial correlations in their output to CA1, which could induce deviations from the independent population code outlined here. However, feedback inhibition motifs such as those found in CA1 may counteract such correlations (Renart et al., 2010; Tetzlaff et al., 2012; Bernacchia and Wang, 2013; Sippy and Yuste, 2013; King et al., 2013). Hence, the local inhibitory circuitry in CA1 may actively remove

correlations present in its input in order to generate an independent population code (Ecker et al., 2010).

A major advantage of independently precessing cell populations is that they provide a highly readable, robust and information rich code for working and episodic memory in downstream neocortex. In particular, a downstream decoder with access to an independent population code need only extract the stereotyped correlational patterns associated with travelling waves under a given place field mapping, allowing it to flexibly decode activity across a large number of spatial representations. Decoding in the presence of additional correlations would likely lead to a loss of information (Zohary et al., 1994). While this loss can to some extent be limited by including knowledge of these additional correlations (Nirenberg and Latham, 2003; Eyherabide and Samengo, 2013), this likely requires a high level of specificity and therefore a lack of flexibility in the decoder. The flexibility afforded by an independent population code may therefore provide an optimal format for the representation and storage of the vast number of spatial experiences and associations required to inform decision making and guide behaviour.

2.10 Methods

Simulations of CA1 population activity

In the independent coding model, we simulated data from a population of place cells with place field centres x_c and width σ which precess linearly through a phase range of $\Delta\phi$ over a distance $2R$ on a linear track using Equation (2.22). The initial phase ψ_s was either taken as 0, or a uniform random variable $\psi_s \in [0, 2\pi)$ set at the beginning of each run. In all simulations, parameters were set as: $2R = 37.5$ cm (Maurer et al., 2006a), $\Delta\phi = 2\pi$, $\sigma = 9$ cm, $f_\theta = 8$ Hz (Buzsáki, 2002), $N_{\text{spikes}} = 15$ (Huxter et al., 2003). Finite numbers of place cells were simulated with place field centres x_c which were either uniformly distributed along a linear track with equal spacing or randomly sampled from a uniform distribution over the track. All cells were therefore identical up to a shift in place field centre x_c. Simulations were performed using Matlab 2010b and 2013b.

Simulations of population activity generated through coordinated assemblies used Equations (2.26-2.30), with the single cell properties simulated as for the independent coding model. The peer interaction timescale was set to $\tau = 25$ ms (Harris et al.,

2003), and the interaction length for asymmetric excitation was set to $\ell = 10$ cm with an excitatory amplitude of $w_E = 1/4$. The amplitude of the inhibitory weights was varied until the same number of spikes were generated as in the independent coding simulation (for the parameters used in these simulations, the inhibitory amplitude was $w_I = 1/18$).

Experimental datasets

We used data recorded from CA1 during navigation along a linear track. For details of experimental data see Mizuseki et al. (2014). For the analysis performed in this study, simultaneous recordings of a large number of coactive cells in CA1 is required, which restricted the number of suitable datasets. In particular, we used datasets *ec016.233*, *ec016.234*, *ec016.269*, *ec014.468*, *ec014.639*.

Prediction analyses (Section 2.5)

To replicate the results of Harris et al. (2003), we simulated constant speed movement along a linear track, with lap-by-lap running speeds drawn from a normal distribution with mean 35 cm/s and standard deviation of 15 cm/s. We simulated motion in each direction, using the same set of place fields in each case. We estimated the preferred firing phase at each location from the simulated data using the methods stated in Harris et al. (2003), using either single-direction data or data consisting of runs in both directions to generate nondirectional or directional phase fields. The prediction analysis was performed according to the methods given in Harris et al. (2003). Specifically, models of place fields and phase fields are fitted via maximum likelihood on a training dataset. These models are then used to predict the firing probability at each point in time given the animal's location and the LFP theta phase on a test dataset, under the assumption of Poisson firing with instantaneous rate determined by the fitted model. Finally, the predictability (or information) is quantified as the difference in the log likelihood of the full model versus a null model with a constant firing rate. By calculating this measure with a logarithm of base 2, we arrive at a measure of information in bits, and by dividing by the recording time of the test dataset we arrive at a measure in bits per second. The separation of the data into training in test datasets is a form of cross-validation, which guards against overfitting.

For these initial simulations (Figure 2.8), we used the simulated value of phase locking rather than estimating it from the data. To display the peer prediction perfor-

mance shown in Figure 2.8C, the optimal prediction timescale for each phase locking value was chosen. This was done separately for the peer only case and the peer plus phase field case.

We then performed additional, more detailed simulations to test the performance of simulated and experimental data when using the new directional phase fields. We separated datasets according to the running direction along a linear track, analysing each direction individually. In addition to fitting the place field, phase field and peer factor used by Harris et al. (2003), we also fitted a velocity modulation factor given by:

$$A(v) = \frac{\sum_t n_t w(|v - v_t|)}{\sum_t r_0(x_t)\, dt w(|v - v_t|)} \tag{2.35}$$

which estimates the changes in firing rate of a cell according to running speed. In the above equation, the notation follows that of Harris et al. (2003) (their Supplementary Information), i.e., w is a Gaussian smoothing kernel of width 3.5 cm/s, n_t is the number of spikes fired by the cell in time bin t, r_0 is the estimated firing rate field at location x, x_t is the animal's location in time bin t and v_t is its velocity. Our simulations showed that, using the methods of Harris et al. (2003), the phase locking parameter k was underestimated outside of the place field centre. Misestimation of phase field parameters introduces false peer predictability in simulated datasets. We therefore replaced their location-dependent estimation with a fixed value equal to the phase locking estimated in regions where the place field is over 2/3 its maximum value. We also found that the 5 cm spatial smoothing kernel used by Harris et al. (2003) resulted in a high level of spurious peer prediction in simulations based on independent coding, since it extended the boundaries of place fields, allowing non-overlapping peer cells to compensate via inhibitory weights. A smaller kernel of 3.5 cm reduced the rate of false positive for peer prediction and was therefore used instead. We simulated 300 cells in each session of which we randomly sampled 15 for analysis in order to match the number of place cells typically recorded experimentally. 28 laps were simulated for each session and 10 sessions were simulated in total (representing the 2 running directions over the 5 experimental sessions we analysed). Peer prediction was performed at a timescale of 25 ms (the optimal timescale in Harris et al. (2003)).

Changes in sequence properties with running speed (Section 2.6)

To compare the sequence path length in spiking data generated from the independent coding model to experimental data, we followed the decoding methods outlined in

Maurer et al. (2011). Briefly, this involves constructing trial averaged time by space population activity matrices in order to decode the location represented by the population in each time bin over an average theta cycle. The decoded path length is measured as the largest distance between decoded locations within the theta cycle. To test the influence of phase locking in this analysis, k was varied incrementally from 0 to 6 and the sequence path length for the resulting data was calculated in each case. We used the same spatial and temporal bins (0.7 cm and 20° of LFP θ) as the original study.

To calculate the fast and slow slopes, we generated the contour density plots described by Maurer et al. (2011) using the same parameters as the sequence path length analysis. We simulated 100 trials for each running speed. We then divided these 100 trials into 10 subsets of 10 and applied the contour analysis to each subset. We fitted the fast slope to the 95% contour of the central theta peak, and measured the slow slope as the line joining the maximum of the top and bottom peaks of the central 3. We averaged over the results from each subset to obtain the final value. The analytical value for the fast slope in the limit of high phase locking is $FS = v_p/(360 f_\theta)$, where the denominator arises due to the normalisation to cm/deg in the analysis of Maurer et al. (2011). Similarly for zero phase locking, $FS = v/(360 f_\theta)$. The analytical value for the slow slope is independent of phase locking, $SS = v/(360 f_\theta)$. Upper and lower bounds for the slow slope were therefore fitted assuming the reported running speed is accurate, and that the LFP theta frequency is in the range $4\text{Hz} < f_\theta < 12\text{Hz}$.

Shuffling analyses (Section 2.6)

To reproduce the results of Foster and Wilson (2007), we generated data from 1000 theta cycles, each with a running speed drawn from the same distribution as for the prediction analysis. Following the protocol outlined by Foster and Wilson (2007), we found the set of all spike phases for each cell when the rat was at each position and analysed events defined as 40 ms windows around firing rate peaks. Spike phases were calculated by interpolation between LFP theta peaks. For the shuffling analysis, each spike in an event was replaced by another spike taken from the same cell while the animal was at the same location. The new spike time was then calculated from its phase by interpolation between the closest two LFP theta troughs of the original spike, as reported in the original study. 100 such shuffles were performed for each event, and the correlation between cell rank order and spike times was calculated in each case.

For the corrected shuffling procedure, we followed the methods of Foster and Wil-

son (2007) but with the following adjustments: The correlations between spike times and place field rank order within an event calculated in the original study were replaced with circular-linear correlations between spike phase and place field peaks in order to remove issues arising from conversion between spike time and spike phase (Kempter et al., 2012); a minimum running speed of 20 cm/s and a maximum running speed of 100 cm/s were imposed; the LFP phase was measured using a Hilbert transform rather than a linear interpolation between theta peaks; spikes that occurred more than 50 cm away from the place field peak were discarded from the analysis. The circular-linear correlation requires a mild restriction of the range of possible regression slopes between the circular and linear variables, which in this case describes the distance travelled by a theta sequence within a theta cycle (Kempter et al., 2012). We set this range as $25 - 80$ cm/cycle, i.e. around the size of a place field. For simulations using this shuffling procedure, we simulated 300 cells in each session on a linear track and randomly sampled 15 of these for further analysis. We again simulated 10 sessions with 28 laps each, for which the number of detected events was similar to that of the experimental dataset. We generated a large number of such datasets in order to obtain a distribution of shuffling test results to compare against the experimental dataset.

Dependent and independent cells (Section 2.6)

To reproduce the results of Dragoi and Buzsáki (2006), we simulated population activity on a linear track. To recreate the experimental conditions of Dragoi and Buzsáki (2006), we set the track length as 250 cm and simulated 8 sessions (i.e., 4 animals by 2 running directions), each with 25 place cells. As the original experiment consisted of continuous locomotion around a rectangular track, we wrapped the boundaries of the linear track and simulated continuous sessions rather than single laps. Place fields were randomly distributed over the track following a uniform distribution. Running speed on each lap was drawn from the same distribution as the prediction and shuffling analyses. Phase locking was set to 0.5. We calculated the dependent and independent cell pairs following the methods of Dragoi and Buzsáki (2006), which uses temporal bins of 2 s to calculate firing rate correlations and a shuffling procedure to find significantly correlated cells.

Dragoi and Buzsáki (2006) did not state the number of dependent and independent cell pairs obtained from their analysis. Therefore, to compare the results of our simulations to their experimental data, we estimated the number of points in their cross-

correlogram lag plot for dependent and independent cell pairs (their Figure 3B) and compared the result to the same measure in our simulations. CCG plots were calculated using the methods described in Dragoi and Buzsáki (2006). Using this method, we found that 33% of cell pairs were dependent compared to an estimated 30-35% in Dragoi and Buzsáki (2006).

To calculate the reliability of temporal lags between dependent and independent pairs, Dragoi and Buzsáki (2006) took the central cloud of the CCG-lag vs place field distance scatter plot (their Figure 2A) and calculated the correlation between these two variables. However, the method for isolating the central cloud from the surrounding clusters was not disclosed. Without this information, we were unable to reproduce this analysis.

To test for differences between place field separations of dependent and independent cell pairs, we again considered only cell pairs whose CCG lags passed the inclusion criteria (as described in Dragoi and Buzsáki (2006)). We compared the vectors of cell pair separations for each group.

Decoding individual sequences (Section 2.6)

To reproduce the results of Gupta et al. (2012), we used the significant sequence testing protocol and Bayesian decoding algorithm described therein, with spatial binning set as 3.5 cm, as in the original study. Briefly, the significant sequence testing analysis tests if population activity within a theta cycle has significant sequential structure, whereas the Bayesian decoding algorithm generates a time by space probability distribution which is used to decode the ahead and behind lengths represented by the theta sequence. For Figure 2.14A, we varied phase locking and running speed independently and generated spiking data for each pair of values. In the simulations used to generate Figure 2.14, we assumed that the number of spikes fired per theta cycle does not vary with running speed, as such a dependence introduces an additional change of the decoded sequence path length with running speed. In order to best match the fraction of theta cycles with 3 or more cells active reported by Gupta et al. (2012), each simulated theta cycle contained 12 place cells with place fields randomly distributed over a region of space 94.5 cm ahead or behind the rat. We then applied the significant sequence detection methods for each resulting data set to obtain the fraction of significant sequences in each case. For Figure 2.14B, we used $k = 0.5$ and generated 1000000 theta cycles, each with a running speed drawn from a normal distribution with mean 30 cm/s and

standard deviation 10 cm/s. Running speeds less than 10 cm/s were discarded and the remaining theta cycles were tested for significant sequential structure. For Figure 2.14 C&D, we applied the Bayesian decoding algorithm to these significant sequences in order to calculate the path length, ahead length and behind length. In addition, we applied the same analysis to another dataset simulated with $k = 0$.

Remapping simulations (Sections 2.7-2.8)

To simulate remapping in the coordinated assembly model, we simulated spiking activity for a population of 300 cells on a linear track with weights given by Equation (2.26). To simulate the remapped population, we left this set of weights intact but randomly reassigned the place and phase fields of each cell, such that phase coding and rate coding were perfectly remapped but peer interactions were preserved between environments.

To simulate remapping in the linear phase coding model, we assumed that phase lags were preserved between environments. The remapped population was simulated by randomly permuting the place field centres of cells while leaving the phase fields of each cell intact.

To simulate remapping in the sigmoidal phase coding model, we assumed that the field of elevated frequency is locked to the place field before and after remapping. Hence, place fields were randomly permuted and the single cell frequency was defined to increase within the new place field.

Chapter 3

Phase Coding in Grid Cell Modules

3.1 Introduction

In this section we extend the phenomenological models of Chapter 2 to entorhinal grid cells. In particular, while the results of the last section suggest that linear phase coding, in which a fixed phase chart underlies the ordering of cells at theta timescales, is inconsistent with CA1 global remapping, we found it to be fully consistent with the forms of remapping observed in grid cell modules (Fyhn et al., 2007). However, the spatial symmetries of grid cell firing fields complicate the simple picture analysed for place cells in the previous chapter, and it is therefore not clear that the dynamics of linear phase coding under fixed phase charts and the corresponding constraints for firing field remapping discussed in the previous chapter apply to grid cell modules.

In this chapter, we show that the spatial symmetries of grid cell activity patterns impose strong constraints on linear phase coding which create problems for generating self-consistent phase coding in two-dimensional environments. By analysing the properties of sigmoidal phase coding in grid cells, we go on to show that the basic form of sigmoidal phase coding outlined in Chapter 2 faces similar problems with two-dimensional phase coding in grid cells. To overcome these problems, we introduce a more biophysically grounded form of sigmoidal phase coding which includes an active synchronisation term in order to reset the intracellular theta phase between firing fields. This model can account for phase precession in open environments in both grid cells and place cells and provides the basis for a mechanistic model of phase precession which we discuss in Chapter 4.

3.2 Grid cell firing rate model

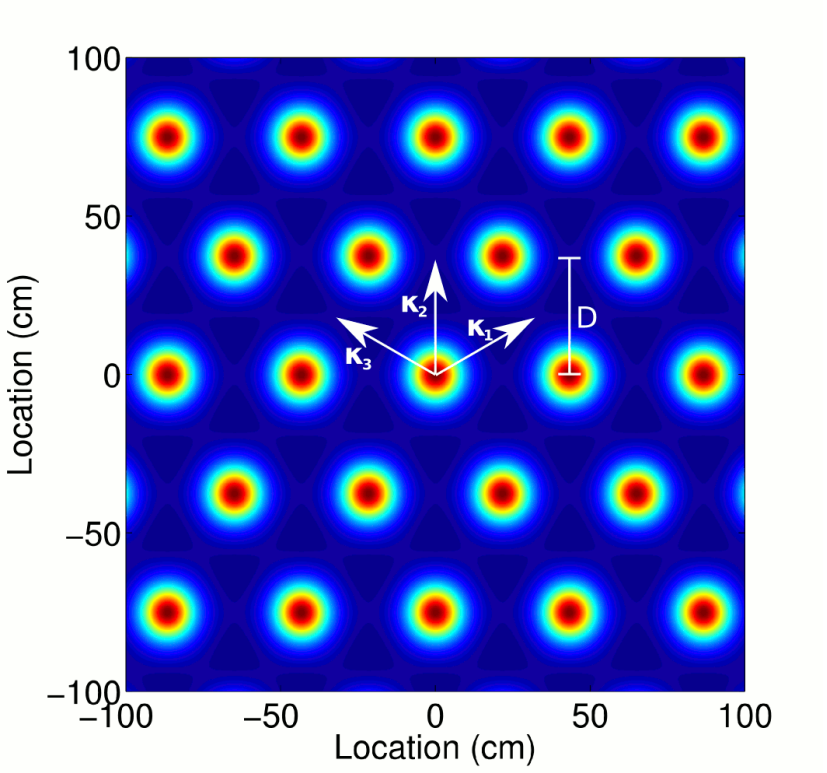

Figure 3.1: Firing rate of a single grid cell over space, or equivalently a snapshot of the firing rate of a grid module, with orientation $\phi_x = 30^\circ$

To describe the firing rate of a grid cell as a function of the animal's location, we constructed a model based on the combined activity of three plane waves at different orientations. Specifically, the firing rate r_x of a grid cell as a function of the animal's location $\mathbf{x}$ can be modelled as a product of von Mises functions:

$$r_x(\mathbf{x},\mathbf{x_c}) = A\exp\left(k_x\cos\left(\boldsymbol{\kappa_1}\cdot(\mathbf{x}-\mathbf{x_c})\right)\right)\exp\left(k_x\cos\left(\boldsymbol{\kappa_2}\cdot(\mathbf{x}-\mathbf{x_c})\right)\right)\exp\left(k_x\cos\left(\boldsymbol{\kappa_3}\cdot(\mathbf{x}-\mathbf{x_c})\right)\right) \tag{3.1}$$

where $\boldsymbol{\kappa_i}$ are two-dimensional wavevectors for these three plane waves which determine the orientation and scale of the grid map, $\mathbf{x_c}$ is the location of any grid field centre, which sets the spatial phase of the cell and k_x sets the grid field size relative to their separation (Figure 3.1). In particular, a large value of k_x will lead to narrow, highly peaked grid fields.

This model describes the firing rate of a grid cell in terms of three plane waves at different angles, which integrate the animal's motion along three directions. For isotropic grid maps (i.e., without shear or squeezing), the wavevectors are separated

by exactly 60°:

$$\boldsymbol{\kappa_1} = \frac{2\pi}{D}(\cos(\phi_x), \sin(\phi_x)) \tag{3.2}$$

$$\boldsymbol{\kappa_2} = \frac{2\pi}{D}(\cos(\phi_x + \pi/3), \sin(\phi_x + \pi/3)) \tag{3.3}$$

$$\boldsymbol{\kappa_3} = \frac{2\pi}{D}(\cos(\phi_x + 2\pi/3), \sin(\phi_x + 2\pi/3)) \tag{3.4}$$

where ϕ_x is the orientation of the grid and D determines the grid scale. Specifically, if we define d to be the shortest distance between grid field peaks, then $d = (2/\sqrt{3})D$ (compare Figure 3.1 to Figure 3.2, top panel). Note also that these vectors form an overcomplete, non-orthogonal basis as $\boldsymbol{\kappa_3} = \boldsymbol{\kappa_2} - \boldsymbol{\kappa_1}$.

This firing rate exhibits translational symmetry. For the isotropic case described in Equations (3.2)-(3.4), the firing rate function is invariant under spatial translations $\boldsymbol{\Delta}$ of the form:

$$\mathbf{x_c} \to \mathbf{x_c} + \boldsymbol{\Delta}, \quad \boldsymbol{\Delta} = \frac{2}{3}D((i-j)\hat{\boldsymbol{\kappa}}_\mathbf{1} + (i+2j)\hat{\boldsymbol{\kappa}}_\mathbf{2}) \qquad i, j \in \mathbb{Z} \tag{3.5}$$

where $\hat{\boldsymbol{\kappa}}_\boldsymbol{i} = \boldsymbol{\kappa_i}/|\boldsymbol{\kappa_i}|$ are the wavevectors after normalisation to unit length. This set of translations $\boldsymbol{\Delta}$ corresponds to the set of vectors between a given grid field peak and all other grid field peaks. In addition to these translations of $\mathbf{x_c}$, the firing rate is invariant under the same set of transformations of the animal's location $\mathbf{x}$.

3.3 Desiderata for phase coding in grid cells

Certain properties are generally assumed to be necessary for phase coding in grid cells, either explicitly or implicitly. In phenomenological models of grid cells in one-dimensional environments, firing fields are typically modelled as a simple sinusoid (or a similar periodic function), and the firing phase is assumed to precess over 2π at a constant rate between successive grid field peaks, so that the firing phase returns to the same value whenever the animal arrives at a location for which the grid cell has the same spatial phase (e.g., Thurley et al., 2013; Jaramillo et al., 2014). This requires that the precession frequency of a grid cell is proportional to the distance between grid field peaks and inversely proportional to running speed, $f_\phi = d/v$. A similar property which is generally assumed tacitly rather than explicitly in models of grid cells is that, at any point in time, two grid cells with the same spatial phase, orientation and grid spacing (i.e., two identical grid cells) should have the same intrinsic theta phase.

In the more general two-dimensional case, these properties can be formally expressed as translational symmetries in both time and space. In particular, they are specific cases of a more general assumption that the theta phase in grid cell populations should respect the same translational symmetries as the firing rate. The first property states that the time-translation symmetry inherent in the firing rate as an animal travels along a straight path between grid fields is also respected by the firing phase. Specifically, given a trajectory $\mathbf{x}(t) = \mathbf{v}t + \mathbf{x_0}$, if $r_x(\mathbf{x}(t+T), \mathbf{x_c}) = r_x(\mathbf{x}(t), \mathbf{x_c}) \forall t$, then $\phi(t+T, \mathbf{x_c}) = \phi(t, \mathbf{x_c}) \forall t$. Here, T is a temporal shift which leaves the firing rate invariant. In the simple one-dimensional case described in the above paragraph, the only possible values are $T = nd/v$ for integer n. However, the general two-dimensional case can be more complex, depending on the running direction of the animal.

The second property described above states that the spatial translation symmetry present in the firing rate distribution over a grid cell module is also respected by the intrinsic theta phase distribution over the grid cell module at any instant in time. Specifically, if $r_x(\mathbf{x}(t), \mathbf{x_c} + \mathbf{\Delta}) = r_x(\mathbf{x}(t), \mathbf{x_c}) \forall \mathbf{x_c}$, then $\phi(t, \mathbf{x_c} + \mathbf{\Delta}) = \phi(t, \mathbf{x_c}) \forall \mathbf{x_c}$. Here, $\mathbf{\Delta}$ is the spatial translation which leaves the population firing rate map invariant. In the simple one-dimensional case this translation can only take on values $\mathbf{\Delta} = nd$, but in the two-dimensional case $\mathbf{\Delta}$ can take on any of the values described by the symmetry of Equation (3.5).

We now consider these issues more systematically, first considering the general case of linear phase coding in grid cells in two dimensions and then comparing to the case of sigmoidal phase coding in two dimensions. We show below that these seemingly innocuous assumptions lead to strong and previously unappreciated restrictions on grid cell theta phase coding in open environments which call into question the validity of the assumptions underlying previously proposed models in one dimension.

3.4 Linear phase precession model

We now consider the simplest possible extension of the linear travelling wave model to grid cells. We consider phase coding in a single module of grid cells consisting of a single orientation ϕ_x and grid spacing d but a range of grid phases determined by the firing field vertices $\mathbf{x_c}$. This model of phase precession in grid modules consists of two basic assumptions: firstly, phase precession in each grid cell is linear, so that the cells have a frequency which is constant across space and over time, depending only on velocity and grid scale; secondly, cells with the same spatial (grid) phase have the

same intrinsic theta phase at any instant in time (i.e., the spatial translation symmetry is respected). We show below that this simple model faces problems in generating phase coding across different directions in two dimensions.

Under the assumption of linear theta phase coding, the MPO phase of the cell is:

$$\psi(\mathbf{x_c}, t) = \omega t - \boldsymbol{\kappa_\psi} \cdot \mathbf{x_c} + \psi_0 \tag{3.6}$$

where $\boldsymbol{\kappa_\psi} = (\kappa_{\psi,x}, \kappa_{\psi,y})$ is a wavevector which describes both the wavelength and direction of motion of travelling waves through the population.

Under the spatial symmetry assumption, if two cells have the same spatial phase $\mathbf{x_c^{(1)}} \sim \mathbf{x_c^{(2)}}$ on the grid, they have the same theta phase:

$$\psi(\mathbf{x_c^{(1)}}, t) \equiv \psi(\mathbf{x_c^{(2)}}, t) \mod 2\pi \tag{3.7}$$

so that:

$$\psi(\mathbf{x_c^{(1)}}, t) - \psi(\mathbf{x_c^{(2)}}, t) = \boldsymbol{\kappa_\psi} \cdot (\mathbf{x_c^{(1)}} - \mathbf{x_c^{(2)}}) = 2\pi n \tag{3.8}$$

for some integer n.

To understand how this constraint affects the travelling wave dynamics, we can consider a single grid tile defined by the region $\mathcal{D} = \{(x,y) | 0 \leq x \leq d, 0 \leq y \leq \frac{\sqrt{3}}{2} d\}$. All points of a single grid tile can be assigned a unique spatial phase (x,y) apart from the boundaries, where each point is identified with a point on the opposite side (see Figure 3.2). Hence, Equation (3.8) places constraints on the theta phase on the grid tile boundaries. Given a cell location on the grid $\mathbf{x_c} = (x,y) \in \mathcal{D}$, the boundary conditions are:

$$\psi((0,y),t) \equiv \psi((d,y),t) \mod 2\pi \tag{3.9}$$

$$\psi((x,0),t) \equiv \psi((x+d/2, \sqrt{3}/2d),t) \mod 2\pi \qquad 0 \leq x \leq d/2 \tag{3.10}$$

$$\psi((x,0),t) \equiv \psi((x-d/2, \sqrt{3}/2d),t) \mod 2\pi \qquad d/2 \leq x \leq d \tag{3.11}$$

Applying the first constraint gives $\kappa_{\psi,x} = 2\pi n/d$, the second gives $\kappa_{\psi,y} = 2\pi(2m - n)/(\sqrt{3}d)$ while the third constraint is redundant. Hence, the only possible wavevectors for linear travelling wave dynamics on a grid lattice are $\boldsymbol{\kappa_\psi} = 2\pi(n, (2m-n)/\sqrt{3})/d$ for integers m, n.

These wavevectors can be decomposed into the vector basis of the firing rate map $\boldsymbol{\kappa_i}$ by setting $\boldsymbol{\kappa_\psi} = \alpha\boldsymbol{\kappa_1} + \beta\boldsymbol{\kappa_2}$ for $\alpha, \beta \in \mathbb{R}$. Noting that our choice of tiling $\mathcal{D}$ assumes a grid orientation of $\phi_x = 30^\circ$, this can be solved to find $\alpha = n$, $\beta = m - n$. Hence, defining $i = n$ and $j = m - n$, the wavevectors consistent with the translational symmetry of grid cell firing rate maps are seen to be given by arbitrary discrete combinations

of the grid vectors, $\boldsymbol{\kappa_\psi} = i\boldsymbol{\kappa_1} + j\boldsymbol{\kappa_2}$. For a given mode (i, j), the wavelength is therefore $\lambda_{i,j} = 2\pi/|\boldsymbol{\kappa_\psi}| = \sqrt{3}d/(2\sqrt{i^2 + j^2 + ij})$.

This result discretises both the direction and wavelength of travelling waves, which has important implications. For example, the model of phase precession in place cells described in Chapter 2 predicts that travelling waves propagate in the direction of movement of the animal, whereas this is not physically possible for all running directions in the grid cell model. Secondly, it predicts that both the wavelength of the travelling wave and the rate at which phase precesses as the animal travels through the firing field depend on the running direction of the animal. We now analyse these properties in more detail, and show that the resulting dynamics are incapable of producing a robust two-dimensional phase code at high directional resolution.

We first analyse the changes in wavelength with direction of wave propagation in the model, depending on the mode (i, j). The simplest case is given by $i = j = 0$, where the phase over the grid is constant, so that all cells are synchronous and the wavelength is undefined. The two longest wavelength modes which exhibit phase precession are:

$$\lambda_{-1,0} = \lambda_{0,-1} = \lambda_{-1,1} = \lambda_{1,-1} = \lambda_{1,0} = \lambda_{0,1} = \frac{\sqrt{3}}{2}d \tag{3.12}$$

$$\lambda_{-2,1} = \lambda_{1,-2} = \lambda_{-1,-1} = \lambda_{-1,2} = \lambda_{2,-1} = \lambda_{1,1} = \frac{d}{2} \tag{3.13}$$

while all other modes have increasingly shorter wavelengths. These two sets of wavevectors with the longest and second longest wavelength allow the network to represent 12 equally spaced running directions, with a resolution of 30° (Figure 3.3). While a higher directional resolution can be achieved by including higher order modes, these involve shorter wavelengths and require that the wavelength switches between these discrete modes at increasingly fine grained changes in direction. Figure 3.4 shows how the wavelength varies across different modes, showing that rapid fluctuations in wavelength are required to account for small changes in direction.

We next analyse the phase precession frequency over these modes. To do this, it is necessary to invoke the assumption that theta phase respects the time translation symmetry of the grid map (as discussed above). In particular, if the animal moves in a direction along which there exists a translational symmetry $\boldsymbol{\Delta}$, each cell should precess through an integer number of cycles over the time $T = |\boldsymbol{\Delta}|/v$. Assuming that the animal moves in the direction of the travelling wave $\boldsymbol{\kappa_\psi}$, we can then calculate the frequencies which satisfy this time translation symmetry as $f_\phi = n/T$. For the two longest wavelength modes described above, the wavelength is equal to $\lambda = |\boldsymbol{\Delta}|/2$ (see

Figure 3.3), so that the possible frequencies are given by:

$$f_{-1,0} = f_{0,-1} = f_{-1,1} = f_{1,-1} = f_{1,0} = f_{0,1} = f_\theta + n_1 \frac{1}{\sqrt{3}} \frac{v}{d} \tag{3.14}$$

$$f_{-2,1} = f_{1,-2} = f_{-1,-1} = f_{-1,2} = f_{2,-1} = f_{1,1} = f_\theta + n_2 \frac{v}{d} \tag{3.15}$$

where n_i are arbitrary integers. Hence, linear phase coding requires that wavelength, direction and frequency are all discretised in grid cell modules.

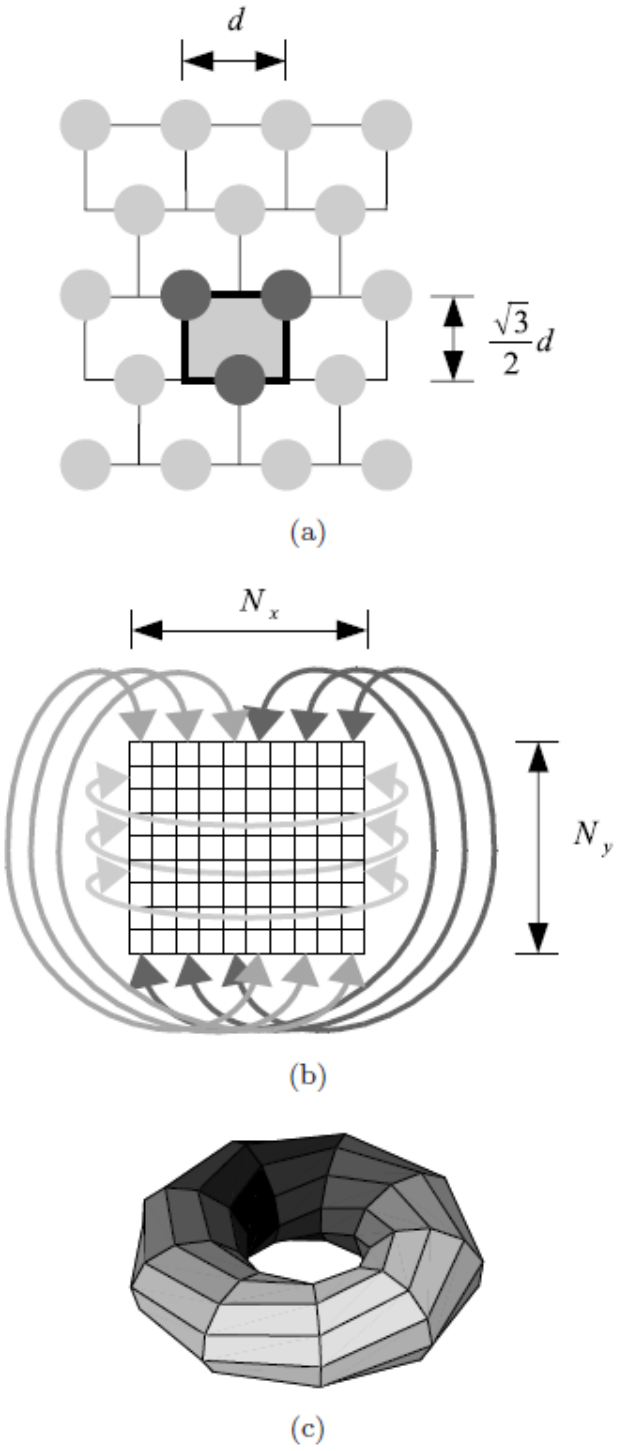

Figure 3.2: Boundary conditions using a rectangular tessellation of the grid pattern. Figure taken from Guanella et al. (2007)

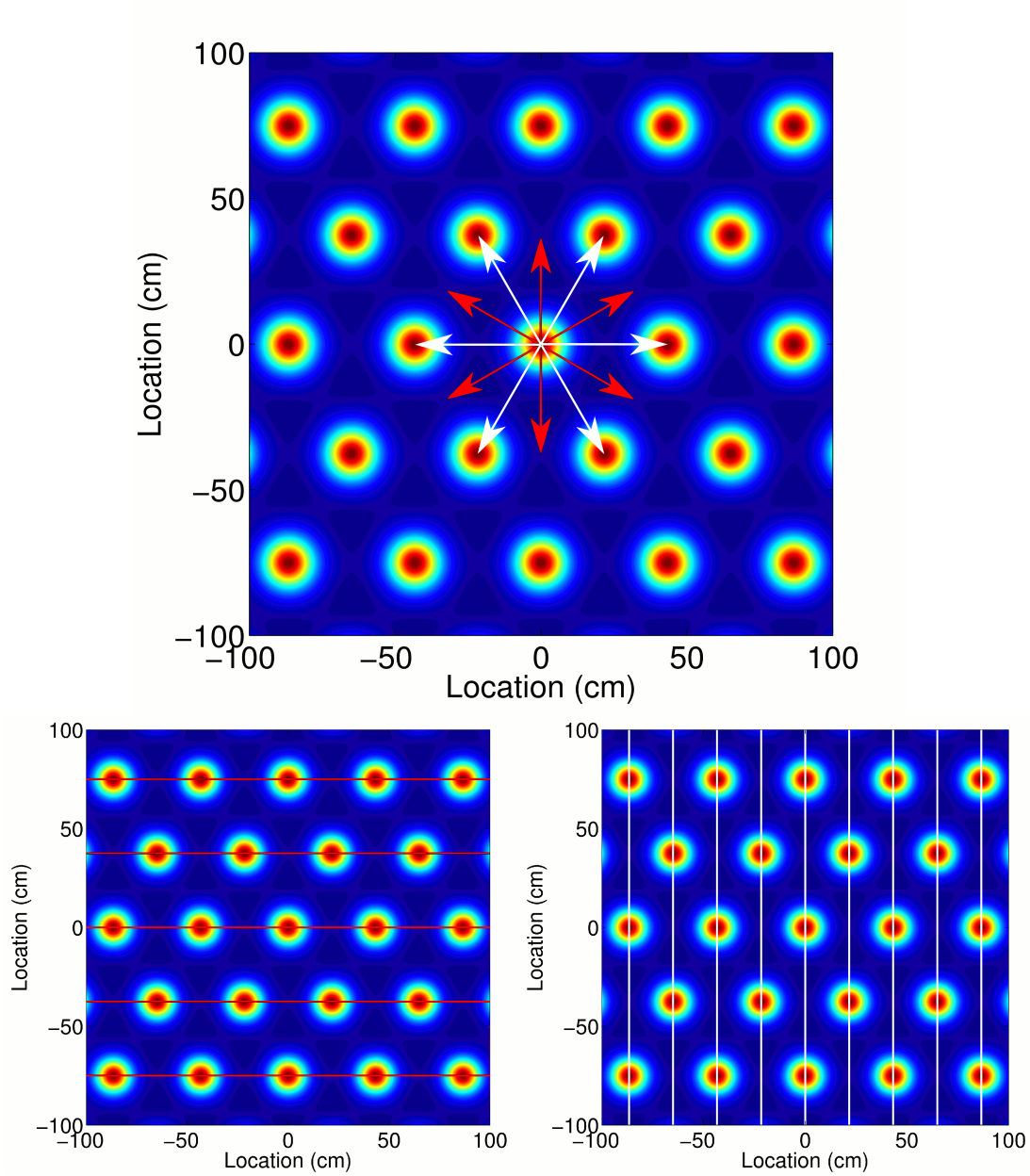

Figure 3.3: *Top:* Possible wavevectors in a grid network. Shown are the set with the longest wavelength (black) and the set with second longest wavelength (white) for phase codes which satisfy the spatial translation symmetry of grid cells. In each case the wavelength is half the distance between successive grid peaks, but this distance depends on direction. Travelling waves with more fine grained directions are possible, but generate increasingly shorter wavelengths. *Bottom:* Two example travelling wave configurations picked from the previous figure. Each self-similar point on the grid has the same phase. The wavelength of the two configurations differ by a factor of $1/\sqrt{3}$.

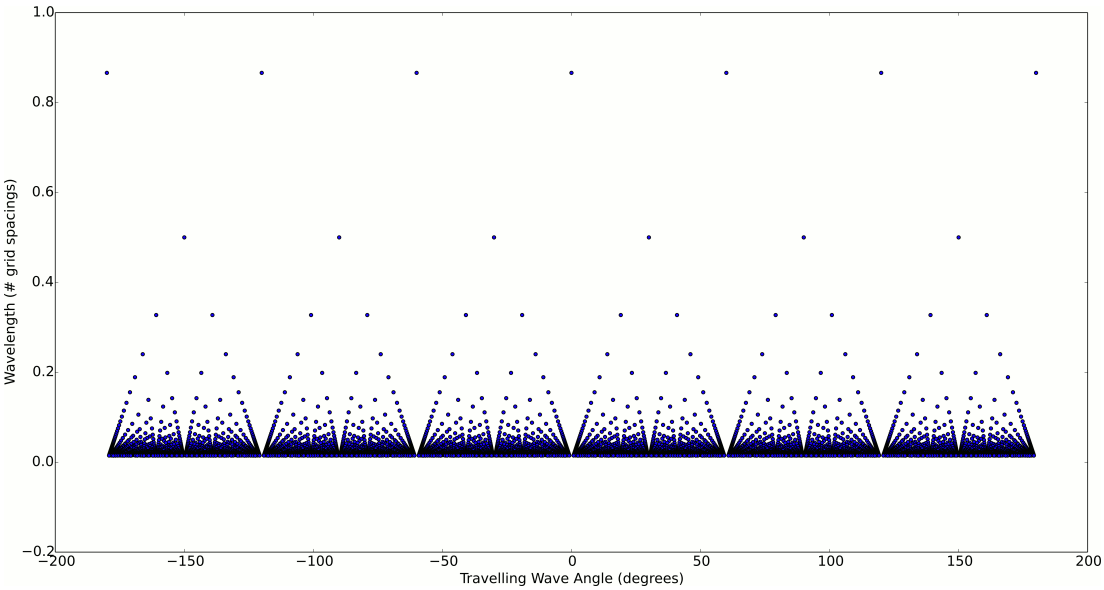

Figure 3.4: Wavelength (normalised by grid scale) plotted against the travelling wave direction for the 500 longest wavelength modes.

Relation to previous models

It is of note that, while the dynamics described in this section appear unnatural, the basic assumptions which enforce these dynamics are present in several existing models. For example, Jaramillo et al. (2014) considered phase coding on a linear track, and suggested a constant intracellular frequency of $f = f_\theta + v/d$ based on the assumption that intracellular theta precesses by one cycle between successive grid peaks. Our analysis shows that, although these assumptions capture the simple one-dimensional trajectory they analysed, they do not generalise to arbitrary two-dimensional trajectories. When analysing phase precession in open environments, Jeewajee and colleagues reported that theta phase in two dimensions correlates best with "distance to the field peak projected onto the animal's current running direction" (Jeewajee et al., 2014), which is mathematically identical to the phase described by the linear travelling wave model described here. The analysis of this section shows that the code suggested by Jeewajee and colleagues cannot be present for arbitrary directions of movement without violating the spatial symmetries of grid cell activity maps. Hence, our analysis reveals previously unappreciated complexities in existing models of phase precession in grid cells.

In summary, we find that the linear phase coding in fixed phase charts we derived for place cells in the previous chapter imply a finite directional resolution for phase coding in grid cells and a dependence of precession frequency on running direction. Although it is possible that grid cells maintain fixed phase charts as we suggested in Chapter 2, this would imply a very limited directional resolution based on a set of discrete network modes. These strong constraints in linear models which are imposed by translational symmetry requirements call into question their biological plausibility, motivating the development of more complex, nonlinear models.

3.5 Rate-coupled frequency model

Due to the finite resolution of directional phase precession using linear phase coding and the dependence of oscillation frequency on direction of movement, we next asked whether a nonlinear phase precession model such as sigmoidal phase coding could provide more natural dynamics while generating the desired translational symmetries. In the sigmoidal model of place cells, we assumed that the intrinsic theta oscillation frequency of a cell covaries with its firing rate. Given that the frequency dynamics

depend only on the firing rate in this model, the spatial translation symmetry inherent in grid module firing rate activity will clearly be present in the theta phase at any instant in time. However, it is not clear whether this frequency can be integrated correctly along different running directions in order to generate the relevant time-translation symmetries in firing phase.

To test this, we extended the sigmoidal model of phase coding in place cells to the case of grid cell firing fields. For analytical tractability, we take the firing rate as a function of location to be:

$$r_x(\mathbf{x},\mathbf{x_c}) = r_0\left[\frac{1}{3}\left(\cos\left(\boldsymbol{\kappa_1}\cdot(\mathbf{x}-\mathbf{x_c})\right)+\cos\left(\boldsymbol{\kappa_2}\cdot(\mathbf{x}-\mathbf{x_c})\right)+\cos\left(\boldsymbol{\kappa_3}\cdot(\mathbf{x}-\mathbf{x_c})\right)\right)+\frac{1}{2}\right] \tag{3.16}$$

where the additional $1/2$ ensures the rate is non-negative.

To understand how a grid cell's theta phase varies along a trajectory through space, we then set the intrinsic theta frequency proportional to the spike rate and solve for the phase:

$$f_\phi = 2\pi\Delta f r_x/r_0 \implies \phi(t,\mathbf{x_c}) = 2\pi\Delta f\int_{t_0}^{t} r_x(\mathbf{x}(\tau),\mathbf{x_c})/r_0 d\tau + \phi(t_0,\mathbf{x_c}) \tag{3.17}$$

Using that $\mathbf{x} = \mathbf{v}(t-t_0)+\mathbf{x_0}$, we find:

$$\phi(t,\mathbf{x_c}) = \tag{3.18}$$

$$2\pi\Delta f\left[\frac{1}{2}(t-t_0)+\frac{1}{3}\sum_{i=1}^{3}\frac{1}{\boldsymbol{\kappa_i}\cdot\mathbf{v}}\left(\sin(\boldsymbol{\kappa_i}\cdot(\mathbf{v}(t-t_0)+\mathbf{x_0}-\mathbf{x_c}))-\sin(\boldsymbol{\kappa_i}\cdot(\mathbf{x_0}-\mathbf{x_c}))\right)\right]+\phi(t_0,\mathbf{x_c}) \tag{3.19}$$

where the above equation holds if $\mathbf{v}\cdot\boldsymbol{\kappa_i}\neq 0$. The result for the special case $\mathbf{v}\cdot\boldsymbol{\kappa_i}=0$ is given in Appendix B.

Given a constant running speed in a straight line, we require that the intracellular theta phase precesses through some multiple of 2π whenever the animal returns to the same spatial phase. For straight runs directly between grid field peaks along a direction $\boldsymbol{\kappa_i}$, this requires that the frequency increases by a factor of $\Delta f = (2/\sqrt{3})kv/d$ for some integer k (proof given in Appendix B). Given this value of rate coupled frequency modulation, we then ask whether movement can be correctly integrated over a different running direction. For directions exactly between two grid vectors ($\mathbf{v} = |\mathbf{v}|\left(\boldsymbol{\kappa_i}+\boldsymbol{\kappa_j}\right)/|\boldsymbol{\kappa_i}+\boldsymbol{\kappa_j}|$, see Figure 3.3 top panel), precession over a multiple of 2π between two grid field peaks requires a precession frequency of $\Delta f = (6/5)k^*v/d$ for some integer k^* (see Appendix B). As no suitably small choices of k, k^* can satisfy

these phase precession constraints in both directions analysed here, these firing rate coupled frequency dynamics alone cannot account for phase precession in different directions. Therefore, the sigmoidal model requires an additional directional dependence of precession frequency as in the linear model.

3.6 Rate-coupled frequency model plus synchronisation to baseline

Phenomenological account

Above we showed that both linear phase coding and sigmoidal phase coding based on rate-coupled theta frequencies have difficulties generating a phase code for grid cells along arbitrary two-dimensional trajectories. However, in the sigmoidal model, key biophysical factors were missing. In particular, grid cells are embedded in a network with theta-rhythmic dynamics, and therefore receive synaptic inputs which would likely provide an additional synchronising drive, pulling the grid cell into phase alignment with the global theta oscillation outside of the firing rate field. To account for this, we introduce a dynamical model for the rate of change in phase by adding a synchronising term in addition to the rate-coupled frequency dynamics described above:

$$\frac{d\phi(t)}{dt} = Br_x(\mathbf{x}(t)) - A\sin(\phi(t)) \tag{3.20}$$

where $\phi(t)$ is the phase of the cell relative to the LFP. The first term represents the rate-coupled frequency of the cell described in the previous section. The second term represents a synchronising influence of medial septum/interneuron input which pulls the phase of the grid cell towards that of the global theta rhythm. Outside of the firing rate field, where $r_x = 0$, the synchronising term will pull the phase towards $\phi = 0$, so that upon entry to the next firing rate field the phase will be correctly aligned. Specifically, if the animal is outside of the firing rate field, we can set $r_x = 0$, in which case a stable locking phase of $\phi = 0$ emerges. Provided that the strength of synchronisation A is sufficiently weak, so that $Br_x \gg A$ within the firing field, phase precession will be relatively unperturbed by the synchronising influence and will occur independently each time the animal crosses an individual grid field (Reifenstein et al., 2012).

Provided that the change in frequency over the firing field is correctly tuned, phase will precess through the correct amount over the firing field. Equation (3.20) clearly shares the spatial translation symmetries of grid cell firing rates at any given point in

time. Moreover, provided that phase is reset between firing fields by the synchronisation term, the time-translation symmetries will also be satisfied. We analyse these dynamics in more detail below.

Semi-biophysical account

While the Equation (3.20) provides a phenomenologically viable model of phase precession in grid cells, the mechanisms underlying the rate-coupled theta frequency oscillations and the synchronisation dynamics are not fully clear. Moreover, the tuning of parameters required in order to ensure the correct precession frequency within the firing field as well as sufficient synchronisation between firing fields merit further investigation. Based on the above phenomenological equation, we now introduce a simple biophysical description with equivalent dynamics.

Specifically, we consider a neuronal oscillator with phase ψ whose baseline frequency $\omega(I)$ is determined by the amplitude of a depolarising current I through its f-I curve (note that we do not make any explicit assumptions about the form of this f-I curve here). Additionally, the oscillator is driven by a pacemaker input which we treat as a weak perturbation to this oscillator (Figure 3.5A), which allows a reduced description in which only phase is considered (e.g., Ermentrout et al., 1986). To achieve this reduced phase description, we introduce an approximation based on the infinitesimal phase response curve of the oscillator $z(\psi)$. The dynamics of an oscillator with frequency ω driven weakly by an external perturbation $Q(t)$ can then be approximated by:

$$\frac{d\psi}{dt} = \omega(I) + z(\psi)Q(t) \tag{3.21}$$

where amplitude variations have been neglected. To model the case of an oscillator driven by a weak pacemaker we consider a perturbation of the form $Q(t) = Q_0\cos(\theta(t))$. Equation (3.21) can then be expressed as:

$$\frac{d\phi}{dt} = \Delta\omega - z(\theta-\phi)Q_0\cos(\theta(t)) \tag{3.22}$$

where $\phi = \theta - \psi$ and $\Delta\omega = \omega_\theta - \omega_\psi$. If z is also sinusoidal, the above equation can be further approximated by averaging out fast fluctuations on sub-theta timescales. To see this, we define the theta-average of a variable as:

$$\langle X\rangle_\theta = \frac{1}{2\pi}\int_0^{2\pi} X d\theta \tag{3.23}$$

Averaging out fluctuations on a sub-theta cycle timescale then gives:

$$\left\langle \frac{d\phi}{dt} \right\rangle_\theta = \Delta\omega - Q_0 \left\langle z(\theta-\phi)\cos(\theta) \right\rangle_\theta \tag{3.24}$$

which for sinusoidal phase response curves of the form $z(\phi) = z_0 + z_1 \sin(\phi)$ is:

$$\left\langle \frac{d\phi}{dt} \right\rangle_\theta = \Delta\omega - Q_0 \left\langle \cos(\theta)\left(z_0 + z_1 \sin(\theta-\phi)\right) \right\rangle_\theta \tag{3.25}$$

$$= \Delta\omega - Q_0 z_1 \left\langle \cos(\theta)\sin(\theta-\phi) \right\rangle_\theta \tag{3.26}$$

$$= \Delta\omega - \frac{1}{2} Q_0 z_1 \left\langle \sin(2\theta-\phi) + \sin(\phi) \right\rangle_\theta \tag{3.27}$$

$$\approx \Delta\omega(I) - \frac{1}{2} Q_0 z_1 \sin(\phi) \tag{3.28}$$

where in the last line it was assumed that ϕ does not change over a single theta cycle. This recovers an equivalent form of Equation (3.20) and provides an explicit set of biophysical parameters to describe the frequency modulation and synchronisation terms. In particular, the strength of synchronisation is given by $A = \frac{1}{2} Q_0 z_1$ and therefore depends on the amplitude of pacemaker drive and the sinusoidal component of the phase response curve.

Equation (3.20), or equivalently Equation (3.28), generates two distinct dynamical states depending on the relative values of A and $\Delta\omega$ (i.e., depending on the amplitude of pacemaker input and excitatory input to the oscillator). The first is stable phase locking and the second is phase precession. Phase locking occurs when $A > |\Delta\omega|$, with a stable locking phase of $\phi_{\text{lock}} = \arcsin\left(\frac{\Delta\omega}{A}\right)$ (Figure 3.5B). Phase precession occurs when $A < |\Delta\omega|$, where there are no stable phases and the oscillator precesses continuously, but nonlinearly, in phase against the pacemaker input (Figure 3.5C).

The general solution to Equation (3.28) is given by:

$$\phi(t) = 2\arctan\left[\frac{A - \sqrt{(\Delta\omega)^2 - A^2}\tan\left(\frac{1}{2}\sqrt{(\Delta\omega)^2 - A^2}(c-t)\right)}{\Delta\omega}\right] \tag{3.29}$$

where c is a constant determined by the initial conditions (Adler, 1946). This equation is valid for both the phase locking and phase precession regimes. In the case of phase precession, where $(\Delta\omega)^2 - A^2 > 0$, this gives the following precession frequency:

$$f = \sqrt{(\Delta\omega)^2 - A^2}/2\pi \tag{3.30}$$

Assuming that the phase precession frequency scales with running speed and field size as $f = v/(2R)$, where R is the radius of the firing rate field (see Chapter 2), we obtain

a constraint on the detuning and synchronization factor:

$$(\Delta\omega(I))^2 = A^2 + (\pi v/R)^2 \tag{3.31}$$

which quantifies how the strength of synchronisation and changes in intrinsic frequency should be tuned in order to precess at the correct rate within the firing rate field.

For the stable phase locking case, where $(\Delta\omega)^2 - A^2 < 0$, the expression for precession frequency yields complex values. To recover the steady state locking dynamics shown in Figure 3.5B, note that for complex arguments the tan function in Equation (3.29) becomes a tanh, and in the limit $t \to \infty$ this tanh term tends to 1 so that the system reaches a steady state independent of the initial condition c. The rate at which the decay to steady state occurs will therefore vary with $\sqrt{(\Delta\omega)^2 - A^2}$. As discussed above, this rate must be fast enough to reset the intrinsic theta phase of the cell between firing fields in order to produce robust phase coding in two-dimensional environments which obeys the time translation symmetries of grid cell firing rates.

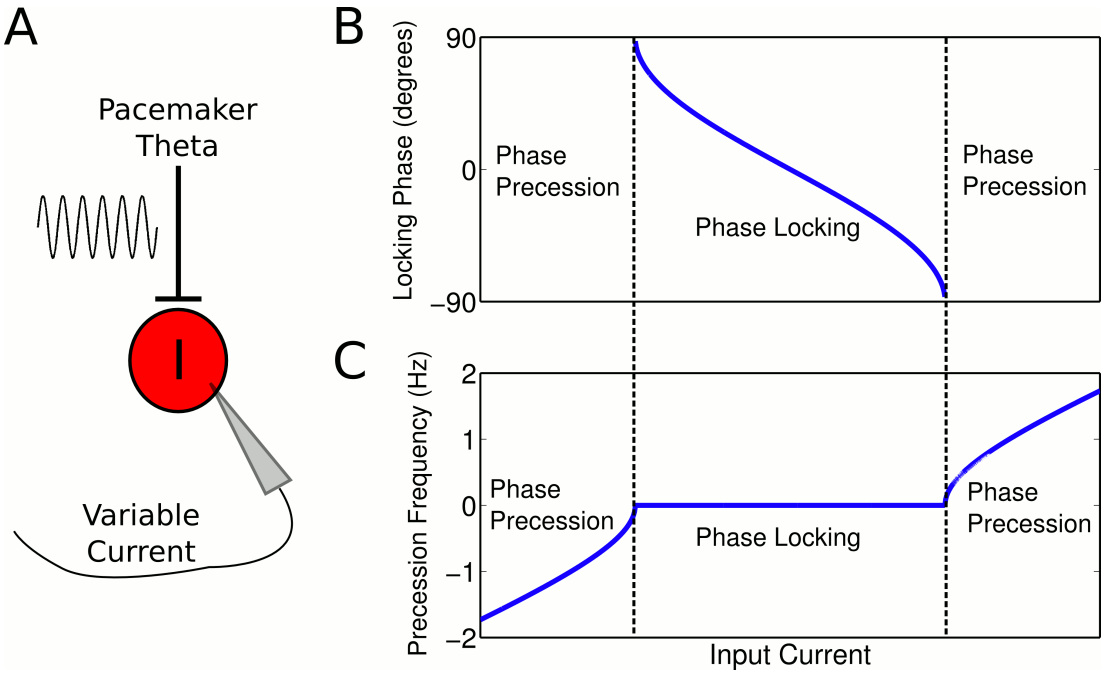

Figure 3.5: (A) A reduced model of a neuronal oscillator driven by depolarizing current and weak pacemaker drive. (B) Phase locking as a function of input current in the reduced model, assuming a linear f-I curve. (C) Precession frequency as a function of input current.

3.7 Discussion

The analysis of this chapter demonstrates that linear travelling wave models of phase precession and simple sigmoidal models of phase precession face difficulties accounting for grid cell phase precession in open environments. To overcome these problems, we have proposed a model based on a firing rate-dependent theta oscillation frequency combined with a synchronising drive which resets intracellular theta phase between firing fields. In order to provide a biophysical grounding for this model, we put forward an analysis based on a neuronal oscillator with an intrinsic, ongoing theta oscillation whose frequency can be modulated via an f-I curve, and is driven by an external theta pacemaker which provides the synchronising influence. In this model, phase precession is initiated independently each time the animal enters a firing field (Reifenstein et al., 2012). Hence, the dynamics of phase precession across a single grid field in entorhinal cortex are identical to those across a place field in CA1 in such a model.

Our model makes several experimentally testable predictions. In particular, the interaction between synchronising drives and rate dependent oscillation frequencies in individual cells can be used to predict the membrane and spike phases for arbitrary two-dimensional trajectories with arbitrary speed profiles. The study of phase precession along two dimensional trajectories has been the focus of several experimental studies in both place cells (Huxter et al., 2008) and grid cells (Jeewajee et al., 2014; Reifenstein et al., 2014). While the phenomology of two-dimensional phase precession has been compared to predictions from various oscillator-interference models (Jeewajee et al., 2014; Reifenstein et al., 2014), our model provides an alternative framework from which to make principled predictions for phase precession in open environments. Additionally, our model predicts that the intracellular theta frequency of grid cells varies over space, so that grid cells oscillate at the same frequency as the LFP between grid fields and reach their highest theta oscillation frequency at the centre of a grid field, where the spike rate is highest.

While the external pacemaker input to the circuit has an empirically established origin in the medial septum, which targets interneurons across the entorhino-hippocampal complex (Freund and Antal, 1988), the biophysical basis for the intrinsic cellular oscillation is less clear. While many cell types in the hippocampus and entorhinal cortex exhibit intrinsic rhythmicity due to the presence of specialised ion channels such as the hyperpolarisation activated cation channel (Leung and Yu, 1998; Hu et al., 2002; Buzsáki, 2002), there is little evidence for an intrinsically generated theta oscillation

in principal cells which persists outside of the firing rate field and whose frequency may be modulated by external inputs as the animal crosses a firing rate field. While subthreshold theta oscillations exist outside of the place field (Harvey et al., 2009; Domnisoru et al., 2013; Schmidt-Hieber and Häusser, 2013), these likely result from a combination of theta rhythmic synaptic input and intrinsic resonances. Interneurons, however, generally spike tonically at theta frequency regardless of the animal's location (Freund and Buzsáki, 1996). As tonic spiking frequencies in neurons can easily be modulated by changing the amplitude of external drive, these cells appear a more natural candidate for the dynamics described here. Moreover, interneurons in CA1 are known to precess in phase at specific locations in an environment, and this precession shows strong functional coupling to individual place cells (Maurer et al., 2006b; Geisler et al., 2007).

In Chapter 4, we propose a mechanistic theory of phase precession based on the rate-coupled frequency dynamics with synchronising drive discussed in this chapter. We show how these dynamics can be achieved in interneurons, generating phase precession in pyramidal cells via their reciprocal synaptic coupling. As the phase precession dynamics we investigate occur independently whenever the animal enters a firing rate field, we focus our analysis on place cells in the CA1 region of the hippocampus in the next chapter. Nevertheless, the results we present for place cells can be considered as equivalent to passes through a single grid field.

Chapter 4

Biophysical Models of Theta Sequences

4.1 Introduction

Place cell populations in the rodent hippocampus generate nested sequential representations of ongoing behavioural events (Skaggs et al., 1996). Event sequences are represented in real-time as slow sequences of firing rate activations, while at the same time a faster, time-compressed representation of these sequences occurs within each cycle of the network theta rhythm (Dragoi and Buzsáki, 2006; Foster and Wilson, 2007). Such sequences are hypothesised to form a substrate for episodic and spatial memory (Pastalkova et al., 2008), but the underlying circuit mechanisms remain unclear.

In contrast to earlier studies, we showed in Chapter 2 that interactions between place cells are not necessary to explain theta sequences. Instead, the organisation of theta sequences can be accounted for by the independent phase precession of each cell. However, the biophysical mechanisms underlying such a coding scheme within the CA1 circuitry are still lacking.

Biophysical explanations for phase precession face a number of challenges. First, precession frequency depends on the running speed of the animal (Geisler et al., 2007). To account for this, models often introduce external velocity-controlled oscillator inputs to place cells which impose this change in precession frequency (e.g., Burgess et al., 2007; Jaramillo et al., 2014), so that this phenomenon is included by hand rather than generated *de novo*. Second, phase precession occurs along arbitrary two dimensional trajectories (Huxter et al., 2008; Climer et al., 2013; Jeewajee et al., 2014). This poses a challenge for models which incorporate fixed spatial asymmetries in order

to account for the change in firing phase over the place field (Tsodyks et al., 1996; Mehta et al., 2002; Chance, 2012; Leung, 2011; Wang et al., 2015), as this can generate phase precession only along a single direction. Finally, phase precession and theta sequences are generated over a large number of distinct spatial maps. This is especially challenging for models in which synaptic coordination underlies the generation of theta sequences (Tsodyks et al., 1996; Geisler et al., 2010; Lisman and Redish, 2009; Wikenheiser and Redish, 2015; Wang et al., 2015), as after remapping the sequences will be disrupted (see Chapter 2).

Here, we present a mechanistic model of CA1 networks in which phase precession is generated by the interactions between individual place cells and interneurons driven by pacemaker inputs. This model accounts for phase precession in open environments, at different running speeds and for the phase precession of interneurons, while allowing sequences to be generated in multiple distinct spatial maps. In contrast to previous hypotheses which viewed phase precession in interneurons as an epiphenomenon inherited from synaptic inputs from phase precessing place cell assemblies (Maurer et al., 2006b; Geisler et al., 2007), interneuron phase precession in this model is crucial for the coordination of spike timing in place cells and the generation of theta sequences. Due to the transient functional coupling between place cells and interneurons, phase precession occurs dynamically whenever a place cell is driven by external inputs, and slow input sequences are automatically compressed into theta sequences. Phase precession and theta sequences are generated *de novo* within the network, without the need for inputs with velocity modulated oscillation frequencies. Hence, while many existing models posit that firing rate fields are an emergent property arising from more fundamental phasic or sequential processes (Burgess et al., 2007; Wang et al., 2015), or suggest that theta sequences reflect active and internally constructed representations of spatial trajectories (Gupta et al., 2012; Wikenheiser and Redish, 2015), our model instead suggests that slow firing rate input sequences to CA1 are fundamental to the emergence of faster sequential activity patterns during theta states.

In contrast to existing models of phase precession, our model suggests that CA1 can function as a flexible compressor of its inputs in order to maintain a representation of temporal order occurring on a behavioural timescale within a faster timescale suitable for synaptic processing in downstream brain areas. We therefore suggest that the same mechanism which generates sequences encoding spatial trajectories can function as a general purpose circuit for encoding temporally extended sequences of events. Finally, we show how such a compression of ongoing experience into theta cycles can

allow supervised learning in classical conditioning task using spike time dependent plasticity. Thus, CA1 may compress ongoing experiences during theta states into fast neural activity patterns suitable for learning and decision making.

4.2 Phase precession emerges in coupled interneuron-pyramidal cell pairs.

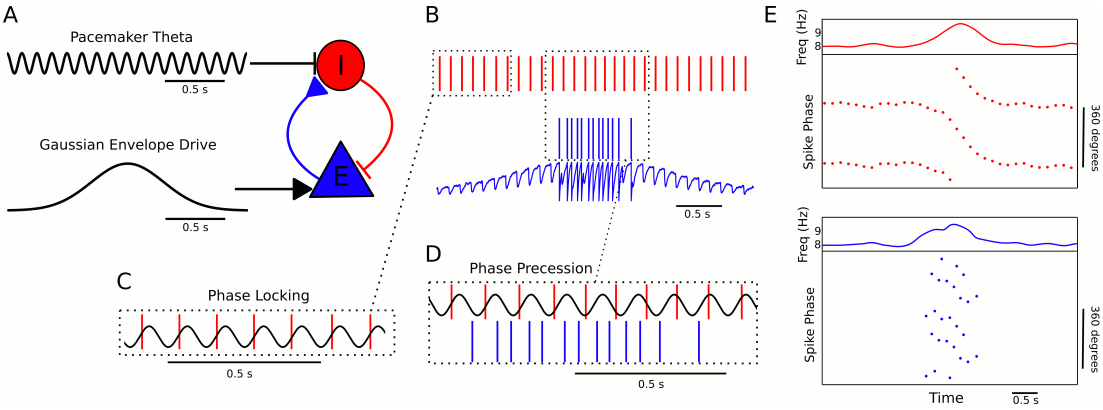

Figure 4.1: (A) A minimal CA1 circuit model. An interneuron (red) is driven by a pacemaker theta oscillation from the medial septum. This interneuron synapses reciprocally onto a pyramidal cell (blue). The pyramidal cell is driven by slower external inputs occurring over behavioural timescales. (B) - (E) A simulation of this network as the animal crosses the place field of the pyramidal cell. (B) Interneuron spiking activity (red lines) and pyramidal cell spikes (blue lines) and membrane potential (blue trace). (C) A sample of the interneuron spike train when the pyramidal cell is inactive (i.e., outside of the place field), with the pacemaker rhythm overlaid for reference. In this case, the interneuron locks to the pacemaker input. (D) A sample of the interneuron and pyramidal cell spike trains inside the place field. In this case, the interneuron precesses in phase against the pacemaker input and the pyramidal cell fires in bursts which also precess in phase. (E) The membrane frequency in the theta band and the spike phases of the interneuron (red) and pyramidal cell (blue) corresponding to the data shown in parts (A)-(D). Phases are replicated over two cycles for clarity.

Given that septal GABAergic projections target interneurons in CA1 (Freund and Antal, 1988), which in turn coordinate the spiking activity of local CA1 pyramidal cells (Royer et al., 2012), we reasoned that phase precession could emerge within the dynamics of interneurons interacting with pyramidal cells and driven by pacemaker

inputs (Figure 4.1A). To investigate the emergence of phase precession in coupled pyramidal cell-interneuron pairs, we constructed a minimal network model based on the known architecture of the CA1 circuit. We first simulated a single interneuron and pyramidal cell, with reciprocal synaptic interactions as shown in Figure 4.1A. The interneuron receives a constant depolarising current which generates tonic spiking as well as a small amount of noise to simulate realistic physiological conditions. In addition, it receives an 8 Hz oscillatory pacemaker current which is sufficient to fully entrain spiking activity when the pyramidal cell is inactive (Figure 4.1B-C). In this case, output from the interneuron drives rhythmic subthreshold theta frequency oscillations in the pyramidal cell (Figure 4.1B). When the pyramidal cell is driven by an external ramp-like input that is strong enough to induce spikes, the resulting synaptic drive to the interneuron advances its spike phase and initiates phase precession in the coupled pair of cells (Figure 4.1D), as evidenced by an increase in each cell's oscillation frequency in the theta band (Figure 4.1E, top panels) and a shift in spike phase of around 360 degrees between place field entry and exit (Figure 4.1E, bottom panels). Hence, the basic architecture of the CA1 circuit driven by pacemaker inputs is sufficient to generate phase precession in place cells and interneurons whenever place cells are driven to spike by slow depolarising drives. While in the present model interneurons fire only one spike per theta cycle, hippocampal interneurons often fire in gamma bursts during theta oscillations, such that multiple spikes occur within a single theta cycle (Varga et al., 2012; Lapray et al., 2012; Katona et al., 2014). We do not address these dynamics, which may involve more complex cellular and synaptic properties than those considered here.

The emergence of these phase locking and precession dynamics can be understood in terms of the model we developed in Chapter 3 (see Figure 3.5). In particular, the interneuron can be understood as a neuronal oscillator with f-I curve and phase response curve, driven by a depolarising current and weak pacemaker input. Phase locking occurs for weak drives (or strong pacemaker inputs) and phase precession occurs for strong drives (or weak pacemaker inputs). Therefore, a change in input current to the interneuron, such as when the animal crosses the place field of the afferent place cell, causes a shift in dynamics from phase locking to phase precession. The phase locking of the cell is robust to fluctuations in input current within a given range, as shown by the wide range of states which exhibit phase locking in Figure 3.5B. Hence, this reduced model explains the dynamics observed in the network simulation of Figure 4.1. Specifically, the interneuron remains in a stable phase locking regime while the

pyramidal cell is inactive, but is pushed into the phase precession regime whenever the pyramidal cell provides sufficient synaptic input. Phase precessing synaptic inputs from the interneuron coordinate the spike timing of the place cell and confer phase precession, but phase precession in the interneuron is relatively insensitive to the timing of place cell inputs, requiring only an overall increase in excitatory input. We note that this mechanism shares some similarities to a previous model designed to account for phase precession in CA3 pyramidal cells (Bose and Recce, 2001).

4.3 Velocity-controlled oscillator dynamics emerge despite fixed pacemaker frequencies

We next investigated whether the model can account for the dependence of precession frequency on the running speed of the animal (Geisler et al., 2007). In a previous phenomenological model, we included such a running speed dependent oscillation frequency but did not propose a biophysical mechanism (see Chapter 2). Existing models of phase precession often include input currents with velocity-controlled oscillation frequencies in order to generate such dynamics (Burgess et al., 2007; Jaramillo et al., 2014). In contrast, phase precession in our reduced model depends on the interplay between pacemaker amplitudes and excitatory drives, so that the precession frequency can be flexibly modulated by varying the relative values of these two variables while keeping input frequencies constant. Specifically, the reduced model predicts that an interneuron receiving an excitatory drive which increases with running speed will show an increase in precession frequency with running speed (Figure 3.5). This change in input current could arise through greater inputs from place cells or through a specialised velocity modulated current. Equally, a change in the amplitude of the pacemaker input with running speed would generate a change in precession frequency in the reduced model.

Recent experiments show that interneurons in CA1 receive a velocity dependent depolarising current from glutamatergic circuits in the medial septum (Fuhrmann et al., 2015). Additionally, the dependence of both the LFP theta amplitude in CA1 (McFarland et al., 1975; Maurer et al., 2005; Patel et al., 2012) and the activity of inhibitory circuitry in the medial septum on running speed (King et al., 1998) suggests that there is likely an increase in the amplitude of pacemaker drive to CA1 with running speed. Based on the predictions of the reduced model of interneuron dynamics, we reasoned

that these phenomena might be sufficient to generate velocity-controlled oscillator dynamics in CA1 circuits.

We tested this hypothesis using the model of Figure 4.1. Our simulations confirm that the rate of phase precession in both the interneuron and place cell, when coupled reciprocally, can be flexibly modulated through changes in pacemaker amplitude and background current to interneurons (Figure 4.2A). We found that a linear increase in pacemaker amplitude with running speed, combined with a linear increase in depolarising current to interneurons with running speed, is sufficient generate an approximately linear increase in precession frequency (Figure 4.2B). Hence, in contrast to existing models, phase precession with a running speed dependent oscillation frequency is generated *de novo* in the local circuitry with inputs at a fixed theta frequency in the present model.

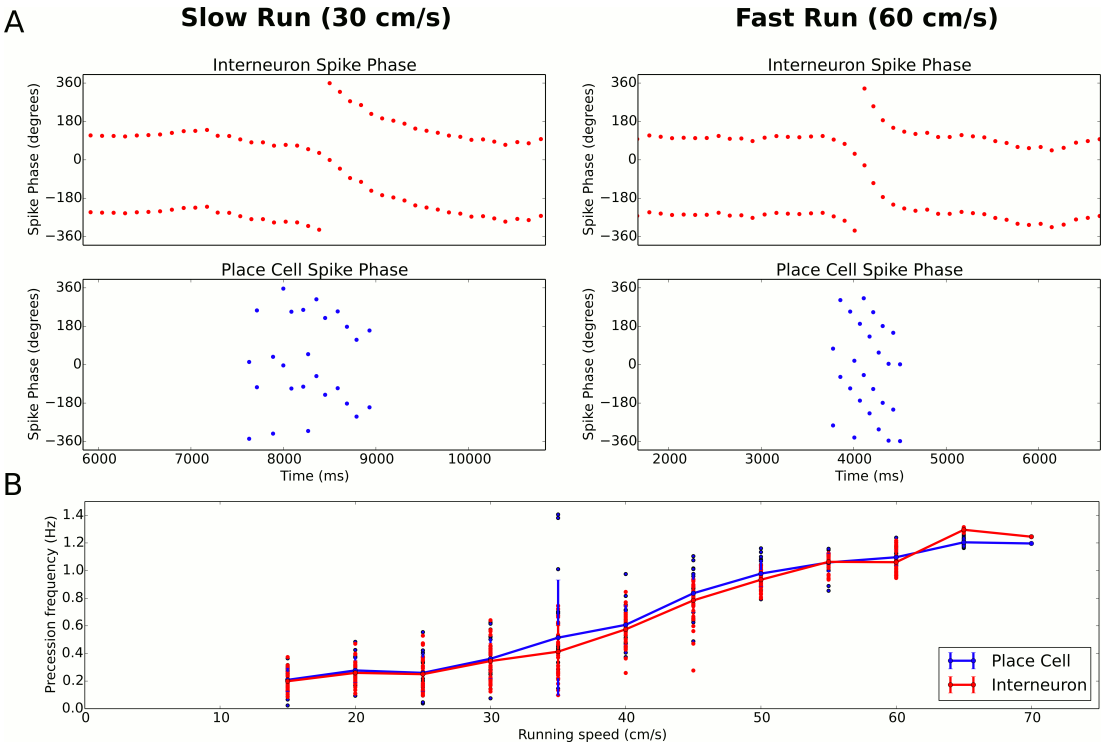

Figure 4.2: (A) Phase precession at a slow and fast running speed, where the pacemaker amplitude and depolarising current to interneurons are varied. (B) Phase precession as a function of running speed. Individual dots illustrate the estimated precessing frequency in the centre of the place field on a single lap. Line and error bars show mean and standard deviation.

4.4 Dorsoventral travelling waves emerge despite coherent pacemaker drives

The phase of population activity varies systematically across the dorsoventral axis of the hippocampus, spanning a range of 180 degrees (Patel et al., 2012). We asked whether the present model can account for these observations. In the reduced interneuron model, there is a range of precisely 180 degrees of possible locking phases to pacemaker input, depending on the strength of the excitatory current (figure 3.5B), while all other spike phases are unstable. This suggests that a gradient in excitatory inputs to interneurons (or alternatively a gradient in input resistance or some intrinsic membrane current) along the dorsoventral axis might be sufficient to generate the observed phase gradient, despite a coherent pacemaker input. To test this hypothesis in a more biophysically detailed setting, we simulated integrate and fire interneurons driven by the same pacemaker inputs but different levels of depolarising input currents.

Figure 4.3A shows three examples of these simulations. In each case, the interneuron is attracted towards a particular stable locking phase of the pacemaker input, but the precise locking phase depends on the strength of depolarising current. In Figure 4.3B we systematically analysed how this locking phase depends on the strength of depolarising current, finding a relationship remarkably similar to that predicted by the reduced model, including a range of 180 degrees of locking phases. Hence, in addition to explaining the change in precession frequency with running speed and place field size, the interplay between excitatory currents and pacemaker inputs can explain the phase gradient across the dorsoventral axis of the hippocampus.

We next tested whether the model can account for phase precession at different dorsoventral locations. Kjelstrup and colleagues found a gradient in place field sizes along this axis ranging from less than 1 meter to approximately 10 meters, and a concomitant gradient in the slope of phase precession (Kjelstrup et al., 2008). We simulated a place cell/interneuron cell pair at the ventral and dorsal pole of CA1, with place field sizes approximately 10 meters and 0.3 meters respectively and interneuron locking phases separated by approximately 180 degrees (Figure 4.3C, D). As in the running speed simulations, it was necessary to alter the amplitude of pacemaker amplitude as well as the depolarising current to the interneuron in order to modulate the slope of phase precession in the interneuron. Unlike the running speed simulations, however, it was also necessary to reduce the excitatory synaptic strength of the ventral place cell in order to ensure that the interneuron precessed sufficiently slowly over the large

place field. Given a dorsoventral gradient in these biophysical parameters, however, we found the gradient in both phase precession and theta phase along the dorsoventral axis could be accounted for in the model. Moreover, the reduced pacemaker amplitude at the ventral pole is consistent with observations of reduced theta power at ventral locations (Patel et al., 2012).

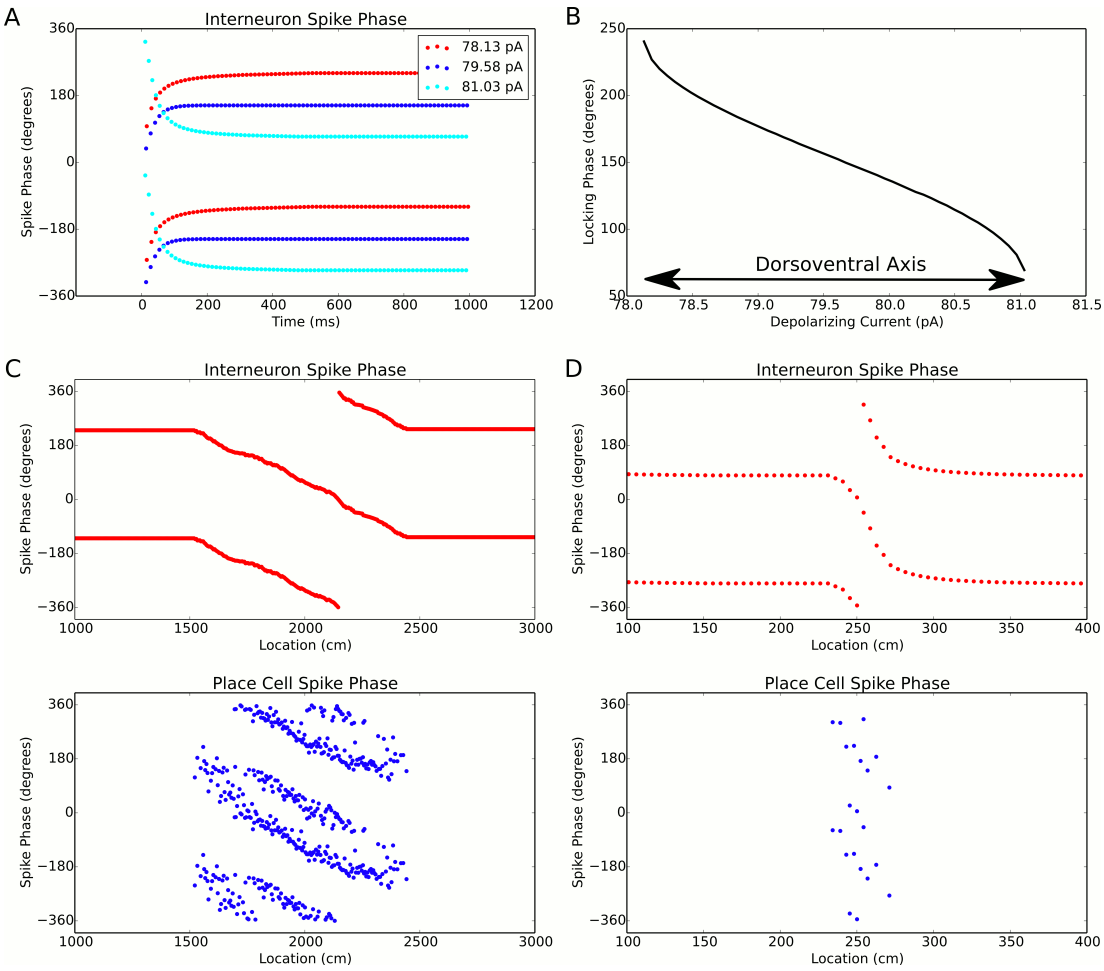

Figure 4.3: Theta dynamics across the dorsoventral axis. (A) Interneuron spike phases for three simulations with different depolarising currents. (B) Interneuron locking phase vs depolarising current (cf. Figure 3.5B). (C) Phase precession in a ventral place cell/interneuron pair (place field size 10 meters). (D) Phase precession in a dorsal place cell/interneuron pair (place field size 0.3 meters). Note the change in both locking phase and precession slope from dorsal to ventral.

4.5 Robust phase precession is generated along two-dimensional trajectories

Finally, we tested whether the model can account for the properties of phase precession in open environments. In open environments, spikes always precess from late to early phases of theta, regardless of running direction (Huxter et al., 2008; Climer et al., 2013; Jeewajee et al., 2014). Assuming the animal passes in a straight line through the centre of a place field at a constant speed, these dynamics arise naturally from the depolarising current envelope in the present model, and no additional directional inputs such as head direction cells are required. Similarly, our model is consistent with sequences observed during backwards travel, in which theta sequences reflect the ordering at which locations are visited rather than head direction (Cei et al., 2014; Maurer et al., 2014).

A more complex feature of phase precession in open environments is observed on passes through the edge of the place field, in which case the firing phase generally precesses through around 180 degrees before shifting backwards in phase rather than continuing to precess (supplementary figure S2b in Huxter et al. (2008)). To our knowledge, this phenomenon has not been explained by existing models of phase precession. In the present model, similar dynamics occur when the interneuron is not driven sufficiently to pass through to the next cycle and is instead attracted back towards the initial phase (Figure 4.4A). These dynamics are similar to those of a pendulum, which will swing through a complete revolution if driven strongly enough, but will fall backwards if not driven over the vertical point.

Given that weak inputs can be insufficient to generate phase precession in the model, we next investigated the robustness of phase precession depending on the strength of current drive to the place cell. In particular, how robust is the circuit to variations in the amplitude of the slow envelope input, and what are the consequences of excessively weak or strong inputs? We found that strong and sustained inputs to place cells can result in precession over multiple theta cycles (Figure 4.4B). However, the pacemaker drive to the interneuron confers some robustness against this effect, as the interneuron can only precess through a discrete number of theta cycles and requires a considerable additional input to precess through two cycles of theta rather than one. Figure 4.5A shows how the number of theta cycles precessed by the interneuron varies with the amplitude of slow envelope. Over a broad range of input currents (or more directly, a range of pyramidal cell spike counts as in Figure 4.5B-C), the interneuron

will continue to precess through exactly one cycle over the place field. These dynamics also place limits on rate remapping within place cells, through which additional task-relevant information is encoded in the firing rate of a place cell within the place field (Allen et al., 2012). We found robust phase precession through one cycle in the interneuron provided the place cell fires between 10 and 25 spikes in the place field. Thus, phase precession is sufficiently robust as to allow considerable rate remapping, but phase precession will be disrupted for excessively large changes in firing rate.

In summary, the model outlined here provides a robust mechanism for phase precession consistent with the circuitry in CA1. The model accounts for the key features of phase precession observed in CA1, including the dependence on running speed, place field size and dorsoventral location, phase precession along two dimensional trajectories, the coupling of phase precession between place cells and interneurons and the phase gradient along the dorsoventral axis. In the following sections we investigate the ability of the model to account for large scale network activity during theta states, including the capacity to generate sequential activity across multiple spatial maps.

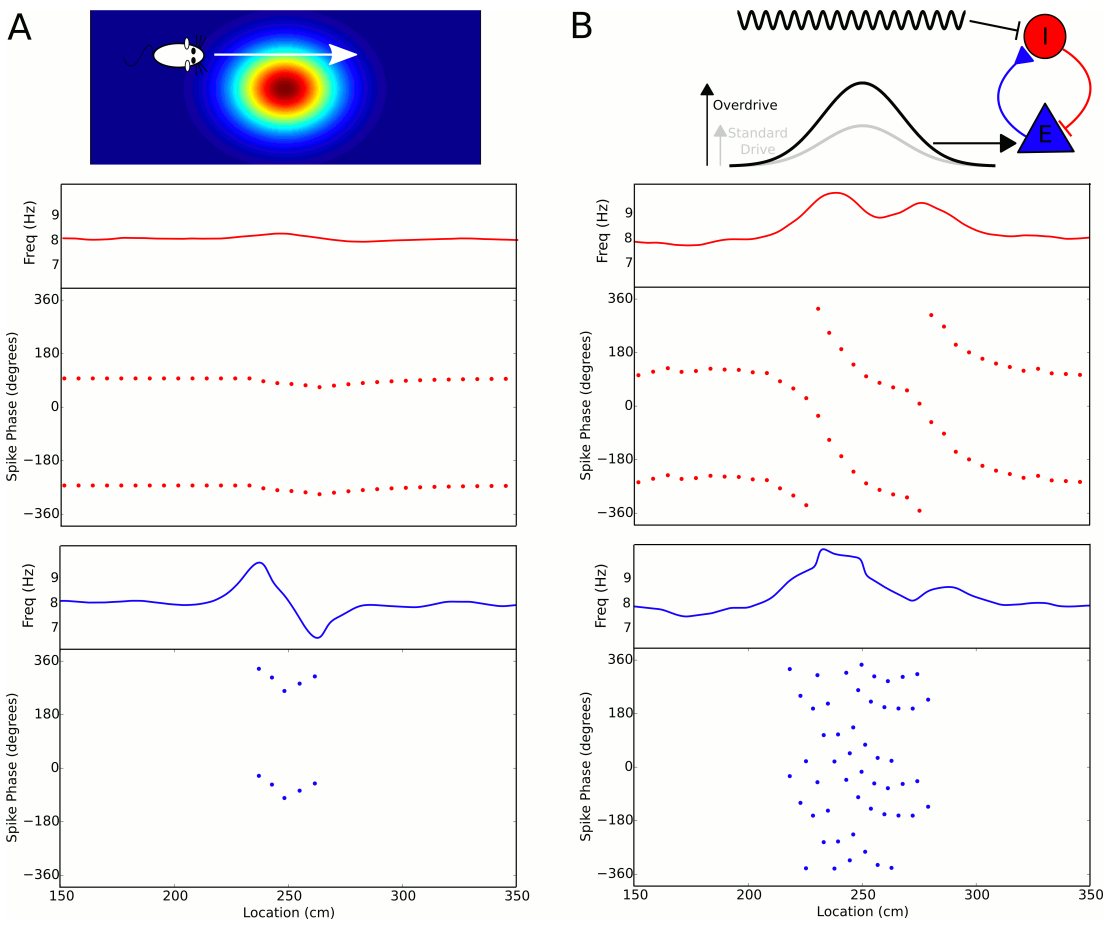

Figure 4.4: (A) Failure to precess through one full cycle. In this case, the external inputs were not strong enough to drive the interneuron past the threshold to be pulled into the next theta cycle, and instead it is pulled back towards the phase it started at. This is also seen in an initial increase followed by a decrease in frequency as the cell precesses before processing in phase against the pacemaker. (B) Precession through two full cycles. In this simulation, the amplitude of the slow envelope current was increased. This results in an increased firing rate of the pyramidal cell and hence an increased excitatory input to the interneuron. As a result, the interneuron received enough drive to pass through two cycles of pacemaker input.

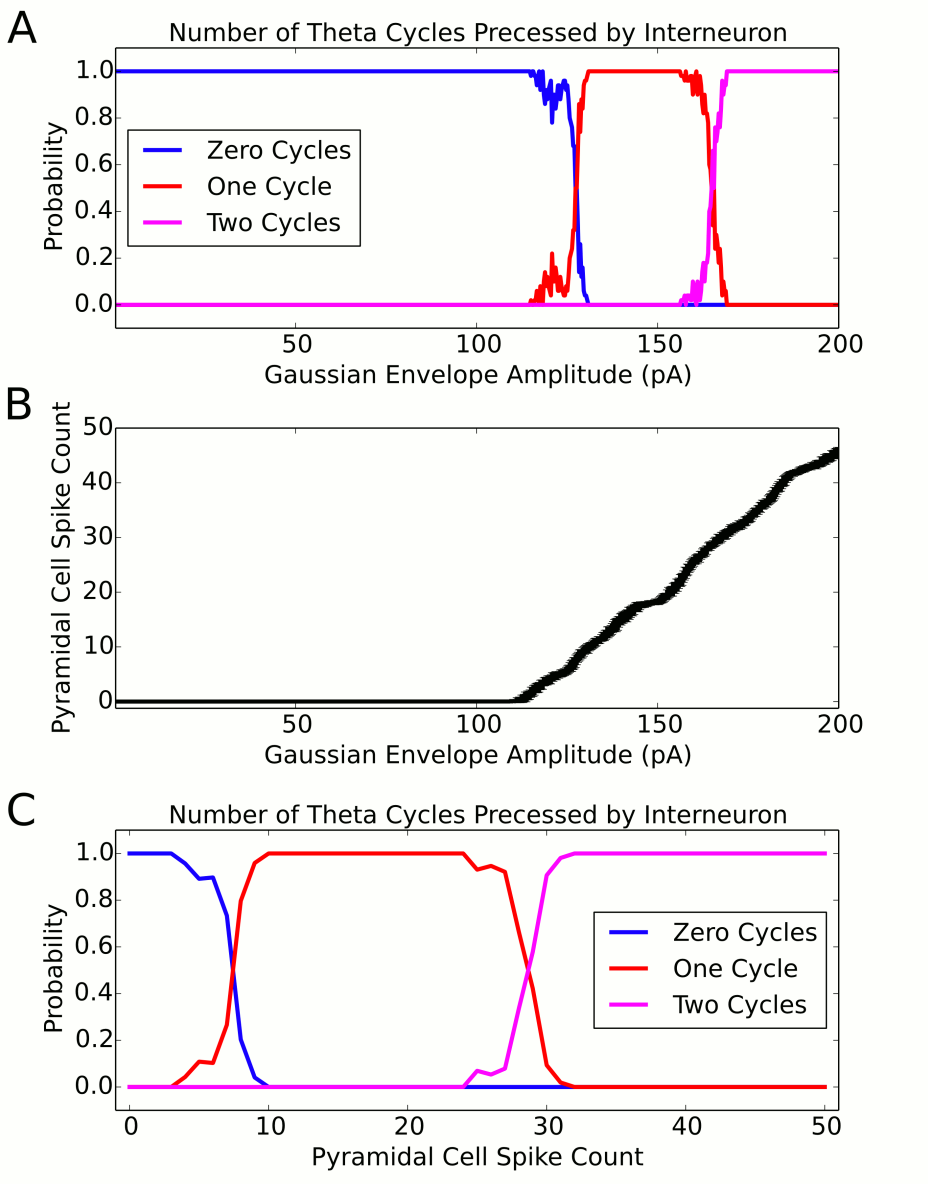

Figure 4.5: (A) The probability of an interneuron precessing through one, two, or three cycles of pacemaker theta phase as a function of the amplitude of the depolarising envelope current onto the place cell. (B) The number of spikes fired by the place cell (with standard deviation shown as error bars) as a function of the amplitude of depolarising envelope current. (C) The probability of the interneuron precession through one, two, or three cycles of pacemaker theta phase as a function of the number of spikes fired by the place cell.

4.6 Functional coupling of a single interneuron to multiple pyramidal cells.

While the network in Figure 4.1 generates phase precession in an isolated place cell and interneuron, CA1 place cells are embedded into much larger networks with far fewer interneurons than pyramidal cells (Freund and Buzsáki, 1996). It is estimated that only 7-11% of CA1 cells are GABAergic interneurons (Woodson et al., 1989; Aika et al., 1994; Bezaire and Soltesz, 2013). The large disparity in the number of place cells and interneurons demands that a single interneuron in the model must couple to multiple pyramidal cells and generate phase precession in each one.

To test if this is possible, we simulated a single interneuron which couples synaptically to two pyramidal cells. Figure 4.6 demonstrates that, if each pyramidal cell receives a depolarising drive at a different time, an interneuron can be selectively recruited for phase precession by multiple pyramidal cells. A consequence of such a mechanism is that the interneuron shows multiple phase precession fields, and that each place cell which couples to that interneuron to generate phase precession shows subthreshold phase precession fields whenever the interneuron precesses. Thus, a key signature of this mechanism is the presence of transient increases in the membrane potential oscillation frequency outside the firing field of a place cell (Figure 4.6B).

While a single interneuron can functionally couple to multiple place cells to generate phase precession when their firing fields are well separated, it is unclear if these dynamics are possible when firing fields overlap. In such a case the net synaptic input to the interneuron may be too strong, such that the precession frequency increases and multiple cycles are precessed (as in Figure 4.4B). Even if the interneuron precesses through just one cycle, synaptic outputs from the interneuron may synchronise all place cells which receive strong inputs from that interneuron. If so, partial overlap between place fields of cells coupled to the same interneuron may disrupt the relationship between spike lags and place field separation required for sequence compression (Skaggs et al., 1996), causing place cells with separated place field centres to spike in synchrony. In the following section, we investigate the ability of a large scale network to generate theta sequences under different place field maps and the influence of place field organization on sequence compression.

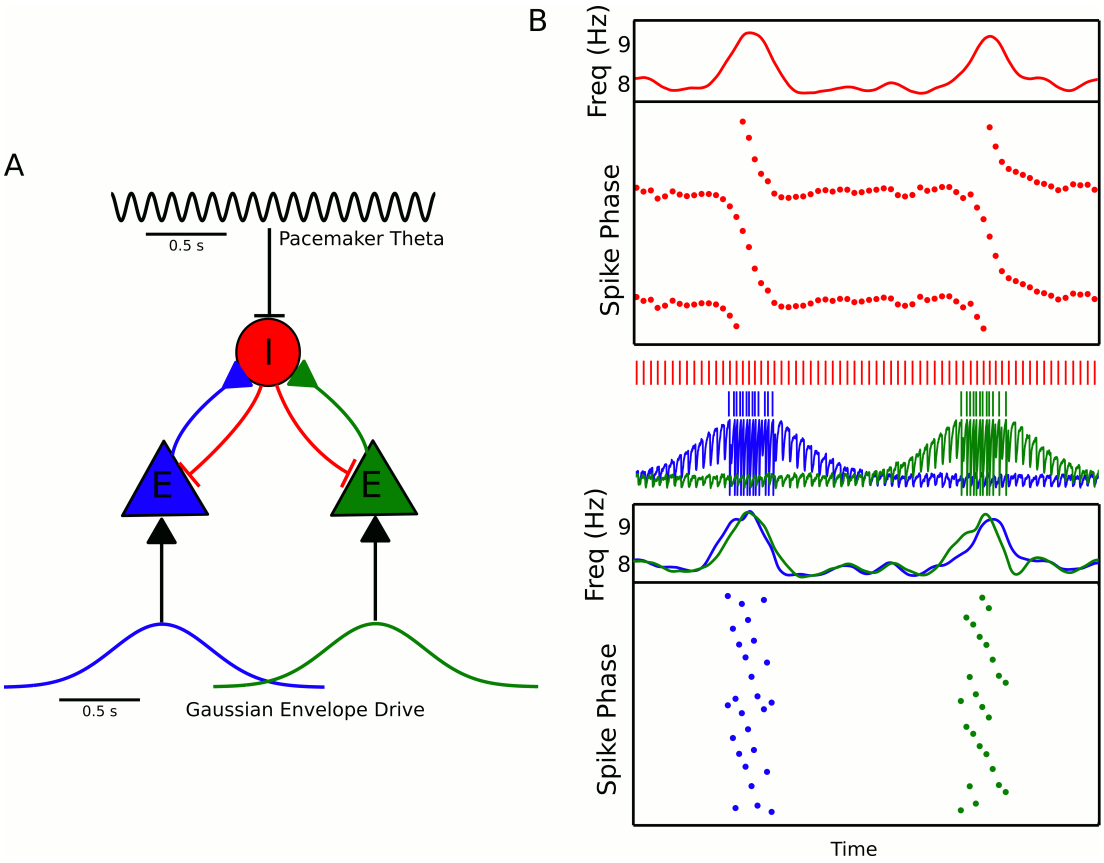

Figure 4.6: (A) Circuit diagram showing two pyramidal cells connected to the same interneuron, receiving slow envelope currents at different points in time. (B) Simulation of this circuit showing the intrinsic theta frequency, spike phases and membrane potentials.

4.7 Theta sequences are disrupted in unconstrained place field maps

We wished to investigate the extent to which the minimal CA1 circuit described in Figure 4.1, when extended to a large scale network, can account for the activity patterns of CA1 populations during theta oscillations. Of particular interest is the relationship between single-cell phase precession and network level sequential activity patterns. While phase precession in individual place cells is generally sufficient to generate population theta sequences (Skaggs et al., 1996), recent evidence suggests that this is not always the case (Feng et al., 2015). Moreover, our previous model demonstrated that, for some forms of phase coding, the emergence of theta sequences from phase precession may be dependent on the spatial organization of place fields (see Chapter 2). In principle, independent coding mechanisms such as the present model can have a higher

representational capacity than mechanisms based on coordinated coding (see Chapter 2), but the extent to which this capacity is compromised by the constraints imposed by circuit connectivity within the present model is unclear. We therefore proceeded to investigate the ability of large scale networks to perform sequence compression on slow place field inputs and the conditions under which single-cell phase precession gives rise to network level sequence compression within the present model.

To address these questions, we quantified the performance of the network in simulations while varying the properties of the spatial maps (i.e., the organisation of the slow envelope inputs to pyramidal cells). In our model of a CA1 network, each pyramidal cell coupled to only one interneuron, and all connections were bidirectional (see Methods). Hence, each interneuron coupled to multiple pyramidal cells. We view this network as a simplified description of the interactions underlying phase precession, with other circuit interactions removed. We hypothesised that place field overlap between pyramidal cells coupled to the same interneuron would be disruptive to theta sequences, such that the degree of sequential organization of spiking activity within theta cycles would depend with the amount of overlap.

To test this, we simulated network activity in two distinct scenarios. In the first scenario, place cells which functionally couple to the same interneuron are optimally arranged in order to maximise their place field separation on the linear track. In the second case, place fields are randomly mapped to the track. In both cases, we varied the number of place cells per interneuron which are active on a linear track of fixed length (i.e., the density of the place code). For the case of random place field mapping, this results in a continuous increase in the probability of place field overlap between place cells coupled to the same interneuron. For the case in which place fields are optimally mapped onto the track, such place field overlap occurs when the density of the code crosses a fixed threshold (Figure 4.7A). Consistent with our hypothesis, Figure 4.7C shows that the network can successfully compress slow input sequences into fast theta sequences for sparse place field maps with low overlap, but that such sequences do not emerge in dense maps with high overlap.

To understand how place field mapping influences the ability of the network to perform sequence compression, we introduced two distinct metrics which measure the extent to which spiking within theta cycles faithfully recapitulates the slow sequence of envelope inputs, which we call the *single-cycle sequence* metric and the *population phase precession* metric (see Methods for details). For the single-cycle sequence metric, we calculated the correlation between spike time and place field centre for all

spikes generated in the place cell population within a single theta cycle, a direct measure of sequence compression at the single-sequence level (Figure 4.7B, red line). The population phase precession metric was calculated by pooling the spikes of all place cells over a full lap and quantifying the correlation between spike phase and the distance of the animal from the place field centre of that cell at the time of that spike (Figure 4.7B, blue line). This measure returns a strong correlation if each individual place cell exhibits a robust correlation between spike phase and location and in addition this relationship is coherent amongst different cells in the population, i.e. if all place cells show a similar relationship between spike phase and location. By requiring that phase precession amongst different cells is coherent, this metric therefore serves as an averaged measure of sequence compression over a dataset.

Applying these measures to simulations with different place field densities, we found that the strength of both single-cycle sequences and population phase precession decreases with increasing place field density on the track, indicating that the ability of the network to compress slow sequences of inputs into fast theta sequences is disrupted. This trend occurs for optimal place field mappings and for random place field mappings (Figure 4.7B, solid vs dashed lines). Random place field mappings, however, show a continuous degradation of network performance with increasing place field density, whereas optimal place field mappings maintain high performance over a range of place field densities before beginning to degrade as place field overlap finally emerges, consistent with the hypothesis that place field overlap of pyramidal cells coupled to the same interneuron disrupts sequence compression (see Figure 4.7A). Therefore, both the number of active place cells in an environment and the spatial organization of their place fields influence the quality of sequence compression. In general, network performance is high when the spatial maps are sparse, but high levels of performance can be maintained with more dense spatial maps provided that the place fields of cells coupled to the same interneuron are well separated.

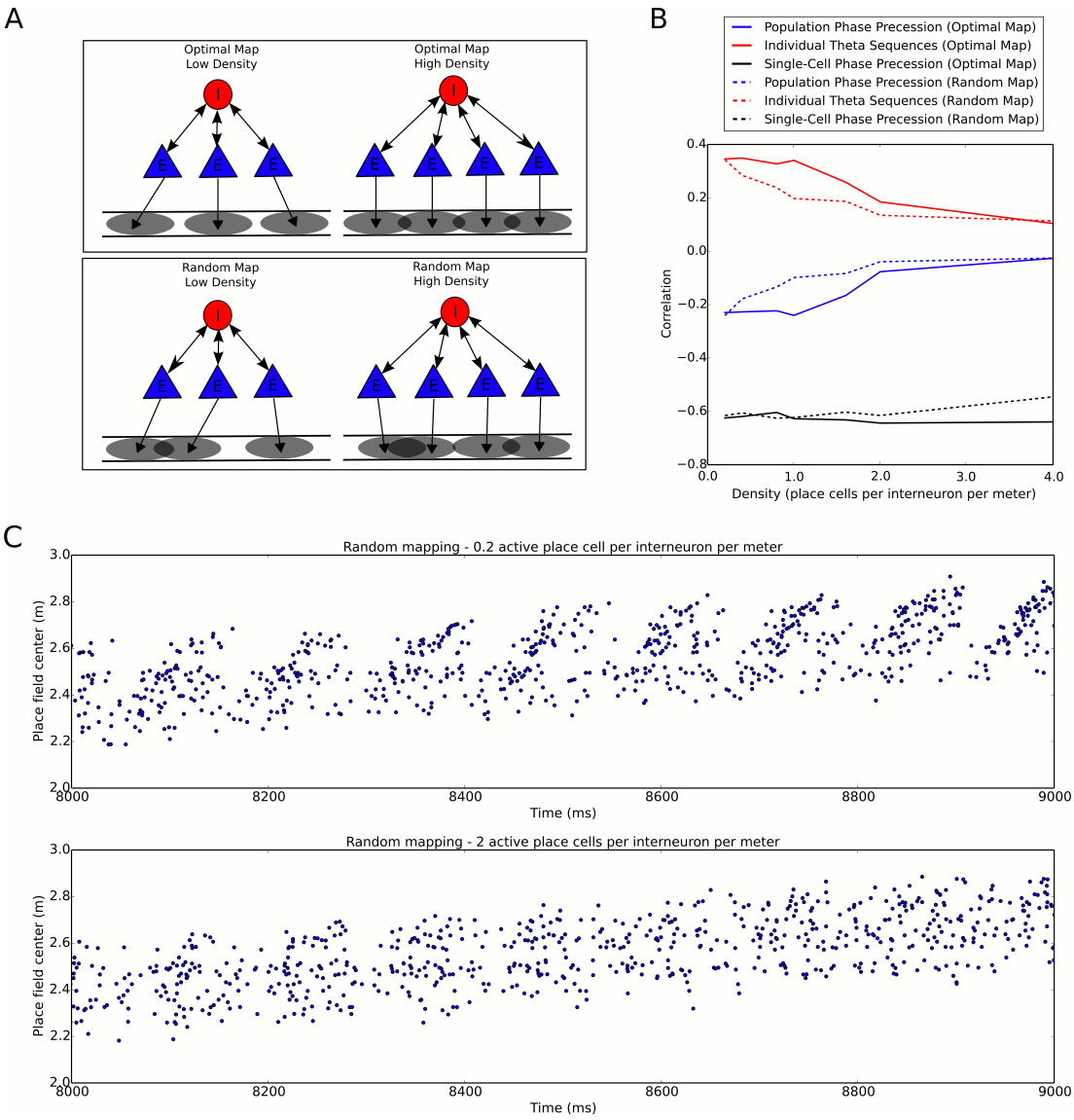

Figure 4.7: (A) Top: Examples of optimal maps given two different place field densities. A set of place cells attached to the same interneuron are mapped onto a linear track. In an optimal map, their place field centres are organised such that their overlap is minimised. For a certain number of place cells per interneuron (here, four) overlap occurs even for an optimal map. Bottom: Example of random maps. The location of each place field on the track is drawn from a uniform probability distribution. In this case, a larger number of place cells per interneuron causes an increase in the probability that place fields will overlap. (B) Network performance vs number of active place cells per interneuron. As more place cells become active (or the number of interneurons is decreased), the compression of inputs into theta sequences is degraded. This is caused by a drop in the coherence of phase precession in the population, despite a relatively constant phase-position correlation in individual place cells. Note that while the population phase precession metric approaches zero, the single-cycle metric approaches a non-zero value reflecting the slow movement of activity through the population on a behavioural timescale. (C) Example network simulations at low and high mapping densities.

Theta sequences are contingent on independent phase precession

It is possible that the observed changes in sequence compression in neuronal populations are caused by changes in the quality of phase precession in individual place cells. Alternatively, they may result from changes in the timing relationships between groups of place cells (i.e., a decoherence of phase precession in neuronal populations). To test this, we next we quantified the fidelity of single-cell phase precession by calculating the correlation between spike phase and location for individual cells on single laps. This measure differs from the population measure in that it doesn't require phase precession amongst different place cells to be coherent at the population level and hence is not in itself sufficient for sequence compression to emerge. We found that this measure of single-unit phase precession remained stable with increasing place field overlap despite the disruption of both single-cycle sequences and population phase precession (Figure 4.7B, black line). Hence, while individual cells continue to precess in phase, the theta lag between cells no longer encodes the distance between their place field centres. This is a consequence of place field overlap between place cells associated with the same interneuron, which causes them to enter synchrony so that the phase lags required for sequence compression cannot be formed. Phase precession therefore leads to robust theta sequences only when pyramidal cells precess independently of one another, whereas interactions via shared interneurons lead to disruption of sequences.

Recent experimental evidence suggests that the formation of theta sequences in a novel environment develops rapidly after first exposure. On the first lap of a linear track place cells exhibit phase precession, in that their frequency is higher than the network theta and their phase shifts continuously from place field entry to exit. Nevertheless, the phase lags between cells are uncoordinated and do not generate population theta sequences, which instead emerge rapidly with further experience (Feng et al., 2015). These observations are consistent with our model, assuming that the initial place field mapping includes interference between phase precessing cells which is then rapidly removed by some decorrelating mechanism with subsequent experience.

Our model suggests two potential mechanisms which could perform this task. First, plasticity between place cells and interneurons could modify the synaptic weights such that place cells with overlapping place fields no longer couple strongly to the same interneurons (Figure 4.8A). Second, the slow envelope inputs to place cells could rapidly reorganise in order to minimise the overlap of place fields of cells coupled to the same interneurons (Figure 4.8B). If a plasticity mechanism were in place, synaptic changes

which allow sequential activity in a new environment would cause disruption in previously stored maps. If place field reorganisation were to underlie the formation of coherent theta sequences, multiple stable maps might be formed without disruption or interference between different representations. Experimental evidence suggests that place field activity is indeed reorganised upon exposure to a novel environment, including a sparsification of the CA1 place code and and a decrease in the number of active place cells (Frank et al., 2004; Karlsson and Frank, 2008). Further, reorganisation of CA1 sequence activity in a novel environment is initially contingent on NMDA receptor-dependent plasticity in upstream CA3, suggesting that it is the external inputs to CA1 place cells which is reorganised rather than the interactions between CA1 place cells (Dragoi and Tonegawa, 2013a). Whether such a reorganisation is consistent with the removal of unwanted place field overlap is yet to be determined.

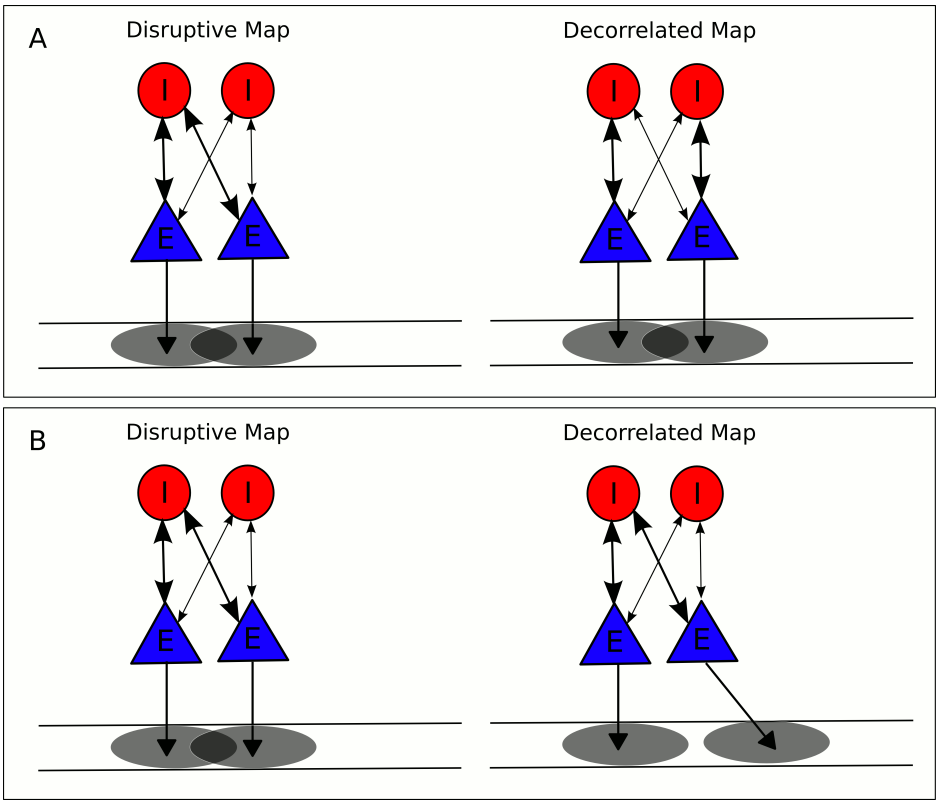

Figure 4.8: Putative mechanisms for removing disruption from network theta sequences. (A) In one possible mechanism, synaptic weights between pyramidal cells and interneurons are altered so that pyramidal cell pairs with overlapping place fields no longer functionally couple to the same interneuron. (B) In a second mechanism, the place fields themselves undergo changes to remove overlap for place cells coupled to the same interneuron.

4.8 Theta sequence generation requires sparse place field maps

We next investigated the consequences of the assumption that place field mapping is organised in order to minimise network interference. What constraints does this assumption impose on spatial mapping? To answer this question, we developed a simplified model of spatial mapping. In this model, place cells can map to different locations on a linear track, under the constraint that place cells which functionally couple to the same interneuron cannot map to locations within a certain distance of each other, which we termed the exclusion zone. For a given number of place cells and interneurons, track length and place field size, how many spatial maps are possible? What fraction of place cells can be active on the track without violating the constraint? We were able to arrive at concrete answers to these questions in the context of the simplified model of spatial mapping (see Appendix C). The maximum fraction of pyramidal cells, F, which can express place fields in a given map is:

$$F < \frac{N_I}{N_P}\frac{L}{D} \tag{4.1}$$

where N_I, N_P are the number of interneurons and pyramidal cells respectively, L is the length of the track and D is the exclusion zone (approximately the size of a place field). The above inequality gives a bound on the coding density of the spatial representation. In particular, it shows that spatial maps generated by this network must be sparse and that the required sparsity depends on the ratio of pyramidal cells to interneurons and the size of the place fields. As this is an upper bound for the fraction of active cells, there is a range of sparsities which are feasible in an operating network (as evidenced in the optimal mapping simulations of Figure 4.7B, where the network performance remains fixed with increasing place cell numbers before place field overlap occurs and performance deteriorates). If the network is close to this upper bound, there will be a high density of subthreshold phase precession fields in place cells and interneurons will precess in phase over most of the environment. If instead the network is operating well below this upper bound, so that the representation is sparser than the minimum requirement, there will be only occasional interneuron and subthreshold phase precession fields. While subthreshold phase precession fields have not yet been investigated, the density of reported interneuron phase precession fields can be high (see Figure 2 of Maurer et al. (2006b)).

4.9 Theta sequences can be generated in a large number of spatial maps

We next asked whether the non-overlap constraint places limits on the capacity of the network for the representation of distinct environments and contexts. Our previous phenomenological model showed that it is possible for a place cell population to show coherent sequential activity patterns within a given spatial map, yet generate incoherent activity patterns within other maps (see Chapter 2). We therefore asked whether the network can perform sequence compression across multiple distinct spatial maps and whether there are any limitations on capacity imposed by the network connectivity.

We quantified the capacity of the network under the non-overlap constraint in three different ways (see Methods). First, we quantified the number of spatial maps available to the network within our simplified model of spatial mapping. To do this, we assume that place cells encode with a given spatial acuity, such that place field locations can be distinguished with a particular spatial resolution x_{res} which is limited by biological noise and variability, and count the number of place field configurations which are distinguishable at this resolution and obey the non-overlap constraint. Second, we quantified the number of possible cell assemblies, i.e. the number of possible sets of coactive place cells which do not generate theta disruption. Each cell assembly might be considered as representing a particular location or context. Finally, we considered the capacity in terms of the number of sequences which can be generated. We consider a sequence to be an ordered set of cell assemblies. A sequence might represent a trajectory through space, or an episode consisting of a sequence of events encoded by individual cell assemblies. We assumed that no two cells in a single sequence can couple to the same interneuron. We note here that, as we have defined a cell assembly as a set of coactive neurons, it does not imply synaptic coordination and may arise from independent coding mechanisms as discussed in Chapter 2.

We find that the number of distinct spatial maps, cell assemblies and sequences which can be generated by the network are each considerably larger than the number that an animal could encounter within its lifetime. For example, assuming a population of 10000 pyramidal cells of which 20 % are active in each map, 1000 interneurons, an exclusion zone between place fields of 1 meter, a linear track of length 5 meters with and with a spatial resolution of only 10 cm (a conservative estimate), the number of spatial maps in which coherent theta sequences are generated is greater than 10^{5000}. For the same population of cells, assuming each cell assembly consists of 100 pyra-

midal cells, there over 10^{500} possible cell assemblies, and assuming a phase sequence consists of 7 cell assemblies (Lisman et al., 1995) there are over 10^{1500} possible sequences. Hence, despite the constraints imposed by the coupling between groups of pyramidal cells and interneurons, the capacity of the network to encode distinct environments, contexts and episodes can be considered to be unlimited from an ethological perspective.

In summary, we find that overlap between the place fields of pyramidal cells which functionally couple to the same interneuron can disrupt sequence compression in the network. The level of disruption increases with the number of active place cells per interneuron. For random place field mappings, maintaining coherent sequence compression requires that place field maps are very sparse. By introducing mechanisms to organise place field maps in order to avoid interference, coherent sequence compression can be maintained with relatively large numbers of active place cells. While such mechanisms reduce the number of spatial maps available to the network, we find that even under these constraints, there is a practically unlimited capacity for encoding distinct spatial maps, cell assemblies and theta sequences in the network.

4.10 Flexible compression of arbitrary input sequences allows learning through STDP

In the model outlined here, slow input sequences of slow current envelopes are compressed into fast, repeating sequences of spiking activity. This runs in contrast to the alternative hypothesis that such sequences are generated by internally coordinated ensemble interactions, which have been hypothesised to generate both phase precession and firing fields as a result of a fundamental sequential organization of network dynamics (Lisman and Redish, 2009; Wikenheiser and Redish, 2015; Wang et al., 2015). What possible functional advantages could arise from the passive compression of slow current inputs, as opposed to the ensemble coordination hypothesis? In this section, we show how the compression of slow input sequences can be used in conjunction with spike time dependent plasticity (STDP) to learn associations in a classical conditioning paradigm.

A longstanding hypothesis for the function of sequence compression is the induction of synaptic plasticity (Skaggs et al., 1996). In particular, STDP can allow causal relationships to be learned by strengthening synapses between cells firing in a partic-

ular (Bi and Poo, 1998). However, the timescale of neuronal activity correlations on which STDP acts is on the order of tens of milliseconds, which is at least an order of magnitude shorter than the timescales of causal relationships typically encountered in behavioural contexts. The model proposed here offers a solution to this disparity in timescales. As an animal explores an environment, the ongoing sequence of behavioural events is compressed into theta sequences representing several seconds of recent and upcoming experiences (Figure 4.9A, B). Because behavioural events extending up to several seconds into the past are represented in an orderly fashion along the descending phase of the theta cycle and events occurring up to several seconds into the future are ordered along the ascending phase, sequence compression using theta oscillations generates an absolute temporal reference frame in neural time for past, present and future events in real time on which STDP can act (Figure 4.9C).

To illustrate this, we consider the case in which a population of CA1 pyramidal cells performing sequence compression on its inputs projects to a downstream neuron which encodes some particular outcome or event of behavioural relevance, termed the *unconditioned stimulus* (Figure 4.9B). This outcome may be a reward, punishment or any other event which the animal might need to remember. When the unconditioned stimulus occurs, the downstream cell signals that event by firing action potentials. Figure 4.9C shows that, if these action potentials lock to the trough of the theta rhythm, a standard STDP rule will cause the set of CA1 pyramidal cells representing experiences which occurred recently before the unconditioned stimulus on a behavioural timescale to undergo an increase in synaptic strength onto the downstream cell. This circuit therefore performs supervised learning, forming an association between the conditioned and unconditioned stimuli (here, the conditioned stimulus can be thought of as the context or location recently before the onset of the unconditioned stimulus, represented via the slow envelope inputs to the CA1 network).

How sequence compression and STDP interact in this context can be understood in the following way. Given a standard plasticity rule of the form:

$$\Delta w(\Delta\tau) = \begin{cases} A_+ e^{-\Delta\tau/\tau_+} & \Delta\tau > 0 \\ -A_- e^{\Delta\tau/\tau_-} & \Delta\tau < 0 \end{cases} \tag{4.2}$$

where $\Delta\tau$ is the spike lag between pre- and post-synaptic cells, the above mechanism transforms the rule to behavioural times via the following effective plasticity rule:

$$\Delta w(\Delta t) = \begin{cases} A_+ e^{-\Delta t/(c\tau_+)} & \Delta t > 0 \\ -A_- e^{\Delta t/(c\tau_-)} & \Delta t < 0 \end{cases} \tag{4.3}$$

where Δt is the behavioural time from the present moment (i.e., past events have $\Delta t < 0$ and future events have $\Delta t > 0$) and c is the compression factor of the CA1 network (see Chapter 2).

If the downstream cell were to lock to a theta phase other than the trough, this would introduce a temporal shift to behavioural time lags at which potentiation and depression of synapses occurs. For example, a downstream neuron which fires at the peak of the theta oscillation will cause a *decrease* in synaptic strength from neurons representing past events and an *increase* in synaptic strength from CA1 pyramidal cells representing the future events (Figure 4.9D). As cells in the ventral striatum are known to precess in phase when ramping up to a reward (van der Meer and Redish, 2011), such a mechanism might serve important functions. In particular, since the reward cell fires nearer to the peak of theta when the animal is further from the reward, this would cause CA1 cell assemblies representing locations ahead of the animal to be associated with the reward when the reward is still far away, and locations behind the animal to be associated with the reward once the reward has been achieved. Thus, sequence compression with theta oscillations allows events occurring further in the past or future to be flexibly and selectively associated with a particular outcome by varying the spike phase of the downstream cell.

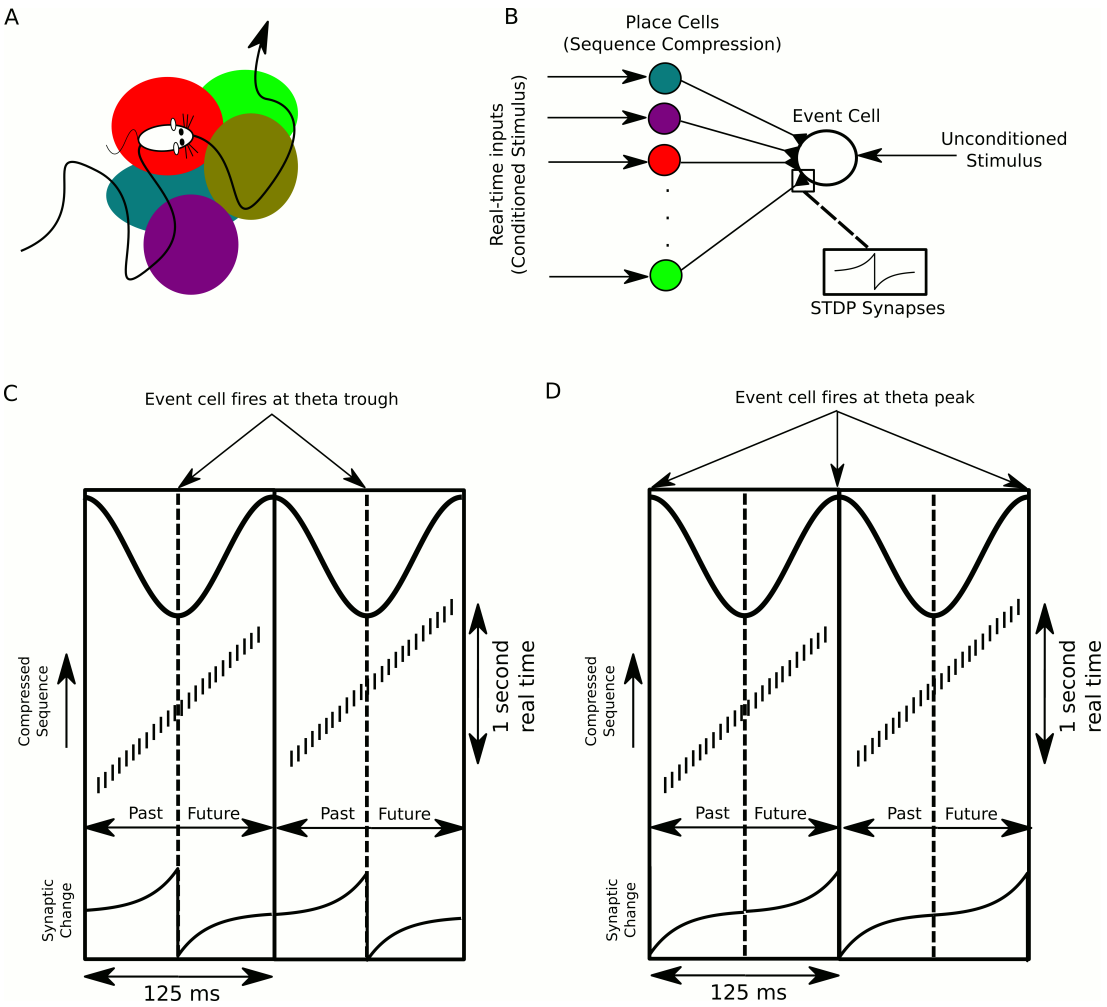

Figure 4.9: A proposed function of sequence compression for supervised learning. (A) The animal explores an environment, activating different cell in CA1 in a particular temporal order on a behavioural timescale. (B) A population of CA1 place cells performs sequence compression on the slow Gaussian envelope inputs. These cells project onto a downstream neuron which signals some event of interest (the unconditioned stimulus). When this event occurs, this cell fires tonically at the trough of the theta cycle. Synapses from CA1 place cells to the event cell are modifiable via STDP. (C) During each cycle of the theta rhythm, CA1 cell assemblies representing past, present and future events in behavioural time are activated sequentially. At the trough of the theta cycle, place cells representing the animal's current location are active, whereas during the descending and ascending phases cells representing past and future locations respectively are active. If the downstream cell signalling the unconditioned stimulus fires an action potential at the trough of the theta cycle, STDP between pre- and post-synaptic spikes establishes an association between cells representing recently visited locations and the event. (D) If instead the downstream cell encoding spikes at the peak of the theta rhythm, an association between cells representing upcoming locations and this cell is formed, whereas cells representing recently visited locations and this cell have their synapses weakened (i.e., the temporal associations are reversed relative to those in (C)).

4.11 Discussion

We show that a minimal model based on the known CA1 network architecture can produce phase precession and theta sequences. The network can flexibly generate phase precession with running speed dependent oscillation frequencies, along arbitrary two dimensional trajectories and across a large number of distinct spatial maps. Phase precession is generated *de novo* within the network, without the need for external inputs with velocity-controlled oscillation frequencies or temporally patterned inputs to place cells. Instead, the phase precession of interneurons, previously assumed to be an epiphenomenon resulting from synaptic inputs from phase precessing place cell assemblies, acts to coordinate pyramidal cells and transfer phase precession to place cell assemblies. Our model can account for phase precession along the dorsoventral axis of the hippocampus, including a gradient in place field size, precession slope and theta phase (Kjelstrup et al., 2008 Lubenov and Siapas, 2009; Patel et al., 2012).

The network automatically compresses slow sequences of current inputs occurring on timescales of seconds into fast sequences of spiking activity within each cycle of the network theta rhythm. The ability of the network to perform such sequence compression, however, depends on the mapping of inputs into the network and the details of the coupling between pyramidal cells and interneurons. Specifically, a single phase precessing interneuron will synchronise all pyramidal cells which receive strong synaptic inputs from that interneuron. Hence, if pyramidal cells are to form asynchronous sequential activity patterns within theta cycles, the external inputs to the network must be such that pyramidal cells which couple strongly to the same interneuron receive temporally segregated inputs at behavioural timescales. We considered two ways in which this could be achieved. In the first case, the mapping of inputs to the network is random, but the sparsity of inputs is sufficiently high that the probability of unwanted overlap is low, and the ability of the network to perform sequence compression is maintained. In the second case, inputs are rapidly reorganised so as to minimise the temporal overlap of inputs to pyramidal cells sharing a common interneuron. This allows network performance to remain high with increasing numbers of active pyramidal cells, and can explain recent observations that theta sequences are absent on the first lap of a novel track, but emerge rapidly with subsequent exposure (Feng et al., 2015). Our model provides a very different interpretation of the results of Feng and colleagues, however. While Feng and colleagues proposed that sequences emerge due to an increase in the synaptic coordination within the CA1 network, our model suggests that sequences in

fact emerge due to a decrease in synaptic coordination between pyramidal cells active within a theta cycle, such that disruptive synchrony is removed in order to generate an independent population code.

We previously presented a phenomenological model which accounts for the statistical properties of CA1 population activity during navigation (see Chapter 2). The present model extends these results by providing a mechanistic basis for independent theta phase coding. In particular, the previous model suggested that the membrane potential oscillations of place cells should lock to the LFP theta rhythm when the animal is outside of their place fields, and display a transient elevation of membrane potential oscillation frequency inside their firing field. This allows remapping without disrupting theta activity provided that this elevation of membrane potential frequency is always locked to the firing rate field. The present model suggests that this increase in frequency is generated via coupling between place cells and interneurons. As a consequence an increase in membrane potential oscillation frequency occurs whenever the place cell is activated by a slow depolarising current, which explains how the theta frequency elevation coincides with the firing rate field. Nevertheless, while our previous model suggested that such a mechanism would allow arbitrary remapping of place field locations, the mechanism we propose here imposes some additional restrictions. These restrictions arise because the increase in membrane potential frequency is common to all pyramidal cells coupled to the same interneuron, which was not a feature of the previous phenomenological model. As in the phenomenological model, place cells in the mechanistic model precess in phase independently of each other provided that the place fields of cells coupled to the same interneuron do not overlap. If these place fields do overlap, the cells enter into a highly synchronous state and theta sequences are disrupted. It is possible that such disruptive synchronisation exists in CA1 networks between a small number of cells, although the failure to observe this in existing datasets suggests that it is rare (see Chapter 2).

In our model, phase precession is generated *de novo* by the dynamics on the local circuitry and allows running speed dependence and directional phase precession in open environments without the need for specialised velocity-controlled input oscillation frequencies or head direction cells. Our model therefore offers significant advantages over existing proposals. O'Keefe and colleagues originally proposed a mechanism based on the interference of oscillations at different frequencies (O'Keefe and Recce, 1993), which has subsequently been developed and extended to grid cells (Burgess et al., 2007). While such models can account for phase precession across run-

ning speeds and in open environments, the velocity dependence is included by hand in these models. Other models include asymmetric excitatory synaptic connectivity (Tsodyks et al., 1996; Wang et al., 2015), spike train adaptation (Harris et al., 2002), asymmetric place fields (Mehta et al., 2002), interference between inputs from entorhinal cortex and CA3 (Chance, 2012) and inheritance from phase precessing synaptic inputs (Jaramillo et al., 2014). Several of these models have difficulties generating phase precession and theta sequences in open environments (Tsodyks et al., 1996; Mehta et al., 2002; Chance, 2012; Wang et al., 2015), inheritance models do not address the *de novo* origin of phase precession (Jaramillo et al., 2014), and it is not clear whether models based on spike train adaptation can account for velocity dependencies (Harris et al., 2002). Hence, a major advance of our model is to account for all of these phenomena within a biophysical framework consistent with CA1.

The model outlined here makes several testable predictions. First, we predict the existence of subthreshold phase precession fields in silent or inactive pyramidal cells. These are most easily observed as transient increases in subthreshold oscillation frequency in the theta band. Second, we predict that pyramidal cells which precess in tandem with a particular interneuron have non-overlapping place fields, and will enter a highly synchronous state if not. Third, we predict that a continuous current injection to a pyramidal cell during theta activity should be sufficient to generate phase precession. Fourth, we predict that phase precession in place cells should be accompanied by the presence of strong, phase precessing inhibitory synaptic inputs. Fifth, entrainment of septal GABAergic inputs should set the basal theta frequency, but precession of CA1 interneurons and place cells against this basal theta should remain intact. Finally, phase precessing interneurons should show reciprocal synaptic connections onto pyramidal cells, and the interneuron to pyramidal cell synapse should be sufficiently strong to synchronise theta activity. Finally, inactivation of phase precessing interneurons should block pyramidal cell phase precession.

Several other brain areas exhibit theta phase precession. These circuits display a variety of different coding properties and circuit connectivities. In CA3, pyramidal cells are connected via dense recurrent collaterals, which have been hypothesised to form a substrate for associative memory. In layer II of the entorhinal cortex, principal cells are connected indirectly via inhibitory interneurons (Couey et al., 2013; Pastoll et al., 2013), and show periodically repeating firing fields which tessellate an environment and may form a substrate for path integration. Do these differences in coding properties and circuit wiring imply a different mechanism for phase precession from

the one outlined here for CA1? It is possible that, despite the presence of recurrent excitation in CA3, phase precession is nevertheless generated via coupling between pyramidal cells and interneurons. In this case, excitatory synapses may simply modulate the theta-scale dynamics generated by excitatory-inhibitory coupling, or they may primarily subserve slower timescale dynamics via attractor mechanisms. Grid cell circuitry is similar to that outlined here for CA1, in that stellate cells are connected with local interneurons without direct recurrent connectivity. Hence, the mechanism outlined here could account for phase precession over each individual firing field in grid cells. However, the periodic firing fields of each grid cell cover a large fraction of the environment, so that firing field overlap between any two grid cells is on average greater than that for place cells. Hence, if phase precession in grid cells is subserved by the mechanism described here, the capacity for remapping should be vastly restricted in comparison to place cells due to the higher coding density (see Figure 4.7B). Indeed, grid cells generally remap via simple affine transformations such as rotation, translation and shear. Future work should investigate whether the mechanism outlined here can be implemented in attractor networks, either with recurrent excitation as in CA3, or with patterned excitatory and inhibitory connectivity as in models of grid cell modules. In this case, the slowly varying inputs to excitatory neurons would arise primarily from internally generated attractor dynamics rather than external inputs as we have considered in this study.

We find that the network considered has a vast capacity for the compression of sequences of events on behavioural timescales into theta sequences. The number of episodes which could be represented by the network is practically unlimited in comparison to the number of events which are encountered by an animal within its lifetime. The storage of such events into long term memory, however, is not addressed by this model. We suggest that the network considered here provides a flexible format for the representation of experienced events in real time, but that the capacity to store experienced events into long term memories is likely to be far more limited. During a cognitive task, the hippocampus may provide a time-compressed running narrative of recent and upcoming events in a suitable format for decoding in downstream brain areas such as the prefrontal cortex. This compression serves a dual purpose. First, the sequence compressed representation contains information about the temporal order at which place cells were activated in a format suitable for neural decoding in the performance of cognitive functions, which may explain the importance of the hippocampus for processing of temporal order (Kesner et al., 2002; Devito and Eichenbaum, 2011;

Davachi and DuBrow, 2015). Second, sequence compression orders neuronal activity into a temporal reference frame in which separate phases represent past, present or future behavioural events. Within such a reference frame, STDP can form associations between ongoing experiences in the recent past or future with an outcome such as reward or punishment. This allows the contingencies between specific behaviours and their outcomes to be learned. Crucially, such a mechanism requires that ongoing experiences are compressed and aligned into a common temporal reference frame at timescales relevant for STDP. This compression is not a feature of many models of phase precession, in which it is often assumed that the sequential organisation of CA1 activity is generated via synaptic coordination of cell assemblies, and that firing fields emerge as an epiphenomenon from these more fundamental sequential processes (Wikenheiser and Redish, 2015; Wang et al., 2015).

We hypothesise that, during theta oscillations, CA1 provides a time-compressed ongoing narrative of behavioural sequences. During theta states, which typically emerge during active behaviour, associations are formed between ongoing behavioural events and specific outcomes such as reward or punishment. During sharp wave ripple states, which typically occur during immobility, the network can then explore its state space in order to test outcomes of different behavioural choices based on these stored associations. Importantly, place cell activity is relatively sparse and asynchronous during theta states (Mizuseki and Buzsaki, 2014), so that downstream cells might be driven only at subthreshold levels by place cell ensembles, allowing supervised learning between these inputs and the conditioned stimulus as shown in Figure 4.9. During sharp wave ripples, however, activity is highly synchronous, and may drive these downstream cells to spike if strong associations have formed during theta states. This allows a form of mental exploration in which possible behavioural sequences can be simulated and the likely outcomes determined based on associations learned during theta states. Hence, we hypothesise that a major function of CA1 during theta states is to compress ongoing events into neuronal sequences in order to store associations in synaptic projections to downstream brain areas, which are then utilised during sharp wave ripple states for mental exploration, planning and decision making.

4.12 Methods

Numerical simulations

Simulations were performed using the Brian simulator (Goodman and Brette, 2009).

Neuron Model

We modelled the network using leaky integrate and fire neurons with conductance based synapses. For example, excitatory neurons were modelled by the following equation:

$$\frac{dV_m(t)}{dt} = -\left(V_m(t) - E_0\right)/\tau_m - \sum_{j=1}^{N_I} g_{I,j}(t)\left(V_m(t) - E_I\right)/C_m + I_{\text{Ext}}/C_m + \sigma_n \eta(t)/\tau_m \tag{4.4}$$

where V_m is the membrane potential, E_0 is the resting potential, τ_m is the membrane time constant, $g_{I,j}$ is the conductance of the synapse from presynaptic interneuron j, E_I is the inhibitory reversal potential, I_{Ext} is an external current input, σ_n is the noise amplitude and η is a normally distributed random variable. When the membrane potential V_m reaches the threshold V_θ, a spike occurs and the membrane potential is reset to V_r. Inhibitory cells were modelled using the same equation, but with excitatory rather inhibitory synaptic conductances.

The synaptic conductances were governed according to:

$$\frac{dg_{I,j}(t)}{dt} = -g_{I,j}/\tau_I + \sum_i w_j \delta\left(t - t_i^{(j)}\right) \tag{4.5}$$

where $t_i^{(j)}$ is ith spike of cell j and w_j the synaptic weight. Excitatory synapses were modelled in the same way.

External Inputs

For interneurons, the external current was of the form:

$$I_{\text{Ext}}^I = I_0^I - I_\theta \cos\left(\omega_\theta t\right) \tag{4.6}$$

where I_θ is the amplitude of the pacemaker current. To simulate a trajectory through a place field, the external current injected to the place cell was of the form:

$$I_{\text{Ext}}^E(t) = I^E \exp\left(-\frac{|\mathbf{x}(t) - \mathbf{x_c}|^2}{2\sigma^2}\right) \tag{4.7}$$

where $\mathbf{x}(t) = \mathbf{x_0} + \mathbf{v}t$ is the trajectory of the animal through the place field. For simulations through the edge of the place field the trajectory was a straight line offset from the place field centre $\mathbf{x_c}$ by 14 cm, otherwise the trajectory passed through the centre.

Synaptic Connectivity (Section 4.7)

Synaptic weights from pyramidal cell i to interneuron j were defined as:

$$w_{ij}^E = C_{ij} w^E \tag{4.8}$$

where C_{ij} is a connectivity matrix with binary entries $C_{ij} \in \{0,1\}$. The connectivity matrix satisfies the following conditions: $\sum_j C_{ij} = 1$ for all i and $\sum_i C_{ij} = N_p/N_I$ for all j. This ensures that each pyramidal cell connects to exactly one interneuron and that each interneuron receives connections from the same number of pyramidal cells. Similarly, synaptic weights from interneuron j to pyramidal cell i were defined as:

$$w_{ji}^I = (C_{ij})^T w^I \tag{4.9}$$

where the inhibitory connectivity matrix is simply the transpose of the excitatory connectivity matrix. This ensures that interneurons project to the same pyramidal cells from which they receive connections. Synaptic weights between neurons of the same type were set to zero.

Synaptic weights were tuned using constraints from the literature. We first tuned the inhibitory synaptic weight such that they drove approximately 10 mV amplitude subthreshold theta oscillations in the pyramidal cell (Harvey et al., 2009). Excitatory synapses were then tuned in order to generate phase precession over 360 degrees in the coupled pair of cells when pyramidal cells fired realistic numbers of spike on a pass through the place field (approximately 10-15 spikes, Huxter et al., 2003). Specific parameter values used in simulations are provided below.

Model Parameters

The following parameters were fixed, independent of running speed:

$\tau_m^I = 40$ ms, $\tau_m^E = 20$ ms, $V_\theta = -50$ mV, $V_r = -70$ mV, $V_0 = -65$ mV, $C_m^I = 200$ pF, $C_m^E = 155$ pF, $\tau_I = 10$ ms, $\tau_E = 2$ ms, $E_I = -70$ mV, $E_E = 0$ mV, $f_\theta = 8$ Hz, $w^E = 0.5$ nS, $w^I = 25$ nS, $dt = 0.1$ ms, $\sigma = 40$ cm, $\sigma_n^I = 0.15$ mV.

Running Speed Dependence (Section 4.3)

We varied several parameters to model the changes with running speed. Firstly, the injected current to the place cell depends on running speed according to Equation (4.7), where the width of the Gaussian in time varies with running speed. In addition to the temporal duration of current injection (as determined by the trajectory $\mathbf{x}(t)$), the amplitude of current input I_0^E was varied with running speed. In addition, the noise to the place cell was varied with running speed. The amplitude and noise term were varied so that the width of the place field (measured as the distance from first to last spike on a single lap) and the number of spikes fired during a pass through a place field were constant across running speeds. Increasing noise tends to spread out the place field, whereas increasing the input current amplitude tends to increase both the number of spikes fired and the width.

The inputs to the interneuron were also running speed dependent. Specifically, the pacemaker amplitude I_{MS} and the baseline current I_0^I were varied with running speed. By lowering the pacemaker input, the range of inputs currents over which phase locking occurs is reduced, but the nonlinear transition from phase locking to phase precession is less severe. This effectively allows a wider range of currents over which slow phase precession can be achieved and increases the stability of phase precession within this range. For these reasons, we reduced the pacemaker amplitude at lower running speeds and also reduced the baseline current so as to allow a slow precession frequency.

The depolarising current input to the interneuron was set as:

$$I_0^I = (79.3 + 0.03v) \quad p\mathrm{A} \tag{4.10}$$

The septal pacemaker input was:

$$I_\theta = 0.065v \quad p\mathrm{A} \tag{4.11}$$

The amplitude of current injection to the place cell was:

$$I^E = (110 + 0.5v) \quad p\mathrm{A} \tag{4.12}$$

The noise to the place cell was varied with running speed as:

$$\sigma_n^E = (1.75 - 0.025v) \quad \mathrm{mV} \tag{4.13}$$

In each of the above equations v is measured in cm/s.

Dorsoventral Changes (Section 4.4)

To model changes in theta dynamics along the dorsoventral axis, we simultaneously varied the place field width σ, excitatory synaptic weight w^E, depolarising current to interneurons I_0^E and the pacemaker drive I_θ. For Figure 4.3A, B, only I_0^E was varied and all other parameters were as above. For Figure 4.3C, D, we chose two parameter sets representing the dorsal and ventral poles. For the dorsal pole, the parameters were: $\sigma = 40$ cm; $I_0^I = 80.7$ pA; $I_\theta = 2.6$ pA; $w^E = 0.5$ nS. For the ventral pole, the parameters were: $\sigma = 800$ cm; $I_0^I = 79.49$ pA; $I_\theta = 0.2$ pA; $w^E = 0.108$ nS.

Calculation of Precession Frequency

To estimate the theta frequency of the simulated neurons, the membrane potential was bandpass filtered at $6.25 - 10$ Hz and the instantaneous phase was calculated via a Hilbert transform. The phase was unwrapped then and smoothed using a moving average of width 250 ms and the gradient was calculated at each time point to obtain the instantaneous frequency.

To determine the precession frequency at different running speeds, we calculated the average membrane frequency within a radius of 15 cm around the place field centre on each pass through the place field. To remove artefactual frequency estimates arising due to the bursting dynamics within theta cycles, we excluded individual runs based on the variability of the instantaneous place cell frequency within this 15 cm radius. Specifically, we excluded runs on which the standard deviation was greater than 1.75 times the mean standard deviation over all runs at that speed. This excludes cases in which the estimated frequency fluctuated rapidly on a short timescale.

Analysis of Phase Precession Statistics (Section 4.7)

To estimate the strength of phase precession in each pyramidal cell, we calculated the Pearson correlation between the vector of spike phases Φ and the vector of the animal's location X at the time of each spike on a single lap. The phase offset was chosen in order to minimise this correlation, i.e. to obtain the most negative possible correlation between spike phase and the animal's location (Foster and Wilson, 2007; Feng et al., 2015). Specifically, given the vectors X and Φ, we calculated the correlation $\rho(X, \Phi + \widetilde{\phi})$, where $\widetilde{\phi} = \text{argmin}(\rho(X, \Phi + \phi))$.

To obtain the measure of population phase precession, we pooled the spikes of all

pyramidal cells on a single lap. We again calculated the correlation between the vector of pooled spike phases Φ_{pop} and the vector whose entries are given by the distance of the animal from the place field centre of the corresponding cell in the pooled spike phase vector at the time of that spike X_{pop}. As for the single cell case, the phase offset was chosen in order to minimise this correlation by calculating $\rho(X_{\text{pop}}, \Phi_{\text{pop}} + \widetilde{\phi}_{\text{pop}})$, where $\widetilde{\phi}_{\text{pop}} = \text{argmin}(\rho(X_{\text{pop}}, \Phi_{\text{pop}} + \phi_{\text{pop}}))$.

To measure the strength of sequential activity in the population, we analysed the data on a cycle-by-cycle basis. For each cycle, the Pearson correlation between the vector of spike times in the population and the vector whose entries are given by the place field centre corresponding to each spike in this first vector was calculated. Theta windows for this method had a temporal width equal to the period of the pacemaker input to the network. The offset of theta windows was given by the phase offset $\widetilde{\phi}_{\text{pop}}$ which maximised the population phase precession measure. This allows for the possibility of an offset between the simulated CA1 network theta activity and the septal input oscillation.

Place Field Mapping (Section 4.7)

For network simulations, the number of simulated pyramidal cells was held constant ($N_p = 1000$) and the number of interneurons was varied. This choice was made to avoid changes in correlation values introduced by changes in sample size. The number of interneurons was always chosen to be a divisor of the number of pyramidal cells so that there was an equal number of place cells for each interneuron. Each simulated place cell was given exactly one place field. For random place field mapping, place field locations were generated by a uniform distribution over a linear track. For optimal place field mapping, place field locations were defined so that the place cells associated with a single interneuron were equally spaced along the track and so that the entire population of place cells uniformly covered the track.

Chapter 5

Conclusions

5.1 Summary of results

In this thesis, I have developed a detailed account of the phenomenological properties and biophysical mechanisms of population activity during theta oscillations in the rodent hippocampus. In Chapter 2, I developed a phenomenological model based on the assumption that place cells code independently of each other during theta oscillations, and compared this to an alternative model in which cells encode via coordinated synaptic interactions within the local circuitry in order to produce theta sequences. By comparison of these models to experimental data, I found empirical support for the independent coding hypothesis, and showed how previous evidence presented in support of coordination during theta oscillations is consistent with independent coding.

Through a detailed analysis of the properties of independent coding models and coordinated coding models under place field remapping, I uncovered an important functional benefit of independent coding. In coordinated coding models, interactions between cells can disrupt sequential activity patterns after place fields are remapped. In independent coding models, however, it is possible for place fields to be remapped without interference between spatial representations in different environments. Specifically, I found that this ability to remap flexibly is possible provided that individual cells exhibit sigmoidal phase coding, wherein their intrinsic theta frequency increases as the animal crosses the place field. For linear phase coding, in which the oscillation frequency of each cell remains fixed over space, I found that remapping generally disrupts theta sequences.

In Chapter 3, I investigated the phenomenological properties of phase coding in grid cells during theta oscillations. By extending the linear and sigmoidal models of

place cells developed in Chapter 2 to grid cells, I showed that the translational symmetries of their firing rate fields impose additional constraints on the phenomenological properties of theta phase coding in two-dimensions. To overcome these constraints, I developed a more complex model in which grid cell firing phase depends on a combination of a location-dependent intracellular theta frequency and a synchronising pacemaker drive. I showed how this model can generate a robust theta phase code for grid cells in two-dimensions which satisfies the symmetry properties of grid cell activity.

In Chapter 4, I proposed a detailed biophysical mechanism based on the dynamics outlined for grid cells in Chapter 3. Specifically, I showed that phase precession emerges in coupled interneuron-pyramidal cell pairs driven by pacemaker inputs. I showed that this model can account for many challenging features of phase precession, including the dependence on running speed, dorsoventral location and phase precession in two-dimensional environments. I then investigated the ability of the proposed mechanism to account for large scale network activity during theta oscillations. I found that the network has a vast capacity for the generation of theta sequences in different spatial maps, but also identified important constraints on the sparseness and organisation of place field maps under which robust theta sequences can be generated. Finally, I proposed a mechanism by which this network can use spike time dependent plasticity in order to learn associations between events occurring during behaviour.

5.2 Implications for hippocampal function

The models of CA1 presented in this thesis imply a vast capacity of the CA1 network for the encoding of trajectories and episodic memories in different environments and contexts. These results are in contradistinction to a growing body of work which suggests that the hippocampus exhibits a repertoire of intrinsically organised sequential activity patterns, and hence a limited range of representational patterns (Lisman and Grace, 2005; Dragoi and Tonegawa, 2011, 2013b; Wikenheiser and Redish, 2015). Specifically, the results of this thesis suggest that the hippocampus compresses arbitrary sequences of inputs in real-time into faster sequential representations. In this view, theta sequences represent a passive representation of ongoing events at neural timescale, as opposed to active, internally constructed representations which are anchored by and aligned to sensory inputs (Lisman and Grace, 2005; Dragoi and Tonegawa, 2011, 2013b; Aghajan et al., 2015; Wikenheiser and Redish, 2015; Wang et al., 2015). Hence, while O'Keefe and Dragoi have proposed that the activity of place cell

ensembles embodies the Kantian notion of an innate, internally constructed spatial representation through which sensory experience is embedded and interpreted (O'Keefe and Nadel, 1978; Wills et al., 2010; Dragoi and Tonegawa, 2014), the models proposed in this thesis are more akin to the Lockean "tabula rasa" or blank slate, in which arbitrary novel spatial representations can be constructed from sensory inputs.

The results presented here are consistent with the two-stage model of memory formation (Buzsaki, 1989), in which episodes are represented in real time during theta oscillations before being consolidated later during sharp wave-ripple states. Our results provide an account of the phenomenology and mechanisms of the first stage in this model. Specifically, the generation of sequential representations of arbitrary sequences of events may be achieved through the independent phase precession of each cell and used to establish associations during these episodes according to the supervised learning mechanism presented in Chapter 4. However, the phenomenology and mechanisms of the second stage, which occur during sharp wave-ripples, were not addressed.

The results herein are also consistent with Marr's proposal that the hippocampus has the capacity to index arbitrary cortical input patterns (Marr, 1971). However, the proposed mechanisms extend this concept to the indexing of arbitrary sequences of inputs via theta compression. Finally, as the model presented here allows the compression of arbitrary sequences of inputs to the hippocampus, the proposed mechanism offers a unified account of the involvement of the hippocampus in encoding spatial trajectories (Dragoi and Buzsáki, 2006; Foster and Wilson, 2007), sequences of sensory stimuli (MacDonald et al., 2013), and memory episodes (Pastalkova et al., 2008) during theta oscillations. As such, this work makes contributions towards a unified understanding of hippocampal function.

5.3 Future work

Several important questions have been raised in this thesis that warrant further investigation. In Chapter 2, I suggested that CA3 may generate sequences with temporally coordinated activity patterns within theta cycles, in contrast to the independent population code in CA1. I further suggested that CA1 may actively decorrelate these inputs in order to orthogonalise the information contained within the population during theta cycles. It will therefore be important to test whether CA3 does indeed exhibit coordinated spatiotemporal activity patterns, and if so, to investigate the mechanisms by

which CA1 may remove these correlations.

In Chapter 3, we found that linear phase coding in grid modules requires strong constraints for two-dimensional phase precession which appear unbiophysical, due to the discrete changes in precession frequency with direction of movement. Nevertheless, these dynamics are possible, and may be tested by analysing the theta frequency of cells for different running directions. By testing whether precession frequency varies with running direction for grid cells, it will therefore be possible to validate the model, or alternatively to rule out linear phase coding entirely.

The biophysical model of Chapter 4 makes several salient experimental predictions. For example, it predicts the existence of subthreshold phase precession fields in the membrane potential oscillations of place cells. Moreover, it predicts that phase precession in pyramidal cells is contingent on the precession of synaptically coupled phase precessing interneurons, and that current injection to a place cell outside of its place field should initiate phase precession. These predictions are within the grasp of current experimental techniques. By testing these predictions empirically, it should be possible to find clear evidence for or against the proposed mechanism.

Finally, the model of Chapter 4 leaves open several theoretical questions. For example, can the same mechanism persist in CA3, where recurrent excitation may interfere with the proposed dynamics? Can the mechanism coexist with attractor dynamics, such that the slow depolarising inputs to cells come from within the network rather than external inputs? In grid cell modules, the density of firing rate fields is much higher than in place cell populations. What are the implications for grid cell remapping under the biophysical mechanism proposed in this thesis, given the constraints imposed by firing field overlap? Perhaps most importantly, what possible mechanisms or learning rules could allow place field mapping under the proposed mechanism without introducing interference between competing pyramidal cells?

Appendix A

Remapping with Fixed Phase Sequences

In this appendix the structure present in a population of place cells with a linear phase code in two dimensions is described, not considering any rate coding. We then investigate the constraints when remapping between different place field configurations in an open environment, assuming the original set of phase lags between cells in the population is fixed. We then present a set of transformations which obey these constraints, allowing a prediction of the set of possible remappings in a network with a fixed set of theta phase lags.

Definition of a Phase Chart

In the linear travelling wave model, the MPO phase $\psi(\mathbf{x_c}, t)$ in each cell can be separated into a temporal component ωt and a spatial component $\theta_P = \boldsymbol{\kappa} \cdot \mathbf{x_c}$ which sets a fixed phase lag between any two cells in the population (see Equation (2.25)). Since the temporal component is the same for each cell, we can disregard the temporal dynamics and focus only on the spatial component θ_P when analysing the properties of networks with fixed phase lags.

During each theta cycle, a phase sequence is swept out. Only those cells within the rate coded area around the rat fire an action potential during a phase sequence, but every single place cell can be assigned an MPO phase, whether or not it fires. In the linear travelling wave model the relative phase between two cells $\Delta\theta_P$ depends only on the direction the rat is moving (determined by $\boldsymbol{\kappa}$) and the relative place field locations (determined by $\mathbf{x_c}$ for each cell).

If the rat is running in the direction $\boldsymbol{\kappa}$, the set of cells with a phase θ_P have place fields $\mathbf{x_c}$ given by:

$$C(\theta_P, \boldsymbol{\kappa}) = \left\{ \mathbf{x_c} \in \mathbb{R}^2 \middle| \, \mathbf{x_c} \cdot \boldsymbol{\kappa} \equiv \theta_P \bmod 2\pi \right\} \tag{A.1}$$

Equation (A.1) shows that, in the linear travelling wave model, the set of cells with the same phase corresponds to periodic parallel lines extending across the whole environment (Figure A.1). Each $C(\theta_P, \boldsymbol{\kappa})$ is a cell assembly active at phase θ_P in the sequence ordered along the direction $\boldsymbol{\kappa}$. A phase sequence consists of the set of cell assemblies $C(\theta_P, \boldsymbol{\kappa})$ with phases $\theta_P \in [0, 2\pi)$ for a particular $\boldsymbol{\kappa}$. In turn, a phase chart is the full set of phase sequences consisting of one $\boldsymbol{\kappa}$ for each running direction.

In this description, we have treated the set of cells as a two dimensional continuous sheet, so that we can assign a place field to each point in a two dimensional environment. This is an idealized case, but a finite sampling of cells from this idealized case would not affect any of the arguments here. Moreover, since we are neglecting rate coding in this analysis, the definition of a phase sequence describes the sequence of MPO phases of all cells in the population, rather than the sequence of spikes which are localized to the vicinity of the animal.

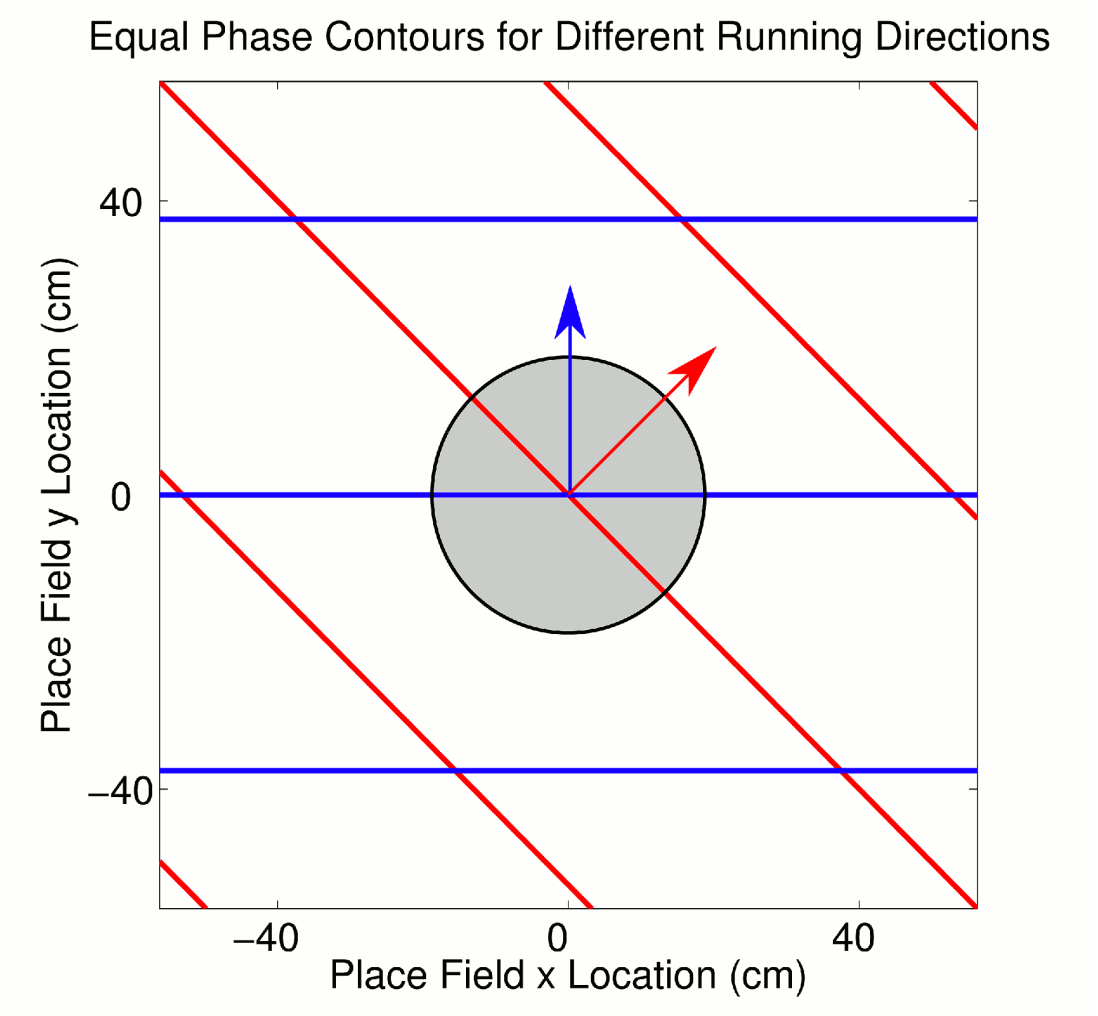

Figure A.1: **Equal phase contours in the linear travelling wave model.**
The set of cells with a given phase θ_P maps onto parallel lines in the environment with spacing equal to the size of a place field and orientation aligned with the current running direction (shown by arrows). The phase lag between any two cells is fixed according to a linear population phase gradient $\boldsymbol{\kappa}$ along the direction of movement. The grey circle illustrates the spiking population, but the phase lags between cells are independent of this rate code.

Constraints Under Remapping with a Fixed Phase Chart

We now assume that this phase chart remains fixed under remapping, so that the set of phase lags remains, even though the cells can be assigned new place fields. This situation might arise if the phase differences between cells in the population is fixed anatomically, for example by upstream pacemakers. If $\mathbf{x_c}$ is the location of a place field before a remapping f, we denote the remapped place field as $\mathbf{x'_c} = f(\mathbf{x_c})$. Here, we set constraints on the possible remappings which ensure that the new place fields still display spatially ordered sequences under the same phase chart.

Constraint 1

After remapping, the new phase sequences should still sweep out paths in the environment, i.e. they should map out parallel lines which are ordered along a direction of movement, and each should represent a unique such direction as before.

For the remapped assemblies within a phase sequence to map out straight lines as in the original place field configuration, we require that:

$$f(C(\theta_P, \boldsymbol{\kappa})) = C(\theta'_P, \boldsymbol{\kappa'}) = \left\{\mathbf{x'_c} \in \mathbb{R}^2 |\ \mathbf{x'_c} \cdot \boldsymbol{\kappa'} \equiv \theta'_P \bmod 2\pi\right\}, \tag{A.2}$$

for some new direction $\boldsymbol{\kappa'}$.

Constraint 2

Since the phase lags are preserved, we require that:

$$\Delta\theta'_P = \Delta\theta_P \tag{A.3}$$

for each pair of assemblies within each phase sequence.

In words, these constraints are 1) parallel lines of place fields are mapped to parallel lines and 2) phase differences among these parallel lines are preserved.

Affine Transformations Allow Remapping within a Fixed Phase Chart

Affine transformations have the property that sets of parallel lines remain parallel (constraint 1). They also preserve the ratios of distances along straight lines, meaning that constraint 2 is automatically satisfied, although with a possible spatial scaling.

We can demonstrate mathematically that the affine transformation:

$$\mathbf{x_c} \to M\mathbf{x_c} + \mathbf{a}, \quad M \in GL_2, \quad \mathbf{a} \in \mathbb{R}^2 \tag{A.4}$$

satisfies the above constraints (GL_2 is the group of all invertible 2×2 matrices, called the general linear group), as shown below:

$$\text{Given} \quad \mathbf{x_c} \cdot \boldsymbol{\kappa} \equiv \theta_p \bmod 2\pi \quad \text{and} \quad \mathbf{x'_c} = \mathrm{M}\mathbf{x_c} + \mathbf{a} \tag{A.5}$$

$$\text{Let} \quad \boldsymbol{\kappa'} = \left(M^{-1}\right)^T \boldsymbol{\kappa}, \quad \text{and} \quad \theta'_P = \theta_P + \mathbf{a} \cdot \left(\left(M^{-1}\right)^T \boldsymbol{\kappa}\right) \tag{A.6}$$

$$\text{Then} \quad \mathbf{x'_c} \cdot \boldsymbol{\kappa'} = \mathbf{x_c} \cdot \boldsymbol{\kappa} + \mathbf{a} \cdot \left(\left(M^{-1}\right)^T \boldsymbol{\kappa}\right) \tag{A.7}$$

$$\implies \mathbf{x'_c} \cdot \boldsymbol{\kappa'} \equiv \theta'_P \bmod 2\pi, \tag{A.8}$$

so that subsets with a given wave vector $\boldsymbol{\kappa}$ and phase θ_P are transformed to a new wave vector $\boldsymbol{\kappa'}$ and phase offset θ'_P. The transformation M can include scaling - in order to preserve phase precession, such a scaling would require a commensurate scaling of place field size in the direction of $\boldsymbol{\kappa'}$. Clearly, the transformation preserves phase differences along each direction.

Appendix B

Derivation of Grid Cell Precession Frequencies in the Sigmoidal Model

Here, we calculate the phase precessed along different running directions in the rate-coupled frequency model. First, for runs when $\mathbf{v} = |\mathbf{v}|\hat{\boldsymbol{\kappa}}_\mathbf{1}$ (we choose the first grid vector for concreteness), we use Equation (3.18) and calculate the phase precessed between successive firing fields:

$$\phi(t+\sqrt{3}d/v, \mathbf{x_c}) - \phi(t, \mathbf{x_c}) = 2\pi\Delta f \left\{ \frac{\sqrt{3}}{2}\frac{d}{v} \right. \tag{B.1}$$

$$\left. + \frac{1}{3}\sum_{i=1}^{3} \frac{1}{\boldsymbol{\kappa_i}\cdot\mathbf{v}} \left[\sin\left(\boldsymbol{\kappa}_i \cdot \left(\mathbf{v}\left(t+\sqrt{3}\frac{d}{v}-t_0\right)+\mathbf{x_0}-\mathbf{x_c}\right)\right) - \sin\left(\boldsymbol{\kappa}_i\cdot((t-t_0)+\mathbf{x_0}-\mathbf{x_c})\right)\right] \right\} \tag{B.2}$$

We note that $\boldsymbol{\kappa_1}\cdot\mathbf{v} = 4\pi v/(\sqrt{3}d)$, so that the first summand vanishes since the two sin terms differ by exactly two cycles.

To calculate the second and third summands, we note that $\boldsymbol{\kappa_2}\cdot\mathbf{v} = 2\pi\cos(\pi/3)v/d = \pi v/d$ and $\boldsymbol{\kappa_3}\cdot\mathbf{v} = 2\pi\cos(2\pi/3)v/d = -\pi v/d$, due to the 60 degree angle between successive grid vectors. From this it is easily seen that the second and third summands also vanish, as in each case the two sin terms differ by exactly one cycle.

Having demonstrated that the sum in Equation (B.1) vanishes, the total phase precessed is seen to be $\Delta\phi = \sqrt{3}\pi\Delta f d/v$. By requiring that $\Delta\phi = 2\pi k$ for some integer k, the result stated in the main text of Chapter 3 is obtained.

Next, we calculate the phase precessed along a trajectory exactly between two grid vectors, $\mathbf{v} = |\mathbf{v}|(\boldsymbol{\kappa_2}+\boldsymbol{\kappa_3})/|\boldsymbol{\kappa_2}+\boldsymbol{\kappa_3}| = v(\hat{\boldsymbol{\kappa}}_\mathbf{2}+\hat{\boldsymbol{\kappa}}_\mathbf{3})/\sqrt{3}$. In this case, $\boldsymbol{\kappa_1}\cdot\mathbf{v} = 0$, so that Equation (3.18) is not valid. Instead, the integral is given by:

$$\phi(t,\mathbf{x_c}) = 2\pi\Delta f \left[\left(\frac{1}{2} + \frac{1}{3}\cos\left(\boldsymbol{\kappa_1}\cdot(\mathbf{x_0}-\mathbf{x_c})\right) \right)(t-t_0) \right. \tag{B.3}$$

$$\left. + \frac{1}{3}\sum_{i=2}^{3} \frac{1}{\boldsymbol{\kappa_i}\cdot\mathbf{v}} \left(\sin(\boldsymbol{\kappa_i}\cdot(\mathbf{v}(t-t_0)+\mathbf{x_0}-\mathbf{x_c})) - \sin(\boldsymbol{\kappa_i}\cdot(\mathbf{x_0}-\mathbf{x_c}))\right) \right] + \phi(t_0,\mathbf{x_c}) \tag{B.4}$$

We can then calculate the phase precessed along a trajectory directly between grid peaks along such a direction $\Delta\phi = \phi(t+d/v,\mathbf{x_c}) - \phi(t,\mathbf{x_c})$ by setting the initial location $\mathbf{x_0} = \mathbf{x_c}$ to obtain:

$$\Delta\phi = 2\pi\Delta f \frac{d}{v}\frac{5}{6} \tag{B.5}$$

By setting the total phase precessed $\Delta\phi = 2k\pi$ as before, we obtain the required frequency for this run as $\Delta f = (6/5)kv/d$.

Appendix C

Remapping Capacity in the Biophysical Model

Here we quantify the capacity of the network under the assumption that pyramidal cells which couple to the same interneuron cannot have overlapping place fields. We use three distinct measures of the network capacity: the number of spatial maps at a given spatial acuity; the number of cell assemblies; the number of phase sequences.

Number of Distinct Spatial Maps

To determine the number of spatial maps available in the network, we considered a simplified model in which each place cell can map to a set of discrete locations on a linear track of length L. Specifically, the track is divided into equal bins of size $x_{\mathrm{res}} = L/N_{\mathrm{bins}}$, where N_{bins} is the number of bins and x_{res} determines the spatial resolution of the place map. To avoid finite size effects, we assume periodic boundaries (i.e., a circular track). The number of place fields to be mapped onto the track depends on both the number of place cells N_p and the average number of place fields per place cell F (which can be greater or less than one). Given a number of interneurons N_I, the population of N_p place cells is divided into N_I equal subsets, so that each interneuron is associated with the same number of place cells. We assume that there is an exclusion zone of size D which sets the minimum distance for which place cells associated with the same interneuron can be mapped, so that $N_d = D/x_{\mathrm{res}}$ is the minimum separation in terms of the number of bins. In general, multiple cells may map to the same bin, or no cells may map onto a given bin, provided that the non-overlap constraint is obeyed.

We can then consider the number of ways in which FN_p place fields can be mapped

onto the track without violating this constraint. We can calculate this number by counting the number of possible choices for each for each place field i, where $1 \leq i \leq FN_p$. For the first place field $i = 1$, there are $N_p N_{\text{bins}}$ possible choices, since we can choose from N_p place cells and N_{bins} spatial locations. For the next choice $i = 2$, there are $N_p N_{\text{bins}} - N_d N_p / N_I$ choices, due to the exclusion zone about the first cell, which excludes N_p / N_I cells from being mapped onto N_d of the possible bins. In general, there are $N_p N_{\text{bins}} - (i-1) N_d N_p / N_I$ for the ith choice. Hence, the total number of combinations is:

$$N = \prod_{i=1}^{FN_p} \left(N_p N_{\text{bins}} - (i-1) \frac{N_p}{N_I} N_d \right) \tag{C.1}$$

which can be simplified by noting that $N_d = N_{\text{bins}} D / L$ so that:

$$N = (N_p N_{\text{bins}})^{FN_p} \prod_{i=1}^{FN_p} \left(1 - (i-1) \frac{D}{L N_I} \right) \tag{C.2}$$

The above analysis gives the number of ordered choices of place cells and spatial bins, but overcounts the number of distinct maps by allowing the same map to be obtained through multiple choice sequences. This can be corrected by a factor of $(FN_p)!$ to obtain the number of distinct maps:

$$N_{\text{maps}} = \frac{(N_p N_{\text{bins}})^{FN_p}}{(FN_p)!} \prod_{i=1}^{FN_p} \left(1 - (i-1) \frac{D}{L N_I} \right) \tag{C.3}$$

Taking the logarithm and applying Stirling's approximation gives:

$$\log N_{\text{maps}} \approx FN_p \left(1 + \log L - \log x_{\text{res}} - \log F\right) + \sum_{i=1}^{FN_p} \log \left(1 - (i-1) \frac{D}{L N_I} \right) \tag{C.4}$$

In general $\frac{D}{L N_I} \ll 1$, so that an approximation of $\log(1-x) \approx -x$ can be made. However, FN_p can be sufficiently large that for higher terms in the sum this approximation begins to break down.

One special case of the above result is of particular interest. Setting $N_I = N_p$, we retrieve the case in which overlap between place fields of cell pairs with a shared interneuron is not a constraint, but maintain the constraint on overlap between multiple place fields of the same place cell. By comparison of the number of maps in the independent case $N_{\text{maps}}^{\text{ind}}$ to the number of maps in the general case, we can see how the proposed mechanism constrains remapping in comparison to a fully independent population code:

$$\log N_{\text{maps}}^{\text{ind}} - \log N_{\text{maps}} = \sum_{i=1}^{FN_p} \log\left(\frac{1-(i-1)D/LN_p}{1-(i-1)D/LN_I}\right) \tag{C.5}$$

$$= \sum_{i=1}^{FN_p} \log\left(\frac{N_p}{N_I}\frac{1/N_p-(i-1)D/L}{1/N_I-(i-1)D/L}\right) \tag{C.6}$$

$$\approx \sum_{i=1}^{FN_p} (\log N_p - \log N_I) \tag{C.7}$$

$$= FN_p(\log N_p - \log N_I) \tag{C.8}$$

where N_I is the number of interneurons in the constrained map.

Number of Cell Assemblies

We define a cell assembly to be a set of coactive cells. We now calculate the number of cell assemblies which contain n place cells under the non-overlap constraint. To construct a cell assembly satisfying the constraint, it is sufficient to simply select n distinct interneurons and then select a place cell associated with each interneuron. The number of possible cell assemblies N_{CA} is therefore:

$$N_{\text{CA}} = \begin{pmatrix} N_I \\ n \end{pmatrix} \left(\frac{N_P}{N_I}\right)^n; \qquad n \leq N_I \tag{C.9}$$

As before, we can simplify this using Stirling's approximation:

$$\log(N_{\text{CA}}) \approx N_I \log N_I - (N_I - n)\log(N_I - n) + n(\log N_p - \log N_I - \log n) \tag{C.10}$$

Number of Phase Sequences

A phase sequence is defined as an ordered set of cell assemblies (Hebb, 1949). We assume that a phase sequence is a discrete sequence of m cell assemblies, and that no two cells in a phase sequence can couple to the same interneuron. A phase sequence can then be constructed by repeatedly constructing cell assemblies as above, where the available interneurons for each subsequent cell assembly is given by those not already selected in previous assemblies within the sequence. The number of phase sequences N_{PS} is then:

$$N_{\mathrm{PS}} = \prod_{i=1}^{m} \begin{pmatrix} N_I - (i-1)n \\ n \end{pmatrix} \left(\frac{N_P}{N_I}\right)^n; \qquad n \leq \frac{N_I}{m} \tag{C.11}$$

which can be approximated as:

$$\log N_{\mathrm{PS}} \approx \sum_{i=1}^{m} \left[(N_I - (i-1)n)\log(N_I - (i-1)n) - (N_I - in)\log(N_I - in) + n(\log N_p - \log N_I - \log n)\right] \tag{C.12}$$

Bibliography

Adler, R. (1946). Study of locking phenomena in oscillators. *Proceedings of the IEEE*, 61(10):1380–1385.

Aghajan, Z. M., Acharya, L., Moore, J. J., Cushman, J. D., Vuong, C., and Mehta, M. R. (2015). Impaired spatial selectivity and intact phase precession in two-dimensional virtual reality. *Nature Publishing Group*, 18(1):121–128.

Ahmed, O. J. and Mehta, M. R. (2012). Running Speed Alters the Frequency of Hippocampal Gamma Oscillations. *J Neurosci*, 32(21):7373–7383.

Aika, Y., Ren, J. Q., Kosaka, K., and Kosaka, T. (1994). Quantitative analysis of GABA-like-immunoreactive and parvalbumin-containing neurons in the CA1 region of the rat hippocampus using a stereological method, the disector. *Experimental Brain Research*, 99(2):267–276.

Allen, K., Rawlins, J. N. P., Bannerman, D. M., and Csicsvari, J. (2012). Hippocampal Place Cells Can Encode Multiple Trial-Dependent Features through Rate Remapping. *J Neurosci*, 32(42):14752–14766.

Alme, C. B., Miao, C., Jezek, K., Treves, A., Moser, E. I., and Moser, M.-B. (2014). Place cells in the hippocampus: Eleven maps for eleven rooms. *Pnas*, 111(52).

Amaral, D. G. and Witter, M. P. (1989). The three-dimensional organization of the hippocampal formation: a review of anatomical data. *Neuroscience*, 31(3):571–591.

Amsel, A. (1993). Hippocampal function in the rat: cognitive mapping or vicarious trial and error? *Hippocampus*, 3(3):251–256.

Anderson, P., Morris, R., Amaral, D., Bliss, T., and O'Keefe, J. (2007). *The Hippocampus Book*.

Bannerman, D. M., Grubb, M., Deacon, R. M. J., Yee, B. K., Feldon, J., and Rawlins, J. N. P. (2003). Ventral hippocampal lesions affect anxiety but not spatial learning. *Behavioural Brain Research*, 139(1-2):197–213.

Battaglia, F. P., Sutherland, G. R., and McNaughton, B. L. (2004). Local sensory cues and place cell directionality: additional evidence of prospective coding in the hippocampus. *J Neurosci*, 24(19):4541–4550.

Bennett, A. T. (1996). Do animals have cognitive maps? *The Journal of experimental biology*, 199(Pt 1):219–224.

Bernacchia, A. and Wang, X. (2013). Decorrelation by recurrent inhibition in heterogeneous neural circuits. *Neural Computation*, pages 1732–1767.

Bezaire, M. J. and Soltesz, I. (2013). Quantitative assessment of CA1 local circuits: Knowledge base for interneuron-pyramidal cell connectivity. *Hippocampus*, 23(9):751–785.

Bland, S. K. and Bland, B. H. (1986). Medial septal modulation of hippocampal theta cell discharges. *Brain research*, 375(1):102–116.

Bose, A. and Recce, M. (2001). Phase precession and phase-locking of hippocampal pyramidal cells. *Hippocampus*, 11(3):204–215.

Bragin, A., Jandó, G., Nádasdy, Z., Hetke, J., Wise, K., and Buzsáki, G. (1995). Gamma (40-100 Hz) oscillation in the hippocampus of the behaving rat. *The Journal of neuroscience : the official journal of the Society for Neuroscience*, 15(1 Pt 1):47–60.

Brandon, M. P., Bogaard, A. R., Libby, C. P., Connerney, M. A., Gupta, K., and Hasselmo, M. E. (2011). Reduction of theta rhythm dissociates grid cell spatial periodicity from directional tuning. *Science (New York, N.Y.)*, 332(6029):595–599.

Burak, Y. and Fiete, I. R. (2009). Accurate path integration in continuous attractor network models of grid cells. *PLoS Computational Biology*, 5(2).

Burgess, N. (2008). Grid cells and theta as oscillatory interference: Theory and predictions. *Hippocampus*, 18(12):1157–1174.

Burgess, N., Barry, C., and O'Keefe, J. (2007). An oscillatory interference model of grid cell firing. *Hippocampus*, 17(9):801–812.

Bush, D. and Burgess, N. (2014). A hybrid oscillatory interference/continuous attractor network model of grid cell firing. *The Journal of neuroscience : the official journal of the Society for Neuroscience*, 34(14):5065–79.

Buzsaki, G. (1989). Two-stage model of memory trace formation: A role for 'noisy' brain states.

Buzsáki, G. (2002). Theta Oscillations in the Hippocampus. *Neuron*, 33(3):325–340.

Buzsáki, G. (2010). Neural syntax: cell assemblies, synapsembles, and readers. *Neuron*, 68(3):362–385.

Buzsáki, G., Anastassiou, C. A., and Koch, C. (2012). The origin of extracellular fields and currents EEG, ECoG, LFP and spikes.

Buzsáki, G., Horváth, Z., Urioste, R., Hetke, J., and Wise, K. (1992). High-frequency network oscillation in the hippocampus. *Science (New York, N.Y.)*, 256(5059):1025–1027.

Buzsaki, G., Leung, L. W. S., and Vanderwolf, C. H. (1983). Cellular bases of hippocampal EEG in the behaving rat. *Brain Research Reviews*, 6(2):139–171.

Buzsáki, G. and Moser, E. I. (2013). Memory, navigation and theta rhythm in the hippocampal-entorhinal system. *Nature neuroscience*, 16(2):130–8.

Cei, A., Girardeau, G., Drieu, C., Kanbi, K. E., and Zugaro, M. (2014). Reversed theta sequences of hippocampal cell assemblies during backward travel. *Nature Neuroscience*.

Chance, F. S. (2012). Hippocampal phase precession from dual input components. *J Neurosci*, 32(47):16693–703a.

Climer, J. R., Newman, E. L., and Hasselmo, M. E. (2013). Phase coding by grid cells in unconstrained environments: two-dimensional phase precession. *The European journal of neuroscience*, 38(4):2526–41.

Cohen, S. J., Munchow, A. H., Rios, L. M., Zhang, G., Ásgeirsdóttir, H. N., and Stackman, R. W. (2013). The rodent hippocampus is essential for nonspatial object memory. *Current Biology*, 23(17):1685–1690.

Colgin, L. L., Moser, E. I., and Moser, M. B. (2008). Understanding memory through hippocampal remapping.

Couey, J. J., Witoelar, A., Zhang, S.-J., Zheng, K., Ye, J., Dunn, B., Czajkowski, R., Moser, M.-B., Moser, E. I., Roudi, Y., and Witter, M. P. (2013). Recurrent inhibitory circuitry as a mechanism for grid formation. *Nature neuroscience*, 16(3):318–24.

Csicsvari, J., Hirase, H., Mamiya, A., and Buzsáki, G. (2000). Ensemble patterns of hippocampal CA3-CA1 neurons during sharp wave-associated population events. *Neuron*, 28(2):585–594.

Czurko, A. (1999). Sustained activation of hippocampal pyramidal cells by 'space clamping' in a running wheel. *European Journal of Neuroscience*, 11(1):344–352.

Davachi, L. and DuBrow, S. (2015). How the hippocampus preserves order. *Trends in Cognitive Sciences*, 19(2):92–99.

Davidson, T. J., Kloosterman, F., and Wilson, M. A. (2009). Hippocampal Replay of Extended Experience. *Neuron*, 63(4):497–507.

Devito, L. M. and Eichenbaum, H. (2011). Memory for the order of events in specific sequences: contributions of the hippocampus and medial prefrontal cortex. *The Journal of neuroscience : the official journal of the Society for Neuroscience*, 31(9):3169–3175.

Diba, K. and Buzsáki, G. (2007). Forward and reverse hippocampal place-cell sequences during ripples. *Nature neuroscience*, 10(10):1241–1242.

Diba, K. and Buzsáki, G. (2008). Hippocampal network dynamics constrain the time lag between pyramidal cells across modified environments. *J Neurosci*, 28(50):13448–13456.

Domnisoru, C., Kinkhabwala, A. a., and Tank, D. W. (2013). Membrane potential dynamics of grid cells. *Nature*, 495(7440):199–204.

Dragoi, G. and Buzsáki, G. (2006). Temporal encoding of place sequences by hippocampal cell assemblies. *Neuron*, 50(1):145–157.

Dragoi, G. and Tonegawa, S. (2011). Preplay of future place cell sequences by hippocampal cellular assemblies. *Nature*, 469(7330):397–401.

Dragoi, G. and Tonegawa, S. (2013a). Development of schemas revealed by prior experience and NMDA receptor knock-out. *eLife*, 2013(2).

Dragoi, G. and Tonegawa, S. (2013b). Distinct preplay of multiple novel spatial experiences in the rat. *PNAS*.

Dragoi, G. and Tonegawa, S. (2014). Selection of preconfigured cell assemblies for representation of novel spatial experiences. *Philosophical transactions of the Royal Society of London. Series B, Biological sciences*, 369(1635):20120522.

Dupret, D., Pleydell-Bouverie, B., and Csicsvari, J. (2010). Rate remapping: when the code goes beyond space. *Neuron*, 68(6):1015–1016.

Dusek, J. A. and Eichenbaum, H. (1997). The hippocampus and memory for orderly stimulus relations. *Proceedings of the National Academy of Sciences of the United States of America*, 94(13):7109–7114.

Ecker, A. S., Berens, P., Keliris, G. A., Bethge, M., Logothetis, N. K., and Tolias, A. S. (2010). Decorrelated neuronal firing in cortical microcircuits. *Science (New York, N.Y.)*, 327(5965):584–587.

Eichenbaum, H. (2004). Hippocampus: Cognitive processes and neural representations that underlie declarative memory.

Eichenbaum, H., Dudchenko, P., Wood, E., Shapiro, M., and Tanila, H. (1999). The hippocampus, memory, and place cells: Is it spatial memory or a memory space?

Eyherabide, H. G. and Samengo, I. (2013). When and why noise correlations are important in neural decoding. *J Neurosci*, 33(45):17921–36.

Feng, T., Silva, D., and Foster, D. J. (2015). Dissociation between the Experience-Dependent Development of Hippocampal Theta Sequences and Single-Trial Phase Precession. *Neuron*, 35(12):4890–4902.

Fenton, A. A., Lytton, W. W., Barry, J. M., Lenck-Santini, P.-P., Zinyuk, L. E., Kubík, S., Bures, J., Poucet, B., Muller, R. U., and Olypher, A. V. (2010). Attention-like modulation of hippocampus place cell discharge. *J Neurosci*, 30(13):4613–4625.

Floresco, S. B., Todd, C. L., and Grace, A. A. (2001). Glutamatergic afferents from the hippocampus to the nucleus accumbens regulate activity of ventral tegmental area

dopamine neurons. *The Journal of neuroscience : the official journal of the Society for Neuroscience*, 21(13):4915–4922.

Foster, D. J. and Wilson, M. A. (2006). Reverse replay of behavioural sequences in hippocampal place cells during the awake state. *Nature*, 440(7084):680–683.

Foster, D. J. and Wilson, M. A. (2007). Hippocampal theta sequences. *Hippocampus*, 17(11):1093–1099.

Frank, L. M., Stanley, G. B., and Brown, E. N. (2004). Hippocampal plasticity across multiple days of exposure to novel environments. *J Neurosci*, 24(35):7681–7689.

Freund, T. F. and Antal, M. (1988). GABA-containing neurons in the septum control inhibitory interneurons in the hippocampus. *Nature*, 336(6195):170–173.

Freund, T. F. and Buzsáki, G. (1996). Interneurons of the hippocampus. *Hippocampus*, 6(4):347–470.

Fuhrmann, F., Justus, D., Sosulina, L., Kaneko, H., Beutel, T., Friedrichs, D., Schoch, S., Schwarz, M., Fuhrmann, M., and Remy, S. (2015). Locomotion, Theta Oscillations, and the Speed-Correlated Firing of Hippocampal Neurons Are Controlled by a Medial Septal Glutamatergic Circuit. *Neuron*, 86(5):1253–1264.

Fuhs, M. C. and Touretzky, D. S. (2006). A spin glass model of path integration in rat medial entorhinal cortex. *J Neurosci*, 26:4266–4276.

Fyhn, M., Hafting, T., Treves, A., Moser, M.-B., and Moser, E. I. (2007). Hippocampal remapping and grid realignment in entorhinal cortex. *Nature*, 446(7132):190–194.

Geisler, C., Diba, K., Pastalkova, E., Mizuseki, K., Royer, S., and Buzsáki, G. (2010). Temporal delays among place cells determine the frequency of population theta oscillations in the hippocampus. *PNAS*, 107(17):7957–7962.

Geisler, C., Robbe, D., Zugaro, M., Sirota, A., and Buzsáki, G. (2007). Hippocampal place cell assemblies are speed-controlled oscillators. *PNAS*, 104(19):8149–8154.

Girardeau, G., Benchenane, K., Wiener, S. I., Buzsáki, G., and Zugaro, M. B. (2009). Selective suppression of hippocampal ripples impairs spatial memory. *Nature neuroscience*, 12(10):1222–1223.

Goodman, D. F. M. and Brette, R. (2009). The brian simulator. *Frontiers in Neuroscience*, 3(SEP):192–197.

Goutagny, R., Jackson, J., and Williams, S. (2009). Self-generated theta oscillations in the hippocampus. *Nature neuroscience*, 12(12):1491–1493.

Griffin, A. L., Eichenbaum, H., and Hasselmo, M. E. (2007). Spatial representations of hippocampal CA1 neurons are modulated by behavioral context in a hippocampus-dependent memory task. *J Neurosci*, 27(9):2416–2423.

Guanella, A., Kiper, D., and Verschure, P. (2007). A model of grid cells based on a twisted torus topology. *International journal of neural systems*, 17(4):231–240.

Gupta, A. S., Van Der Meer, M. A. A., Touretzky, D. S., and Redish, A. D. (2012). Segmentation of spatial experience by hippocampal theta sequences. *Nature Neuroscience*, 15(7):1032–9.

Hafting, T., Fyhn, M., Bonnevie, T., Moser, M.-B., and Moser, E. I. (2008). Hippocampus-independent phase precession in entorhinal grid cells. *Nature*, 453(7199):1248–1252.

Hafting, T., Fyhn, M., Molden, S., Moser, M.-B., and Moser, E. I. (2005). Microstructure of a spatial map in the entorhinal cortex. *Nature*, 436(7052):801–806.

Hampson, R. E., Simeral, J. D., and Deadwyler, S. A. (1999). Distribution of spatial and nonspatial information in dorsal hippocampus. *Nature*, 402(6762):610–614.

Hangya, B., Borhegyi, Z., Szilágyi, N., Freund, T. F., and Varga, V. (2009). GABAergic neurons of the medial septum lead the hippocampal network during theta activity. *The Journal of neuroscience : the official journal of the Society for Neuroscience*, 29(25):8094–8102.

Harris, K. D. (2005). Neural signatures of cell assembly organization. *Nat Rev Neurosci*, 6(5):399–407.

Harris, K. D., Csicsvari, J., Hirase, H., Dragoi, G., and Buzsáki, G. (2003). Organization of cell assemblies in the hippocampus. *Nature*, 424(6948):552–556.

Harris, K. D., Henze, D. A., Hirase, H., Leinekugel, X., Dragoi, G., Czurkó, A., and Buzsáki, G. (2002). Spike train dynamics predicts theta-related phase precession in hippocampal pyramidal cells. *Nature*, 417(6890):738–741.

Harvey, C. D., Collman, F., Dombeck, D. A., and Tank, D. W. (2009). Intracellular dynamics of hippocampal place cells during virtual navigation. *Nature*, 461(7266):941–946.

Hebb, D. O. (1949). *The Organization of Behavior: A Neuropsychological Theory*, volume 44 of *A Wiley book in clinical psychology*. Wiley.

Heckers, S., Zalesak, M., Weiss, A. P., Ditman, T., and Titone, D. (2004). Hippocampal activation during transitive inference in humans. *Hippocampus*, 14(2):153–162.

Holland, P. C. (2008). Cognitive versus stimulus-response theories of learning. *Learning & behavior : a Psychonomic Society publication*, 36(3):227–241.

Howard, M. W., MacDonald, C. J., Tiganj, Z., Shankar, K. H., Du, Q., Hasselmo, M. E., and Eichenbaum, H. (2014). A Unified Mathematical Framework for Coding Time, Space, and Sequences in the Hippocampal Region. *Journal of Neuroscience*, 34(13):4692–4707.

Hu, H., Vervaeke, K., and Storm, J. F. (2002). Two forms of electrical resonance at theta frequencies, generated by M-current, h-current and persistent Na+ current in rat hippocampal pyramidal cells. *The Journal of physiology*, 545(Pt 3):783–805.

Hull, C. L. (1943). *Principles of behavior: an introduction to behavior theory.* Appleton-Century, Oxford, England.

Huxter, J., Burgess, N., and O'Keefe, J. (2003). Independent rate and temporal coding in hippocampal pyramidal cells. *Nature*, 425(6960):828–832.

Huxter, J. R., Senior, T. J., Allen, K., and Csicsvari, J. (2008). Theta phase-specific codes for two-dimensional position, trajectory and heading in the hippocampus. *Nature Neuroscience*, 11(5):587–94.

Jackson, J. and Redish, A. D. (2007). Network dynamics of hippocampal cell-assemblies resemble multiple spatial maps within single tasks. *Hippocampus*, 17(12):1209–1229.

Jadhav, S. P., Kemere, C., German, P. W., and Frank, L. M. (2012). Awake Hippocampal Sharp-Wave Ripples Support Spatial Memory. *Science*, 336(6087):1454–1458.

Jaramillo, J., Schmidt, R., and Kempter, R. (2014). Modeling inheritance of phase precession in the hippocampal formation. *J Neurosci*, 34(22):7715–31.

Jeewajee, A., Barry, C., Douchamps, V., Manson, D., Lever, C., and Burgess, N. (2014). Theta phase precession of grid and place cell firing in open environments. *Philosophical transactions of the Royal Society of London.*, 369(1635):20120532.

Jensen, O. and Lisman, J. E. (2000). Position reconstruction from an ensemble of hippocampal place cells: contribution of theta phase coding. *Journal of Neurophysiology*, 83(5):2602–2609.

Johnson, A. and Redish, A. D. (2007). Neural ensembles in CA3 transiently encode paths forward of the animal at a decision point. *The Journal of neuroscience : the official journal of the Society for Neuroscience*, 27(45):12176–12189.

Karlsson, M. P. and Frank, L. M. (2008). Network dynamics underlying the formation of sparse, informative representations in the hippocampus. *J Neurosci*, 28(52):14271–14281.

Karlsson, M. P. and Frank, L. M. (2009). Awake replay of remote experiences in the hippocampus. *Nature neuroscience*, 12(7):913–918.

Katona, L., Lapray, D., Viney, T. J., Oulhaj, A., Borhegyi, Z., Micklem, B. R., Klausberger, T., and Somogyi, P. (2014). Sleep and Movement Differentiates Actions of Two Types of Somatostatin-Expressing GABAergic Interneuron in Rat Hippocampus. *Neuron*, 82(4):872–886.

Kempter, R., Leibold, C., Buzsáki, G., Diba, K., and Schmidt, R. (2012). Quantifying circular-linear associations: Hippocampal phase precession. *Journal of Neuroscience Methods*, 207(1):113–124.

Kesner, R. P., Gilbert, P. E., and Barua, L. A. (2002). The role of the hippocampus in memory for the temporal order of a sequence of odors. *Behavioral neuroscience*, 116(2):286–290.

King, C., Recce, M., and O'Keefe, J. (1998). The rhythmicity of cells of the medial septum/diagonal band of Broca in the awake freely moving rat: Relationships with behaviour and hippocampal theta. *European Journal of Neuroscience*, 10(2):464–477.

King, P. D., Zylberberg, J., and DeWeese, M. R. (2013). Inhibitory interneurons decorrelate excitatory cells to drive sparse code formation in a spiking model of V1. *J Neurosci*, 33(13):5475–85.

Kjelstrup, K. B., Solstad, T., Brun, V. H., Hafting, T., Leutgeb, S., Witter, M. P., Moser, E. I., and Moser, M.-B. (2008). Finite scale of spatial representation in the hippocampus. *Science (New York, N.Y.)*, 321(5885):140–143.

Kjelstrup, K. G., Tuvnes, F. A., Steffenach, H.-A., Murison, R., Moser, E. I., and Moser, M.-B. (2002). Reduced fear expression after lesions of the ventral hippocampus. *Proceedings of the National Academy of Sciences of the United States of America*, 99(16):10825–10830.

Klausberger, T., Magill, P. J., Márton, L. F., Roberts, J. D. B., Cobden, P. M., Buzsáki, G., and Somogyi, P. (2003). Brain-state- and cell-type-specific firing of hippocampal interneurons in vivo. *Nature*, 421(6925):844–848.

Koenig, J., Linder, A. N., Leutgeb, J. K., and Leutgeb, S. (2011). The spatial periodicity of grid cells is not sustained during reduced theta oscillations. *Science (New York, N.Y.)*, 332(6029):592–595.

Kumaran, D. and Maguire, E. A. (2005). The human hippocampus: cognitive maps or relational memory? *The Journal of neuroscience : the official journal of the Society for Neuroscience*, 25(31):7254–7259.

Lapray, D., Lasztoczi, B., Lagler, M., Viney, T. J., Katona, L., Valenti, O., Hartwich, K., Borhegyi, Z., Somogyi, P., and Klausberger, T. (2012). Behavior-dependent specialization of identified hippocampal interneurons. *Nature neuroscience*, 15(9):1265–71.

Le Duigou, C., Simonnet, J., Teleñczuk, M. T., Fricker, D., and Miles, R. (2014). Recurrent synapses and circuits in the CA3 region of the hippocampus: an associative network. *Frontiers in cellular neuroscience*, 7(January):262.

Le Van Quyen, M., Bragin, A., Staba, R., Crépon, B., Wilson, C. L., and Engel, J. (2008). Cell type-specific firing during ripple oscillations in the hippocampal formation of humans. *The Journal of neuroscience : the official journal of the Society for Neuroscience*, 28(24):6104–6110.

Lee, A. K. and Wilson, M. A. (2002). Memory of sequential experience in the hippocampus during slow wave sleep. *Neuron*, 36(6):1183–1194.

Lengyel, M., Szatmáry, Z., and Érdi, P. (2003). Dynamically detuned oscillations account for the coupled rate and temporal code of place cell firing. *Hippocampus*, 13(6):700–714.

Leung, L. S. (2011). A model of intracellular theta phase precession dependent on intrinsic subthreshold membrane currents. *J Neurosci*, 31(34):12282–12296.

Leung, L. S. and Yu, H. W. (1998). Theta-frequency resonance in hippocampal CA1 neurons in vitro demonstrated by sinusoidal current injection. *Journal of neurophysiology*, 79(3):1592–1596.

Leutgeb, S., Leutgeb, J. K., Treves, A., Moser, M.-B., and Moser, E. I. (2004). Distinct ensemble codes in hippocampal areas CA3 and CA1. *Science (New York, N.Y.)*, 305(5688):1295–1298.

Lisman, J. and Redish, A. D. (2009). Prediction, sequences and the hippocampus. *Philosophical transactions of the Royal Society of London. Series B, Biological sciences*, 364(1521):1193–1201.

Lisman, J. E. and Grace, A. A. (2005). The hippocampal-VTA loop: Controlling the entry of information into long-term memory.

Lisman, J. E. and Jensen, O. (2013). The Theta-Gamma Neural Code.

Lubenov, E. V. and Siapas, A. G. (2009). Hippocampal theta oscillations are travelling waves. *Nature*, 459(7246):534–539.

Luo, A. H., Tahsili-Fahadan, P., Wise, R. A., Lupica, C. R., and Aston-Jones, G. (2011). Linking context with reward: a functional circuit from hippocampal CA3 to ventral tegmental area. *Science (New York, N.Y.)*, 333(6040):353–357.

MacDonald, C. J., Carrow, S., Place, R., and Eichenbaum, H. (2013). Distinct hippocampal time cell sequences represent odor memories in immobilized rats. *The Journal of neuroscience : the official journal of the Society for Neuroscience*, 33(36):14607–16.

MacDonald, C. J., Lepage, K. Q., Eden, U. T., and Eichenbaum, H. (2011). Hippocampal "time cells" bridge the gap in memory for discontiguous events. *Neuron*, 71(4):737–749.

Mankin, E. A., Sparks, F. T., Slayyeh, B., Sutherland, R. J., Leutgeb, S., and Leutgeb, J. K. (2012). Neuronal code for extended time in the hippocampus. *Proceedings of the National Academy of Sciences of the United States of America*, 109(47):19462–7.

Marr, D. (1971). Simple memory: a theory for archicortex. *Philosophical transactions of the Royal Society of London. Series B, Biological sciences*, 262(841):23–81.

Mathis, A., Herz, A. V. M., and Stemmler, M. (2012). Optimal Population Codes for Space: Grid Cells Outperform Place Cells.

Maurer, A. P., Burke, S. N., Lipa, P., Skaggs, W. E., and Barnes, C. A. (2011). Greater running speeds result in altered hippocampal phase sequence dynamics. *Hippocampus*, 747:737–747.

Maurer, A. P., Cowen, S. L., Burke, S. N., Barnes, C. A., and McNaughton, B. L. (2006a). Organization of hippocampal cell assemblies based on theta phase precession. *Hippocampus*, 16(9):785–794.

Maurer, A. P., Cowen, S. L., Burke, S. N., Barnes, C. A., and McNaughton, B. L. (2006b). Phase precession in hippocampal interneurons showing strong functional coupling to individual pyramidal cells. *J Neurosci*, 26(52):13485–13492.

Maurer, a. P., Lester, a. W., Burke, S. N., Ferng, J. J., and Barnes, C. a. (2014). Back to the Future: Preserved Hippocampal Network Activity during Reverse Ambulation. *J Neurosci*, 34(45):15022–15031.

Maurer, A. P. and McNaughton, B. L. (2007). Network and intrinsic cellular mechanisms underlying theta phase precession of hippocampal neurons. *Trends in Neurosciences*, 30(7):325–333.

Maurer, A. P., Vanrhoads, S. R., Sutherland, G. R., Lipa, P., and McNaughton, B. L. (2005). Self-motion and the origin of differential spatial scaling along the septo-temporal axis of the hippocampus. *Hippocampus*, 15(7):841–852.

McFarland, W. L., Teitelbaum, H., and Hedges, E. K. (1975). Relationship between hippocampal theta activity and running speed in the rat. *Journal of comparative and physiological psychology*, 88(1):324–328.

McNaughton, B. L., Barnes, C. A., and O'Keefe, J. (1984). The contributions of position, direction, and velocity to single unit activity in the hippocampus of freely-moving rats. *Experimental Brain Research*, 54(1):195.

McNaughton, B. L., Battaglia, F. P., Jensen, O., Moser, E. I., and Moser, M.-B. (2006). Path integration and the neural basis of the 'cognitive map'. *Nature reviews. Neuroscience*, 7(8):663–678.

Mehta, M. R., Lee, A. K., and Wilson, M. A. (2002). Role of experience and oscillations in transforming a rate code into a temporal code. *Nature*, 417(6890):741–746.

Miles, R. and Wong, R. K. (1986). Excitatory synaptic interactions between CA3 neurones in the guinea-pig hippocampus. *The Journal of physiology*, 373:397–418.

Mizuseki, K. and Buzsaki, G. (2014). Theta oscillations decrease spike synchrony in the hippocampus and entorhinal cortex. *Philosophical transactions of the Royal Society of London. Series B, Biological sciences*, 369(1635):20120530.

Mizuseki, K., Diba, K., Pastalkova, E., Teeters, J., Sirota, A., and Buzsáki, G. (2014). Neurosharing: large-scale data sets (spike, LFP) recorded from the hippocampal-entorhinal system in behaving rats. *F1000Research*, 3:98.

Mizuseki, K., Sirota, A., Pastalkova, E., and Buzsáki, G. (2009). Theta Oscillations Provide Temporal Windows forLocal Circuit Computation in the Entorhinal-Hippocampal Loop. *Neuron*, 64(2):267–280.

Moser, E. I., Roudi, Y., Witter, M. P., Kentros, C., Bonhoeffer, T., and Moser, M.-B. (2014). Grid cells and cortical representation. *Nature reviews. Neuroscience*, 15(7):466–481.

Nadel, L., Samsonovich, A., Ryan, L., and Moscovitch, M. (2000). Multiple trace theory of human memory: Computational, neuroimaging, and neuropsychological results. *Hippocampus*, 10(4):352–368.

Navratilova, Z., Giocomo, L. M., Fellous, J.-M., Hasselmo, M. E., and McNaughton, B. L. (2012). Phase precession and variable spatial scaling in a periodic attractor map model of medial entorhinal grid cells with realistic after-spike dynamics. *Hippocampus*, 22(4):772–789.

Nirenberg, S. and Latham, P. E. (2003). Decoding neuronal spike trains: how important are correlations? *PNAS*, 100(12):7348–7353.

O'Keefe, J. and Conway, D. H. (1978). Hippocampal place units in the freely moving rat: why they fire where they fire. *Experimental Brain Research*, 31(4):573–590.

O'Keefe, J. and Dostrovsky, J. (1971). The hippocampus as a spatial map. Preliminary evidence from unit activity in the freely-moving rat. *Brain Research*, 34(1):171–175.

O'Keefe, J. and Nadel, L. (1978). *The Hippocampus as a Cognitive Map*, volume 3. Oxford University Press.

O'Keefe, J. and Recce, M. (1993). Phase relationship between hippocampal place units and the EEG theta rhythm. *Hippocampus*, 3(3):317–30.

Palm, G., Knoblauch, A., Hauser, F., and Schüz, A. (2014). Cell assemblies in the cerebral cortex. *Biological Cybernetics*.

Pastalkova, E., Itskov, V., Amarasingham, A., and Buzsáki, G. (2008). Internally generated cell assembly sequences in the rat hippocampus. *Science (New York, N.Y.)*, 321(5894):1322–1327.

Pastoll, H., Solanka, L., van Rossum, M. C. W., and Nolan, M. F. (2013). Feedback Inhibition Enables Theta-Nested Gamma Oscillations and Grid Firing Fields. *Neuron*, 77(1):141–154.

Patel, J., Fujisawa, S., Berényi, A., Royer, S., and Buzsáki, G. (2012). Traveling theta waves along the entire septotemporal axis of the hippocampus. *Neuron*, 75(3):410–7.

Penfield, W. and Milner, B. (1958). Memory deficit produced by bilateral lesions in the hippocampal zone. *A. M. A. archives of neurology and psychiatry*, 79(5):475–497.

Petsche, H., Stumpf, C., and Gogolak, G. (1962). The significance of the rabbit's septum as a relay station between the midbrain and the hippocampus. I. The control of hippocampus arousal activity by the septum cells. *Electroencephalography and clinical neurophysiology*, 14:202–211.

Pitkänen, A., Pikkarainen, M., Nurminen, N., and Ylinen, A. (2000). Reciprocal connections between the amygdala and the hippocampal formation, perirhinal cortex,

and postrhinal cortex in rat. A review. *Annals of the New York Academy of Sciences*, 911:369–391.

Reifenstein, E., Stemmler, M., Herz, A. V. M., Kempter, R., and Schreiber, S. (2014). Movement dependence and layer specificity of entorhinal phase precession in two-dimensional environments. *PLoS ONE*, 9(6).

Reifenstein, E. T., Kempter, R., Schreiber, S., Stemmler, M. B., and Herz, A. V. M. (2012). Grid cells in rat entorhinal cortex encode physical space with independent firing fields and phase precession at the single-trial level.

Renart, A., de la Rocha, J., Bartho, P., Hollender, L., Parga, N., Reyes, A., and Harris, K. D. (2010). The asynchronous state in cortical circuits. *Science (New York, N.Y.)*, 327(5965):587–590.

Rennó-Costa, C., Lisman, J. E., and Verschure, P. F. M. J. (2010). The mechanism of rate remapping in the dentate gyrus. *Neuron*, 68(6):1051–1058.

Robbe, D. and Buzsáki, G. (2009). Alteration of theta timescale dynamics of hippocampal place cells by a cannabinoid is associated with memory impairment. *J Neurosci*, 29(40):12597–12605.

Royer, S., Zemelman, B. V., Losonczy, A., Kim, J., Chance, F., Magee, J. C., and Buzsáki, G. (2012). Control of timing, rate and bursts of hippocampal place cells by dendritic and somatic inhibition. *Nature Neuroscience*, 15(5):769–775.

Samsonovich, A. and McNaughton, B. L. (1997). Path integration and cognitive mapping in a continuous attractor neural network model. *J Neurosci*, 17(15):5900–5920.

Sargolini, F., Fyhn, M., Hafting, T., McNaughton, B. L., Witter, M. P., Moser, M.-B., and Moser, E. I. (2006). Conjunctive representation of position, direction, and velocity in entorhinal cortex. *Science (New York, N.Y.)*, 312(5774):758–762.

Schlingloff, D., Káli, S., Freund, T. F., Hájos, N., and Gulyás, A. I. (2014). Mechanisms of sharp wave initiation and ripple generation. *The Journal of neuroscience : the official journal of the Society for Neuroscience*, 34(34):11385–98.

Schmidt, R., Diba, K., Leibold, C., Schmitz, D., Buzsáki, G., and Kempter, R. (2009). Single-trial phase precession in the hippocampus. *J Neurosci*, 29(42):13232–13241.

Schmidt-Hieber, C. and Häusser, M. (2013). Cellular mechanisms of spatial navigation in the medial entorhinal cortex. *Nature Neuroscience*, 16(3):325–331.

Singer, A. C., Carr, M. F., Karlsson, M. P., and Frank, L. M. (2013). Hippocampal SWR Activity Predicts Correct Decisions during the Initial Learning of an Alternation Task. *Neuron*, 77(6):1163–1173.

Sippy, T. and Yuste, R. (2013). Decorrelating action of inhibition in neocortical networks. *J Neurosci*, 33(23):9813–30.

Sirota, A., Csicsvari, J., Buhl, D., and Buzsáki, G. (2003). Communication between neocortex and hippocampus during sleep in rodents. *Proceedings of the National Academy of Sciences of the United States of America*, 100(4):2065–2069.

Skaggs, W. E., McNaughton, B. L., Wilson, M. A., and Barnes, C. A. (1996). Theta phase precession in hippocampal neuronal populations and the compression of temporal sequences. *Hippocampus*, 6(2):149–172.

Solstad, T., Boccara, C. N., Kropff, E., Moser, M.-B., and Moser, E. I. (2008). Representation of geometric borders in the entorhinal cortex. *Science*, 322:1865–1868.

Squire, L. R. and Alvarez, P. (1995). Retrograde amnesia and memory consolidation: A neurobiological perspective.

Sreenivasan, S. and Fiete, I. (2011). Grid cells generate an analog error-correcting code for singularly precise neural computation. *Nature neuroscience*, 14(10):1330–7.

Stark, E., Eichler, R., Roux, L., Fujisawa, S., Rotstein, H. G., and Buzs??ki, G. (2013). Inhibition-Induced theta resonance in cortical circuits. *Neuron*, 80(5):1263–1276.

Stensola, H., Stensola, T., Solstad, T., Frøland, K., Moser, M.-B., and Moser, E. I. (2012). The entorhinal grid map is discretized. *Nature*, 492(7427):72–78.

Stewart, M. and Fox, S. E. (1990). Do septal neurons pace the hippocampal theta rhythm? *Trends in neurosciences*, 13(5):163–168.

Taube, J. S. (2007). The head direction signal: origins and sensory-motor integration. *Annual review of neuroscience*, 30:181–207.

Tetzlaff, T., Helias, M., Einevoll, G. T., and Diesmann, M. (2012). Decorrelation of Neural-Network Activity by Inhibitory Feedback. *PLoS Computational Biology*, 8(8):e1002596.

Thierry, A. M., Gioanni, Y., Dégénétais, E., and Glowinski, J. (2000). Hippocampo-prefrontal cortex pathway: Anatomical and electrophysiological characteristics. *Hippocampus*, 10(4):411–419.

Thurley, K., Hellmundt, F., and Leibold, C. (2013). Phase precession of grid cells in a network model without external pacemaker. *Hippocampus*, 0440(01).

Toates, F. (1997). The interaction of cognitive and stimulus-response processes in the control of behaviour.

Tolman, E. C. (1948). Cognitive maps in rats and men. *Psychological review*, 55(4):189–208.

Tóth, K., Borhegyi, Z., and Freund, T. F. (1993). Postsynaptic targets of GABAergic hippocampal neurons in the medial septum-diagonal band of broca complex. *The Journal of neuroscience : the official journal of the Society for Neuroscience*, 13(9):3712–3724.

Tsodyks, M. V., Skaggs, W. E., Sejnowski, T. J., and McNaughton, B. L. (1996). Population dynamics and theta rhythm phase precession of hippocampal place cell firing: a spiking neuron model. *Hippocampus*, 6(3):271–280.

van der Meer, M. A. A. and Redish, A. D. (2011). Theta phase precession in rat ventral striatum links place and reward information. *J Neurosci*, 31(8):2843–2854.

Vanderwolf, C. H. (1969). Hippocampal electrical activity and voluntary movement in the rat. *Electroencephalography and clinical neurophysiology*, 26(4):407–418.

Varga, C., Golshani, P., and Soltesz, I. (2012). Frequency-invariant temporal ordering of interneuronal discharges during hippocampal oscillations in awake mice. *Proceedings of the National Academy of Sciences*, 109(40):E2726–E2734.

Wallace, D. J. and Kerr, J. N. D. (2010). Chasing the cell assembly. *Current Opinion in Neurobiology*, 20(3):296–305.

Wang, X.-J. (2002). Pacemaker neurons for the theta rhythm and their synchronization in the septohippocampal reciprocal loop. *Journal of Neurophysiology*, 87(2):889–900.

Wang, Y., Romani, S., Lustig, B., Leonardo, A., and Pastalkova, E. (2015). Theta sequences are essential for internally generated hippocampal firing fields. *Nature Neuroscience*, 18(2):282–288.

Wikenheiser, A. M. and Redish, a. D. (2015). Decoding the cognitive map: ensemble hippocampal sequences and decision making. *Current Opinion in Neurobiology*, 32:8–15.

Wills, T. J., Cacucci, F., Burgess, N., and O'Keefe, J. (2010). Development of the hippocampal cognitive map in preweanling rats. *Science (New York, N.Y.)*, 328(5985):1573–1576.

Wilson, M. A. and McNaughton, B. L. (1993). Dynamics of the hippocampal ensemble code for space. *Science (New York, N.Y.)*, 261(5124):1055–1058.

Wood, E. R., Dudchenko, P. A., Robitsek, R. J., and Eichenbaum, H. (2000). Hippocampal neurons encode information about different types of memory episodes occurring in the same location. *Neuron*, 27(3):623–633.

Woodson, W., Nitecka, L., and Ben-Ari, Y. (1989). Organization of the GABAergic system in the rat hippocampal formation: a quantitative immunocytochemical study. *The Journal of comparative neurology*, 280(2):254–271.

Yartsev, M. M., Witter, M. P., and Ulanovsky, N. (2011). Grid cells without theta oscillations in the entorhinal cortex of bats.

Zalesak, M. and Heckers, S. (2009). The role of the hippocampus in transitive inference. *Psychiatry Research - Neuroimaging*, 172(1):24–30.

Zohary, E., Shadlen, M. N., and Newsome, W. T. (1994). Correlated neuronal discharge rate and its implications for psychophysical performance. *Nature*, 370(6485):140–143.

Zugaro, M. B., Monconduit, L., and Buzsáki, G. (2005). Spike phase precession persists after transient intrahippocampal perturbation. *Nature neuroscience*, 8(1):67–71.